Design and fabrication of an on-chip PCR device.

by

G.H.C. Maybery

Thesis presented in partial fulfilment of the requirements for the degree of Master of Engineering in Electronic Engineering in the Faculty of Engineering at Stellenbosch University

Supervisor: Prof. W.J.Perold

April 2019

The financial assistance of the Council for Scientific and Industrial Research (CSIR) towards this research is hereby acknowledged. Opinions expressed and conclusions arrived at, are those of the author and are not necessarily to be attributed to the CSIR.

Declaration

By submitting this thesis electronically, I declare that the entirety of the work contained therein is my own, original work, that I am the sole author thereof (save to the extent explicitly otherwise stated), that reproduction and publication thereof by Stellenbosch University will not infringe any third party rights and that I have not previously in its entirety or in part submitted it for obtaining any qualification.

Date: April 2019

Abstract

Design and fabrication of an on-chip PCR device.

G.H.C Maybery

Thesis:

April 2019

An investigation into microfluidic-based PCR (Polymerase Chain Reaction devices was conducted. A continous-flow serpentine-channel device was fabricated. Channels were etched on a Poly(methyl methacrylate (PMMA substrate using CO_2 laser ablation and channels with dimensions $150 \times 150 \mu m$ were obtained. A PMMA lid was bonded via thermal-assisted solvent bonding using Isopropanol. An in-house external connection schema was fabricated for fluid inlet and outlet ports and pressure driven flow was achieved using a benchtop syringe pump. Notable amplification of a 250bp (NisinA fragment was achieved within 30 minutes, a final concentration of 1.5 μg/L was detected. The relationship between flow rates, temperature zone residency times and amplification efficiency was examined. This device serves as a proof-of-concept for two purposes, to show that fabrication of microfluidic devices can be accomplished in low-tech lab spaces and to provide a roadmap towards the design of a fully-portable, low cost PCR device.

Uittreksel

G.H.C Maybery

Tesis:

April 2019

'n Ondersoek na mikro-uidiese-gebaseerde PCR (Polimerase Kettingreaksie toestelle was uitgevoer. 'n Deurlopende-serpentine-kanaal toestel was vervaardig. Kanale was geëts op 'n Poly (methylmethacrylaat (PMMA substraat met CO2 laser ablasie en kanale met afmetings 150x150μm was behaal. 'n PMMA-deksel was gebind deur middel van hitte-geassisteerde oplosmiddel bindinggebruik Isopropanol. 'N interne eksterne konneksie skema was vervaardig vir inlaat en uitlaat poorte en druk gedrewe was behaal met behulp van a spuitbuisprop. Merkbare amplifikasie van 'n 250bp (NisinA fragment was binne 30 minute bereik, 'n nal konsentrasie van 1.5μg/L was opgespoor. Die verhouding tussen ow tariewe, temperatuursone verblyf tye en amptelike kategese was ondersoek. Hierdie toestel dien as 'n bewys van konsepte vir twee doeleindes, om aan te toon dat vervaardiging van mikro uidiese toestelle kan word behaal in lae-tegnologie laboratoriumruimtes en 'n padkaart na die ontwerp van 'n vol draagbare, laekoste-PCR-toestel.

Acknowledgements

I would like to express my sincere gratitude to the following people and organisations.

Firstly, my parents, without whom I would'nt have been where I am today. Their love and support is unconditional and honestly I am forever greatful. Thanks Mom and Dad, I'm finally done.

Secondly, Professor Willem J. Perold for his continued support and guidance. Prof Perold is always willing to discuss concepts and offer his valuable input on a subject, his infectious positivity made the entire process far more bearable. Thanks Prof for all the help over the years.

Thirdly, to my research group. Thank you for all the input and advice given on my project, some of which was implemented in the final product. I wish you all the best and hope we will stay in contact.

Prof Leon Dicks for tolerating my engineer self in the microbiology lab. Thank you for allowing me to work in your lab, without which I would not have been able to complete the biological side of my project.

Lastly to anyone I missed, you know who you are. To the people closest to me, Deon Nevelling, Joshua Hensberg, Robey Beswick, Jonathan Humphries and Philippa Dietmann. All the late nights listening to my babbling about my project did not go unnoticed. Thanks for all the good times, there will be many more.

Contents

List of Figures

List of Tables

Nomenclature

Abbreviations

LOC	Lab-on-chip
PCR	Polymerase Chain Reaction
HIV	Human Immunodeficiency Virus
AIDS	Acquired Immune Deficiency Syndrome
POC	Point-of-care
SVR	Surface to volume ratio
OTS	Off the shelf
PDMS	Polydimethylsiloxane
PMMA	Poly(methyl methacrylate)
PC	Polycarbonate
μTAS	Micro Total Analysis Systems
EWOD	Electrowetting-on-dielectric
DEP	Dielectrophoresis
MEMS	Micro-Electro-Mechanical Systems
HAR	High aspect ratio
RIE	Reactive ion etching
HF	Hydrofluoric acid

Variables

q	Local heat flux density	$[\mathrm{W/M^2}]$
k	Thermal conductivity	$[\mathrm{W/M{\cdot}}K]$
T	Temperature	[K]
Q	Thermal energy	[J]
C_{th}	Specific heat	$[\mathrm{J/K{\cdot}}kg]$
γ	Surface tension	[N/m]
θ_t	Contact angle with channel top	[rad/m]
θ_r	Contact angle with channel right side	[rad/m]
θ_b	Contact angle with channel bottom	[rad/m]

θ_l	Contact angle with channel left side	[rad/m]
σ_{sv}	Surface energy solid-vapour	[J/m^2]
σ_{sl}	Surface energy solid-liquid	[J/m^2]
σ_{lv}	Surface energy liquid-vapour	[J/m^2]
θ_{Young}	Young contact angle	[rad/m]
ϵ	Dielectric constant	[W/M^2]
η	Dimensionless electrowetting number	[ ]

Chapter 1

Introduction

The contents of this chapter provide an overview of the investigation into portable analytical devices, with specific reference to Polymerase Chain Reaction (PCR) devices based on microfluidic concepts. Relevant background knowledge is presented alongside the motivation for such devices. Briefly, microfluidics is presented as a basis for portable analytical devices and its benefits to this category of devices are discussed. The PCR is presented as a means for disease diagnostics and current implementations are discussed. A literature synopsis is provided to outline the theme of the investigation, relevant literature is presented and critically examined. The goals and objectives of this investigation are defined to ensure a benchmark on which to judge the outcome of this thesis. A general overview of the contributions made by this work are presented and principal results put forth. The structure of the thesis will be briefly outlined to provide an insight into the flow of this investigation.

1.1 Background

It was written in *Nature* that 'microfluidics has the potential to influence subject areas from chemical synthesis and biological analysis to optics and information technology' [14]. Microfluidics is the science and study of liquids in the submilliliter range. At this length of scale liquids display interesting properties in comparison to their macro counterparts. At the micron range, fluids within channels can be manipulated more predictability due to different temporal-spatial properties such as low Reynold's numbers (laminar flow), capillary force's dominance over gravity and surface and interfacial tension. This allows for the production of devices capable of accurately manipulating microliter (10^{-6}) down to the picoliter (10^{-12})L volumes. Applications include a number of tasks, such as performing rapid PCR [15, 10, 16, 17, 18, 19], forming mono-disperse droplets in fluid streams [20] and passively pumping fluids in microchannels [21].

One application which shows particular promise in the microfluidics region is the Polymerase Chain Reaction (PCR), a precursory step to many diagnostic and analytical procedures. The PCR reaction amplifies sequences of genes through a thermo-circulatory process whereby a DNA fragment is exposed to 3 unique temperatures, in the presence of polymerase, nucleotides and other necessary reagents. Once the sample has been exposed to these cycled temperatures, usually from 20-40 cycles, the genetic sequence will be amplified. Conventional PCR machines are large pieces of instrumentation and it is highly unlikely one would find such a device in rural areas. PCR on-chip devices can be fully portable, which would allow for more complex analytical procedures to be performed in an in-field environment. This could help alleviate the diagnostic burdens faced by these communities.

1.2 Motivation

The need for portable, reliable and inexpensive disease testing solutions is an issue that still needs to be solved. Rural areas that lack access to sophisticated medical treatment and diagnostic centers can benefit through the provision of portable disease diagnostic equipment. South Africa suffers from the largest HIV epidemic in the world, with HIV prevalence being as high as 18.9% in the population [22]. An estimated 7.2 million people were living with AIDS/HIV in 2017 in South Africa. Governmental spending was reported at R 2 billion for this time period. These numbers are showing improvement, however, much can still be done to aid in the battle against such diseases [23].

There are a number of genes that can affect the course of the HIV infection in a patient. Genetic mutations have been linked to protein defects (CCR5 delta 32) and HIV drug resistances [24]. Genetic testing can be performed to detect the presence of these genes which could improve patient prognosis.

Diagnosis is not the primary purpose PCR devices, although portable PCR devices do show great promise for in-field use. The improvements that microfluidics offer over conventional machinery such as improved reaction times and reduction in reagent volumes, warrant it's inclusion into laboratory environments.

Over the last 20 years an increasing amount of research has been focused on the production of Lab-on-Chip devices (LOC). These devices, in theory, are capable of performing a number of complex analytical laboratory procedures on a miniaturized platform. These devices are manufactured, not only in an effort to reduce size, cost and complexity of such procedures, but also

to provide a portable solution to those affected by diseases in areas lacking diagnostic infrastructure.

The PCR reaction is an analytical procedure that is capable of amplifying DNA from a single strand to billions of copies. This procedure can be deemed the "revolutionary" discovery within the field of genetics. Through the use of this technique researchers and medical technicians can study DNA fragment samples with increased ease. The introduction of the LOC variant of PCR has provided a number of benefits over traditional methodology. Conventionally, PCR is performed by a device known as a thermal-cycler, a large laboratory based piece of equipment. These devices can typically take anywhere between 120-180 minutes to complete a reaction. Microfluidic PCR devices have reported amplification times within 30 minutes, a significant reduction when compared to traditional machinery. This reduction in time, coupled with their portability, point towards the possibility of being used as Point-of-Care (POC) devices to aid in rapid diagnosis of diseases.

The need for POC disease diagnostic devices is evident. These devices not only offer improved response times and reduced costs, their portability allows them to provide diagnostic solutions for those lacking access. The motivation for this project is to aid research into these portable LOC devices, specifically to provide a microfluidics PCR system that could be used in-field. The device itself should conform to low cost, simple operation and portability criteria as to achieve it's goal of alleviating the diagnostic burden faced by those in rural areas. Secondly, the device should aim to improve on conventional PCR equipment and serve as an investigation into the possibility of acting as a replacement device.

1.3 Literature synopsis

Relevant literature pertaining to microfluidics device fabrication, with specific reference to PCR implementations, was reviewed. The review details fundamental microfluidic laws and discusses their applicability to device design. The evolution of microfluidic fabrication technologies was studied, from their initial fabrication on glass/silicon substrates to the more recent use of thermoplastics as an alternative material. An investigation into current implementations of microfluidic PCR devices was performed and presented.

Microfluidics has it's own set of constraints when compared to it's macro counterpart. Volumes of liquid encapsulated in micro/nano-scale channels display interesting properties, properties that have been leveraged to fabricate microfluidic devices. Due to the increased surface to volume ratio (SVR) at this scale, interfaces tend to play a larger role. Capillary forces become dominant

over gravitational forces, Reynold's numbers tend to fall within the laminar region allowing for concise control, molecular diffusion forms more predictable patterns and due to the reduced volume of liquids, a reduced thermal mass is noted, allowing for rapid heating of samples. It is these and other properties of microfluidics that researchers have harnessed to fabricate a plethora of micro-devices.

Fabrication of microfluidic devices is possible through a number of techniques. During it's initial phase, considerable research was focused on the use of glass and silicon as substrates on which to fabricate channels. Techniques commonly used included dry and wet etching procedures, usually involving a masking process followed by a photo-lithographic step after which, the pattern revealed through a form of exposure. In recent years focus has shifted from glass/silicon substrates to thermoplastics. This class of materials offers some attractive advantages to microfluidic fabrication, such as rapid prototyping, good biocompatability and their cost when compared to traditional substrates.

The use of microfluidics to implement PCR devices has been reported for a number of years. The reduction in volume of analytes and reagants not only leads to reduced costs, but the reduced thermal mass allows for far more rapid heating and cooling of samples, which has led to greatly reduced reaction times. Microfluidic PCR devices can be categorized into two main types, namely stationary and continuous. Stationary PCR involves loading of the sample into discrete wells, which are then exposed to the appropriate temperature cycles. Contrastingly, continuous-flow PCR makes use of a "time-space" principle, whereby temperature zones remain stationary and the sample volume is driven through channels across the temperature regions on the chip.

A number of continous-flow PCR implementations have been proposed, which include serpentine channel flow, oscillatory flow and centrifugal driven flow. A vast number of materials have been investigated as the substrate for such devices and each category of substrate has within it a number of fabrication techniques. Polymer substrates allow for relatively simple fabrication procedures, a feat that aids in rapid prototyping of multiple channel geometries. Lid bonding is an essential step in the construction process and a number of techniques exist to achieve air-tight bonds, each with their own pitfalls, caveats and benefits. Samples are driven through the channels by a variety of methods. Syringe pumps are commonly used to create a pressure-driven flow, however, alternatives such as peristaltic pumps, electro-osmotic flow and others exist.

Microfluidics, as a whole, is presented in the literature, focusing on the development of portable PCR-devices. Current fabrication methodologies were investigated and are discussed.

1.4 Objectives of the investigation

The following is a list of objectives for the investigation:

- Briefly overview a number of relevant microfluidics operation principles.
- Review the generalized construction process of microfluidics devices.
- Investigate current literature with regards to portable PCR-devices.
- Determine the most relevant category of PCR device to be constructed.
- Propose a substrate to be used for the microfluidics channels, based on literature.
- Review heating techniques used in microfluidic devices.
- Design a microfluidics network for a PCR device.
- Decide upon a relevant heating approach and design its implementation.
- Investigate flow control in microfluidics devices and decide upon a relevant implementation.
- Review lid bonding methods for microfluidics devices and decide upon a technique to be used.
- Investigate an alternative to commercially acquired microfluidics connections.
- Integrate the subcomponents of the system to produce a functional device for PCR amplification.
- Design a test protocol for the constructed device.
- Calculate theoretical flow rates, Reynold's numbers and temperature zone residency times for constructed device.
- Calculate actual flow rates, Reynold's numbers and temperature zones residency times based on measured values.
- Compare theoretical and actual calculations for the designed device.
- Evaluate the relationship between residency times and amplification efficiencies.
- Investigate optimal device parameters for efficient DNA amplification.
- Compare the constructed device to those detailed in literature.
- Propose a design for a low cost, commercial PCR microfluidics device.

1.5 Contributions made

The contributions made during this project are outlined below:

- A literature review was performed on techniques used for microfluidic device fabrication, with a focus on portable, low-cost PCR devices.
- Current methodologies for performing PCR were investigated, literature indicated large, non-portable equipment is most commonly used to perform PCR, usually in a laboratory environment. This indicated the need for a portable solution.
- A heating system based on Peltier elements was implemented using off-the-shelf (OTS) controllers. This proved that cost-effective heating implementations for PCR are possible.
- An in-house microfluidic connector scheme was devised which did not rely on expensive commercial connectors.
- A non-expensive microfluidics chip manufacturing process was established. PMMA was etched using CO_2 laser ablation and lid bonding was performed using solvent-assisted thermal bonding.
- A system for performing rapid PCR was manufactured and was capable of notable amplification within 30 minutes (compared to the conventional 150 minute process time).
- A relationship between temperature zone residency periods and amplification efficiencies was proposed.
- A system model/specification sheet was produced for use in future portable PCR device designs.

1.6 Summary

This thesis focuses on the design and fabrication of a microfluidics device capable of rapid DNA amplification through the PCR. A detailed overview of microfluidic device construction is presented with a focus on polymer microfluidics. Principal microfluidic fundamentals are presented and discussed in relation to the PCR. A serpentine-channel microfluidics chip was manufactured on a PMMA substrate, using CO_2 laser ablation. Lid bonding was achieved using solvent-assisted thermal bonding and flow control was achieved by a syringe-pump.

DNA amplification of a 200-bp fragment was performed at varying flow rates to investigate the relationship between temperature zone residency times and

amplification efficiencies. Successful amplification was achieved at greatly improved rates (30 minutes) when compared to conventional laboratory procedures (150-180 minutes.) A specification was produced for future work on a commercially viable, portable PCR device. This device represents a low cost alternative to traditional approaches and provides a possible solution for a LOC implementation of a PCR device.

1.7 Brief Chapter overview

The chapters in this thesis detail the work contributed as follows:

- Chapter 2: A literature review covering microfluidic fundamentals, generalized fabrication procedures for microfluidic devices and an in-depth investigation into microfluidic PCR device's current literature.
- Chapter 3: This chapter presents the fabrication methodology followed to produce the PCR device.
- Chapter 4: Results and characterization techniques are presented.
- Chapter 5: Summarizing and concluding remarks are given.
- Chapter 6: Future recommendations and designs are proposed for use in further investigations.

Chapter 2

Literature Review

2.1 Microfluidics

2.1.1 Introduction

Microfluidics is a promising, relatively new field pertaining to the control and manipulation of droplets within the 10^{-6} to 10^{-9} scale [14]. Microfluidics' potential to provide unique solutions to fields such as analytical chemistry, microbiology and microelectronics is substantial. Systems used within these fields can benefit from attractive properties such as reduced reagent and sample usage, high resolution, faster processing and the laminar flow property of fluids flowing at this scale.The origin of microfluidics stems from a gas chromatograph developed by Standford in 1979 [25], the development of which was promoted by the advancement of silicon manufacturing due to the microelectronics and semiconductor industry. Since then the field has made considerable progress and complex 3D structures are now possible on a variety of substrates, paving the way for a wider range of applications. The adoption of polymers as substrates, specifically Polydimethylsiloxane (PDMS), is providing continually expanding room for applications. Silicon and glass microfluidics have been somewhat replaced by the addition of thermoplastics, stemming from their easier fabrication, optical transparency, flexibility and favorable surface properties.

This review will cover microfluidics and it's role in ongoing research into lab-on-chip devices, with specific focus on PCR microfluidic systems. The fundamental laws governing microfluidic systems will be explained and recent work pertaining to device subcomponents will be presented.

2.1.2 Microfluidics fundamentals

A better understanding regarding the advantages and capabilities that microfluidics offer can be achieved through examining the physical laws that

govern fluids and molecules at this scale.

2.1.2.1 Physics at the micro scale

Microfluidics is only made possible due to the unique properties fluid/gas flows exhibit on a micrometer scale. One would expect that microscopic fluid flows would mimic their macroscopic counterparts and although that is true for some cases, exceptions do exist, and it is these exceptions that brought about the study of microhydrodynamics, the study of fluids at micrometric scales. When we inspect the laws prevalent at a miniaturized scale, it is important to introduce the concept of the scaling law [26]. A "scaling law" defines the rule for variations of the physical quantities of a system, with respect to the dimension l of the system or object. When examining the physical quantities of a system, we are usually left with two considerations:

- the physical quantities that affect the scaling law are constants
- physical quantities appearing in the scaling law are dependent on scale.

When looking at miniaturized systems, a general rule of thumb can be drawn: forces with the weaker exponent tend to dominate the forces in a miniaturized system [26]. Considering the scale laws, we see that when examing forces dominant in the microfluidics context, capillary forces (l^1) are more prevalent than those of gravity (l^3) or centrifugal forces (l^4).

2.1.2.2 Low Reynold's numbers

Microfluidic systems can generally be assumed to operate at low Reynold's numbers ($Re << 1$), with the exception of a few cases that operate at moderate Reynold's numbers ($Re < 100$), as is the case with microheaters which require moderate Reynold's numbers to achieve efficient heating. Incompressible Newtonian fluids at small Reynold's numbers are governed by the Stokes equation,

$$\rho F_i - \frac{\partial p}{\partial x_i} + \mu \frac{\partial^2 u_i}{\partial x_j^2} = 0, \tag{2.1.1}$$

where u_i is the component of velocity along the i axis, p is the pressure and F_i is i^{th} component of the external volumetric force. When obtaining the Stokes equation, we consider the two inertial terms to be negligible when compared to the viscous terms for small Reynold's numbers. This disregard of the inertial terms permits flows, in the absence of any free surfaces or interfaces, to exhibit characteristics such as linearity, reciprocity, uniqueness of solution and reversibility. Microfluidics take advantage of these unique properties of flows at low Reynolds numbers to manipulate fluids and particles precisely and predictably.

2.1.2.3 Capillarity

Capillary action is a dominant force when considered on a microfluidics scale. Microfluidic devices that are capillary force driven are considered "passive" flow devices, as these systems can operate with very little user input. Capillary forces are largely governed by surface tensions, surface chemistry and the geometry of the channels [27]. A large pitfall of conventional microfluidic devices is the need for complex external equipment, i.e. flow control and heaters. The capillary driven devices reduce the need for external flow control and thus simplify the equipment necessary to perform diagnostics, thus bringing microfluidics closer to their ideal form as a fully self-enclosed LOC [28].

To gain a better understanding of how capillary forces operate on a microfluidic level and how researchers leverage these properties to create passive flow devices, we must examine the laws that define capillarity.

Surface Wettability Surface wettability is defined by the contact angle of liquids to the surface. If the angle is $<90°$, the surface is considered wettable. These systems produce negative capillary action, which pulls liquid into the channels. Conversely, for angles $>90°$a positive pressure is generated that forces liquid out of the channels.

Capillary pressure Flow in capillary microfluidics is generated by the capillary pressure within the channels. Capillary forces are as a result of a liquid's surface tension and the adhesive forces at the solid-liquid interface. In general, we can assume that micro-channels utilizing capillary forces are of a rectangular geometry, the capillary force of which is governed by the Young-Laplace equation,

$$P = -\gamma\left(\frac{\cos\theta_t + cos\theta_b}{h} + \frac{\cos\theta_l + cos\theta_r}{w}\right), \tag{2.1.2}$$

where P is the capillary pressure, γ the surface tension, θ_l, θ_r, θ_b and θ_t are the contact angles with the channel sides and h, w are the height and width respectively.

Capillary microfluidic applications Since it's inception around the 1980's, capillary microfluidics has seen a wide range of applications evolve, from it's initial phase where abrupt geometry changes were used to halt flow, pumps that allowed unidirectional flow and dilution devices that leverage capillary and gravitational effects to dilute samples [29].

Capillary microfluidics underwent a resurgence with the emergence of micro total analysis systems (μTAS) in the 90's [30]. Notable work done by Delmarche et. al. [30], illustrates how capillary forces started to integrate with

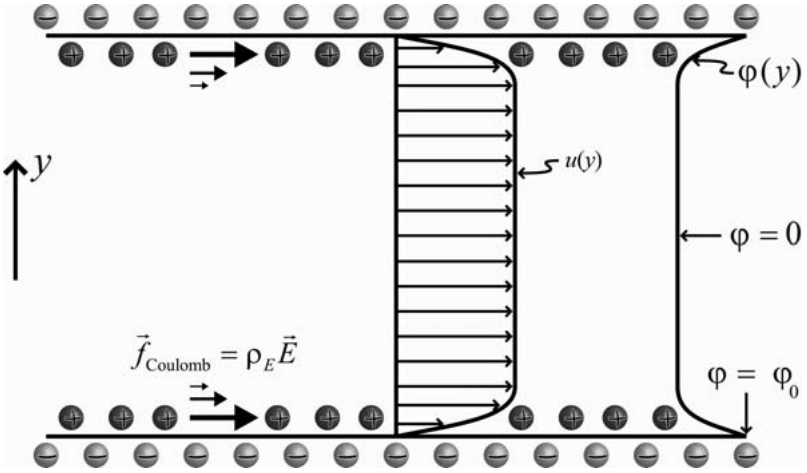

Figure 2.1: Potential distribution and resulting velocity profile from electroosmotic induced flow [1].

biological assays to create self-powered diagnostics devices. A microfluidic network was constructed, consisting of micro-channels patterned with proteins, capillary forces were used to fill these channels and delivery reagents to the appropriate regions[30]. Since these initial designs, complex capillary circuits have been produced, able to deliver reagents to preprogrammed areas on a microfluidic platform.

2.1.2.4 Electro-osmotic flow

Electro-hydrodynamics are subject to different operating conditions at the microfluidics level, where surface to volume ratios are far larger. Surface reactions within a microfluidic channel lead to charge separations at boundary walls. When subjected to a directional electric field $\vec{E}$, these charges will be attracted to the oppositely charged electrode and by viscous drag, set the bulk fluid in motion [1][31]. Uniform fluid flows are produced by this technique and this advantageous fluid flow is known as Electro-osmotic Flow (EOF), and is described by

$$v_{eof} = \frac{\epsilon \xi E}{4\pi\eta}, \tag{2.1.3}$$

where ϵ is the dielectric constant of the fluid, η is fluid viscosity, E is the applied electric field strength and ξ is the Zeta potential of the surface [32].

The study of electro-hydrodynamics at the microfluidic level led researchers to the development of electroosmotic pumps, which provide a pulse free, stable flow, a high level of integration and no mechanical part [33]. Liu and Dasgupta [34] developed one of the earliest versions of an EOP. Consisting of a capillary electrophoresis system, Fe^{2+} was electrophoretically migrated to the reagent

zone and the product was retrieved using electro-osmotic flow. A concentration range within 5-200 mg/L of Fe^{2+} samples were analyzed in this manner.

2.1.2.5 Dielectrophoresis

The separation of charged species has been a topic of research for a number of years. It has been shown that the use of non-uniform ac fields results in the movement of polarized particles, a result of the dielectrophoretic (DEP) force given by

$$\langle \vec{F}_{DEP} \rangle = \frac{1}{2} \upsilon \alpha \bigtriangledown \vec{E}^2_{rms}. \tag{2.1.4}$$

The use of electrophoresis is a well-studied and developed field, used in seperation techniques, such as capillary electrophoresis that can seperate DNA, proteins and other biomolecules. These particles, in a non-uniform electric field, experience movement due to the interaction of their dipole and the spatial gradient of the electric field [35].

2.1.2.6 Electrowetting

Electrowetting refers to a phenomenon whereby a liquid's contact angle on a surface can be modified by the application of an electric field. Typically, the contact angle of a liquid on a surface is dependent on the surface energy of the liquid and the adhesion of the molecules on the surface [36]. Contact angle defines the wettability of a surface. Angles larger than 90° indicate the surface is hydrophobic for that liquid. Hydrophobicity implies that the surface is "non-wettable" or that little to no absorbtion will occur. Hydrophilic surfaces are defined by contact angles less than 90°, implying that the surface is "wettable" for that specific liquid. An illustration regarding the change in contact angle of a liquid can be seen in Figure 2.2.

Young's equation is used to describe the relationship between different interfacial energies and a liquid's contact angle with a surface,

$$\theta_{Young} = \arccos\left(\frac{\sigma_{sv} - \sigma_{st}}{\sigma_{lv}}\right) \tag{2.1.5}$$

where θ is the contact angle and σ_{sv}, σ_{st}, σ_{lv} denote the surface energies between the solid-vapor, solid-liquid and liquid-vapor, respectively. Under the influence of an electric field, an external energy is now present, deemed the electrical/solid energy. This additional energy works in conjunction with the solid/vapor energy to reduce the contact angle and is described by the modified Young-Lippmann equation,

$$\theta_{Young} = \arccos\left(\frac{\sigma_{sv} - \sigma_{st}}{\sigma_{lv}} + \eta\right), \tag{2.1.6}$$

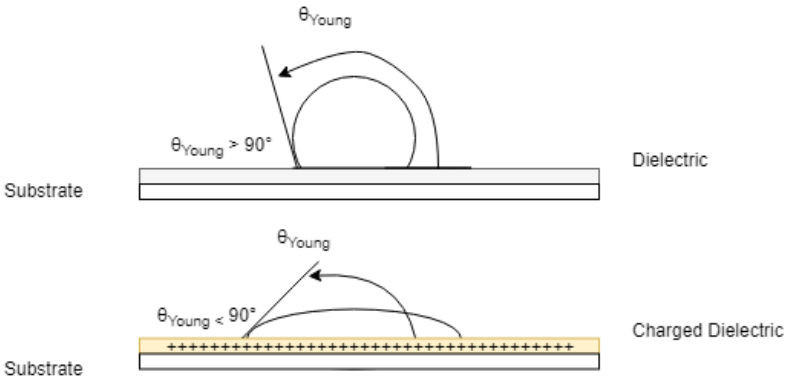

Figure 2.2: Illustration regarding change in liquid contact angle after charging of the dielectric

where η is the dimensionless electrowetting number. This principle of Electrowetting on Dielectric (EWOD) has been leveraged to allow for the transportation of droplets through a system whereby droplets are propelled by the placement of electrodes at interval gaps. Gunji and Masahide [37] used a similar technique to move droplets around an oval track.

2.1.2.7 Microfluidics and thermal transfers

When considering the thermal response of microfluidic systems, it is necessary to review the thermodynamic laws in effect at that scale. Temperature regulation is an important aspect required in a multitude of microfluidic applications, PCR probably being the most notable. We require an understanding of thermal mass and conduction in order to explain most of the observed responses we see in a microfluidics context.

Thermal Conduction Heat conduction is the transport of energy from high energy particles to low energy particles within a material, in the absence of any flow of mass. Incropera et al. (2006) [38] stated that heat conduction is the transportation of vibrational states within a substance, devoid of any mass transport forced by flow or diffusive forces. Heat conduction is the core method for heat transfer in solids and as such the conduction of heat through the micro-channel walls/surfaces is the main mechanism for heat transfer [38]. Essentially, when a temperature gradient exists within a substance, the energy in the high temperature area will migrate towards the lower temperature areas. Fourier's law of heat conduction, credited to Jean-Baptiste Joseph Fourier in 1822, introduced the thermal conductivity parameter (k) and it's relationship to the local flux density and negative temperature gradient:

$$\vec{q} = -k \bigtriangledown T, \tag{2.1.7}$$

where $\vec{q}$ is the local heat flux density in (W/m^2), k the thermal conductivity of a material (W/m·K) and T, the temperature in Kelvin.

When considering a substrate used in a thermal regulatory microfluidics system, special attention should be paid to it's thermal conductivity. Devices requiring rapidly transitioning temperature regions should consider applicable substances with a high thermal conductivity, allowing for the rapid transfer of heat. Stationary PCR devices, in which the sample is held in a reservoir and cycled through 3 temperatures, requires substrates that allow efficient transfer of thermal energy. In contrast, continuous flow PCR, which uses fixed temperature regions that samples flow through, require a substrate that is more stable thermally. Materials with lower thermal conductivity tend to be more stable around a temperature point due to their reduced thermal energy transfer.

Thermal Mass The thermal mass of an object determines the amount of thermal energy an object can store. Thermal mass is dependent on the specific heat of a material, the mass of the body and is expressed as

$$Q = C_{th} \cdot \triangle T, \tag{2.1.8}$$

where Q is the thermal energy in Joules, C_{th} the thermal mass($\frac{J}{K}$) and $\triangle T$ is the change in temperature in (K). Specific heat of a material is defined as the amount of heat to increase the temperature of a mass by 1 degree Kelvin and is defined as,

$$C_{th} = m \cdot C_p, \tag{2.1.9}$$

where C_{th} is specific heat ($\frac{J}{K \cdot kg}$). Using (2.1.8) in (2.1.9), we can relate thermal energy directly to mass, specific heat capacity and the temperature change,

$$Q = m \cdot C_p \cdot \triangle T. \tag{2.1.10}$$

Equation (2.1.10) depicts the relationship between the mass of an object in relation to the thermal energy. In a microfluidics context, the greatly reduced mass of samples leads to a greatly reduced thermal mass. This reduced thermal mass allows for the heating/cooling of samples in a far more rapid manner than previously possible in macro systems, allowing for more time efficient heating cycles. This is one of the greatest advantages when considering thermal transfer in microfluidic systems. PCR microfluidics exploit this specific property to greatly reduce reaction times, as a result of the efficient thermal transfer to microlitre samples.

2.1.3 Conclusion

After reviewing the relevant physical laws at work on a microfluidics level, it is evident that through the leveraging of these unique properties, a plethora of

applications are possible. Whether it be smaller thermal mass, reduced reagent consumption, electro-kinetically driven flow or any of the other benefits, it can be seen why microfluidics has shown great promise for developing a complete LOC device.

2.2 Fabrication and bonding of microfluidic substrates

In this section a general microfluidics model will be proposed in an effort to compartmentalize the components and methods common to microfluidics devices. Each category will be discussed independently and recent work presented for each subcomponent of the model. The model is depicted in Figure 2.3 and it can be seen that microfluidic devices follow a general layout that can be categorized according to their substrates and fabrication methods, lid bonding techniques and flow control systems. This is not an exhaustive model and thus applications requiring specific configurations are not covered. The model can be altered to fit the requirements of such devices by additional subcomponents. An additional subcomponent, temperature regulation, will be discussed due to it's pertinence to PCR devices. However it is not applicable to all microfluidic devices.

2.2.1 Substrate channel fabrication and bonding techniques

The fabrication of microfluidic devices is continuously evolving, improvements in technologies have led to a plethora of new techniques being developed and as such this section will serve as a brief overview of the commonly used methods and substrates in the field. When considering types of materials that microfluidic devices are fabricated from, we can generally assume they will fall under one of two categories, namely silicon/glass-based or thermoplastic/polymer base. The introduction of thermoplastics/polymers to the field is quite recent and researchers are only starting to exploit the favorable characteristics these materials can bring to microfluidics.

2.2.1.1 Silicon/Glass

The fabrication of silicon devices is a mature field, the semiconductor industry has driven the study of this material tremendously in the past 30 years and as a result we have a wealth of knowledge for fabrication of silicon-based devices. Silicon also provides certain advantages when it comes to the integration of devices. However, it's advantages are shadowed by it's price when compared to that of thermoplastics. The environment in which silicon devices are fabricated also needs to be dust free, referred to as a clean room. A clean room is

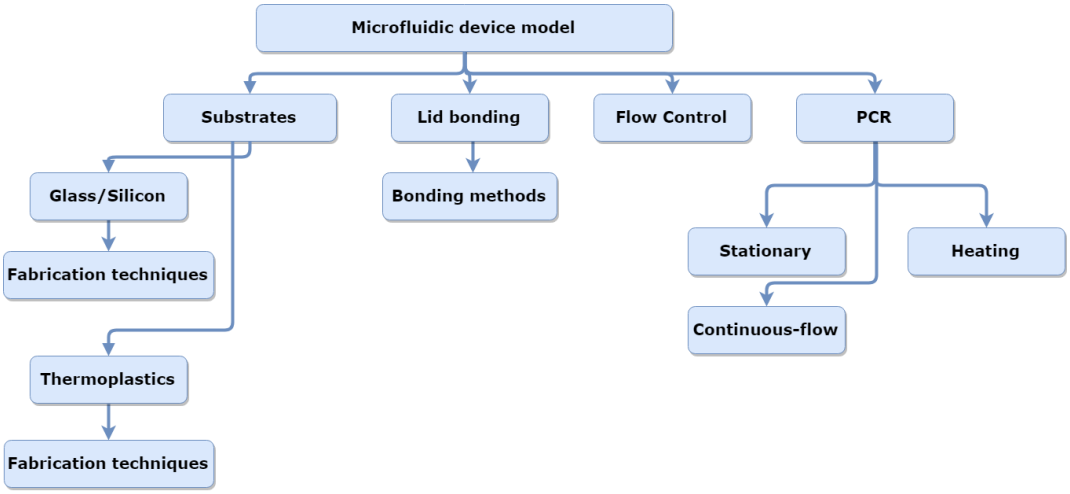

Figure 2.3: Simplified microfluidic device model

an environment in which temperature and humidity are constantly regulated, while the air is circulated. The air is filtered in order to reduce the number of free particles in the air that could otherwise hinder the fabrication of microfluidic devices. The quality of the clean room is assessed by the number of particles smaller than 4 µm in a cubic inch of air [39]. Ratings for clean rooms usually vary, but typical classes for Micro-Electro-Mechanical Systems (MEMS) fabrication are in the range of 1000 to 10 000. A stringent fabrication environment, coupled with the expense of silicon wafers and their biological incompatibility have resulted in a move away from these devices. Applications that require high thermal resilience [40], High Aspect Ratio (HAR), integration with electronic subsystems or integrated electrodes can still benefit from silicon substrates.

The use of glass in microfluidics can be said to be similar to the role of silicon in microfluidics. Glass substrates do offer unique properties that may warrant the additional time, cost and difficulty to produce them. However, they are largely being replaced by the thermoplastic class of substrates. A glass substrate can achieve large temperature gradients due to it's thermal insulating properties. Glass has been used successfully in applications such as LOC PCR devices [41], capillary electrophoresis [42] and gas chromotography [24]. The fabrication techniques for glass microfluidics stem from the silicon manufacturing industry and as such is processed in a very similar manner.

Photolithographic Process Photolithography is a patterning process first used in the printing industry and has been a part of semiconductor fabrication from the 1950's. It is a process whereby a designed mask/pattern is transferred to photoresist on a material surface. The photolithography process usually follows a general methodology, namely photoresist coating, alignment, exposure,

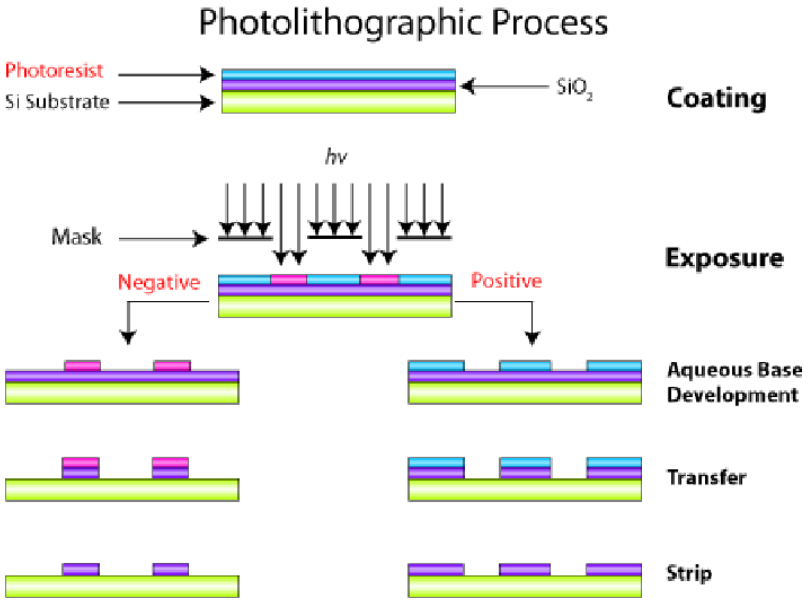

Figure 2.4: Steps involved in a typical photolithographic procedure [2].

development, stripping of photoresist, followed by a hard bake [43]. The first step consists of coating a wafer, usually silicon, in photoresist, a photosensitive material. A mask is then aligned on the now photoresist coated surface and is exposed to ultraviolet (UV) light which passes through the transparent areas of the mask [44]. The photoresist's chemistry is changed by photochemical reactions that occur in UV exposed areas on the chip. Positive photoresist, most commonly used in advanced semiconductor fabrications, requires that the chip be submerged in a developer solution, which dissolves the exposed areas, leaving only the unexposed photoresist on the surface which creates a dark mask/pattern. Once the structure has been embedded in the substrate, the photoresist is stripped away by an appropriate solvent. Figure 2.4 depicts general processes for both positive and negative photoresist. SU-8 has undoubtedly become the most common photoresist used in high aspect ratio (HAR) structures [45]. During the development phase of the photolithographic process, two main techniques are available, namely dry and wet etching.

Dry Etching Dry etching, also known as Reactive Ion Etching (RIE), is a subprocess of photholithography used in micro-fabrication that can achieve HAR strutures in silicon [46]. There are two main techniques when considering dry etching, namely the cryogenic process and the Bosch process, which is the most prevalent of the two [40]. Dry etching involves a passivation step, whereby a C_4F_8-based plasma generates a coating of a polytetrafluoroethylene (PTFE)-like polymer over the exposed surface. Ion bombardment is then used in conjunction with fluoride chemistry to remove the polymer and isotropically etch away the silicon. Most commonly, photoresist and SiO_2 are used as mask

layers. Cryogenic techniques make use of cooled wafers (around -110°C), which provides sidewall passivation and SF_6/O_2 for fluorine radicals for etching [47].

Wet Etching Wet etching of silicon involves the use of "wet" chemicals to etch into the substrate and form structures. However, it has largely been replaced by dry etching due to the advantages it provides. Wet isotropic etching of silicon is performed in HNA solutions. During this redox reaction, HNO_3 oxidizes the Si surfaces, while HF dissolves the generated oxide layer [48]. This solution results in aggressive etching and is largely dependent on the temperature and concentration of the acid. Orientation etching of silicon is possible and relies on the selective etching of the different crystallographic planes [49]. A number of etching solutions are available for this method, however, KOH is the most commonly used, most likely due to it's selective etching of the <100> and <111> crystallographic planes [50].

2.2.1.2 Polymer/Thermoplastics

With the initial boom of the LOC era, glass and silicon microfluidics were at the forefront, with most devices being made from one of the two substrates. However, in the early 1990's polymers were proposed as an alternative to glass/silicon substrates due to their rapid prototyping and reduced expense. Polymers are inexpensive in comparison to glass/silicon substrates. Additionally, there are a wide range of polymers allowing researchers to choose a material that best suits their application [51]. Fabrication techniques for polymers require no hazardous etchants and can be manufactured in relatively simple laboratories, a fact which has driven their use in microfluidics [51].

When introducing polymers as substrates, specifically thermoplastics, the glass transition point of materials (T_g) is an important parameter. Thermoplastics uniquely can undergo softening around the glass transition temperature, which allows their molding/reshaping while retaining the ability to return to their original chemical state upon cooling. This characteristic is exploited in microfluidic fabrication techniques, allowing for rapid prototyping on substrates far more cost efficient than their silicon/glass counterparts. PDMS is currently the most widely used substrate in microfluidic devices, due to its ease of fabrication, biocompatability and cost [52]. Fabrication techniques are far simpler (replica molding, injection molding, hot embossing)[53] than those of silicon/glass substrates (wet etching, RIE). Important to the LOC realization is the need for single-use devices, which can eliminate cross sample contamination. Other polymers used in microfluidic devices include polycarbonate (PC) [54], Poly (methyl methacrylate) (PMMA) [55], polyvinylchloride (PVC) [56], and polyethylene [57]. This section will focus on polymer substrates, their fabrication techniques and recent applications in the LOC field.

		Thermoplastics			
Polymer	**PDMS**	**PC**	**PMMA**	**PS**	**COC/COP/CBC**
Mechanical property	Elastomer	Rigid	Rigid	Rigid	Rigid
Thermal property	80°C	140 - 150°C	100 - 125 °C	90 - 100 °C	70 - 155 °C
Solvent resistance	Poor	Good	Good	Poor	Excellent
Optical transmissivity (Visible range)	Excellent	Excellent	Excellent	Excellent	Excellent
Optical transmissivity (UV range)	Good	Poor	Good	Poor	Excellent
Biocompatibility	Good	Good	Good	Good	Good
Material cost	150 $/kit (1 Kg)	< 3 $/Kg	2 - 4 $/Kg	< 3 $/Kg	20 - 25 $/Kg

Table 2.1: Table summarizing the physical properties of polymers commonly used in microfluidics [12].

2.2.1.3 Fabrication Techniques

The most notable benefit of polymers/thermoplastics is the ease with which microfluidic devices can be fabricated. PDMS, the most commonly used polymer substrate, is a semi-rigid material and as such can be deformed under applied force or air pressure. Thermoplastics such as PC, PMMA and PVC are rigid polymers that offer good mechanical stability, organic solvent resistance and low water absorbtion, all necessary requirements for its use in biomicrofluidics [58]. Polymers are, however, not always perfectly suitable and suffer from drawbacks such as channel deformation [59]. Table 2.1 summarizes the physical properties of polymers and thermoplastics.

Soft-Lithography The introduction of soft-lithography, a polymer molding technique, contributed to considerable advancement in the development of microfluidic devices [60, 61]. Soft-lithography requires the production of a relief master, usually silicon. The polymer is cast onto the stamp and allowed to cure at room or slightly elevated temperatures. Once curing is complete the polymer sheet is then peeled off the silicon stamp, Figure 2.5 depicts this process. During this fabrication technique the silicon master is not exposed to excessive pressure or temperature, which allows the stamp to be used repeatedly. Recently 3-D microfluidic structures have been demonstrated with soft-lithography [62, 63]. Individual layers of the device are cast and a structural support layer is then used to remove the functional layers from the stamp. This is possible due to the excellent adhesion between layers.

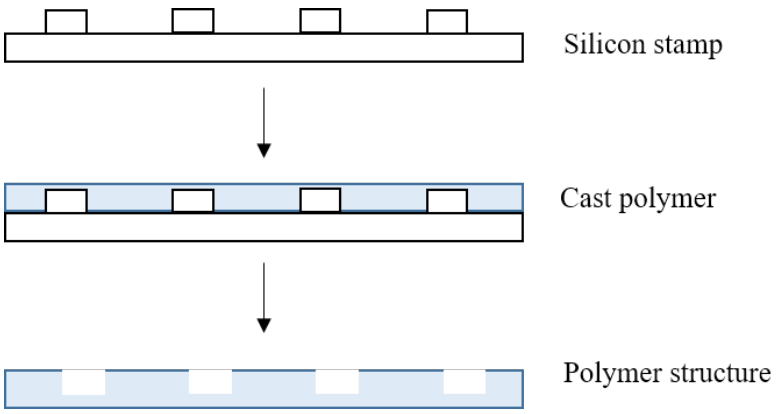

Figure 2.5: Soft-lithography process.

Injection Molding/Micro-molding Micro-injection molding is a process whereby a polymer, usually in granule form, is heated above it's glass transition temperature until it becomes malleable. The polymer is then "injected" into a mold cavity, where it is held for a time. The mold temperature is then reduced, which results in the polymer hardening around the mold [64]. A typical injection molding process is shown in Figure 2.6. This process can be repeated multiple times, with cycle times ranging from seconds to minutes [65, 66, 67]. Injection molding provides accurate resolutions of molded structures [66, 68], low capital costs [68] and short cycle times. These factors point to micro-molding's feasibility as a mass production technique for microfluidic platforms.

Hot embossing/imprinting Hot embossing was one of the initial fabrication methods reported for fabrication of microfluidic structure on polymer substrates [51, 69]. A silicon stamp is designed and transferred to a photomask. A second silicon wafer with a <100> orientation is then coated in a masking material, followed by a layer of photoresist. The photoresist coated wafer is aligned with the mask and exposed to a UV radiation source, resulting in a transference of the image to the silicon. The patterned silicon is etched in a solution of hydrofluoric acid (HF) or KOH, resulting in a silicon wafer with 3-D etched structures. Room temperature or hot embossing of polymers are then possible with use of the silicon stamp. However, many research groups have turned to the use of metal electroforms for use as the stamp [70].

A metal electroform is produced from the silicon master, usually from Ni. This results in an electroform that is a mirror image of the silicon wafer. A second electroform is then produced from the initial electroform, resulting in a electroform stamp that is identical to the silicon master. These metal stamps are more robust when compared to silicon masters, thus allowing for extended usage.

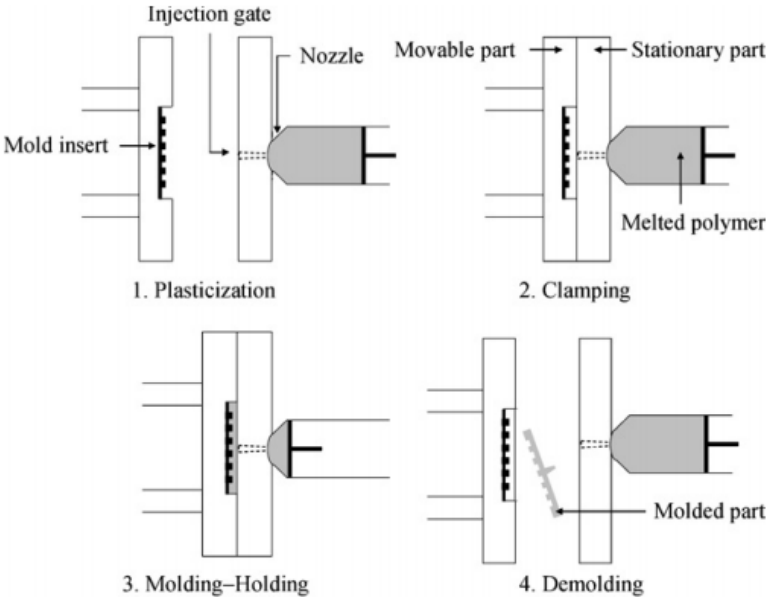

Figure 2.6: Injection molding process [3].

Room temperature imprinting consists of placing the polymer/plastic on top of the silicon/metal stamp. The aligned stack is then placed in a hydraulic press and pressure is typically applied for 10 minutes or less. This method does provide advantages, such as reduced production time, but is typically dependent on a number of parameters, such as applied pressure, imprinting times and polymer characteristics [71]. Hot embossing applies the same principle, but at elevated temperatures. Temperatures approach the glass transition temperature of the polymer, which causes a substrate softening, resulting in more accurate transference of microstructures. The increased temperature also lessens the required pressure and as such stamps can withstand increased imprinting cycles.

Laser ablation Laser ablation is the use of a pulsating radiation source to create polymer microstructures. It is theorized that the radiation source induces bond-breakage in the polymer [72], however, the mechanism of polymer degradation is still under investigation. The polymers also experiences an increase in temperature at the exposed area, which could result in substrate degradation. Two techniques exist for patterning microstructures with laser ablation, namely direct writing and the use of a mask to limit exposed areas.

Direct writing consists of placing the polymer on a programmable laser bed, the laser or laser bed then move to the predesignated points on the polymer that results in the defined structure being formed on the substrate. This is an

advantageous method for structure fabrication due to the fact that no mask is required, thus allowing for rapid design changes, improving the prototype process. The use of masks to predefine areas exposed to radiation is also employed in the fabrication of microstructures in polymers [73].

2.2.1.4 Bonding techniques

A complete, enclosed microfluidic device requires the bonding of a lid to the fabricated channels. Polymers provide a variety of methods for lid bonding, each with their own advantages/characteristics and as such the appropriate polymer/bonding technique must be selected based on device requirements. A number of methods exist for bonding/sealing of microfluidic devices, namely fusion bonding, anodic bonding, solvent bonding and adhesive bonding. This section will detail the different bonding techniques used in microfluidic applications.

Fusion bonding Fusion bonding is the most commonly used polymer bonding technique and under ideal conditions, the resulting bond strength can approach that of the bulk material. Substrates are heated to above or near their T_g under sufficient pressure. The combined pressure and temperature result in a flow of polymer at the interface, resulting in a strong bond due to the interdiffusion of polymers at the surface. Thermal bonding has been reported by a number of researchers, achieving successful bonding with a variety of polymers [74, 75, 58]. Channel deformation is a major drawback when considering this bonding technique. Temperatures and pressure need to be optimized to prevent significant channel deformation.

Anodic bonding Anodic bonding is used to permanently bond silicon to glass in the prescence of an electrostatic field, providing high stability at the glass/silicon interface [76]. Typically, a silicon wafer, placed on the anode, is bound to an alkali-rich conductive borosilicate glass plate placed on the cathode side [77]. The bond is formed through a compound voltage/temperature effect, which results in a hermetically sealed bond at relatively low temperatures ($<$500°C) [78].

Adhesive Bonding Adhesive bonding employs an adhesive to bond two similar/dissimilar materials permanently. Liquid adhesives that bond through solvent evaporation [51] have been investigated. More recently the use of UV-curable adhesives have been employed to bond microfluidic devices [79]. The major limitation of this technique is the flow of adhesive into channels, resulting in channel blockages.

HF welding The use of hydrofluoric acid has been reported to bond glass-glass, glass-silicon and silicon-silicon substrates at room temperature [80]. This

Table 2.2: Solubility parameters for selected polymers/solvent commonly used in solvent bonding [13].

Polymer	**Solubility Parameter (δ)**
PMMA	20.1
PC	19.4
PE	16.3
PVC	19.4
COC	17.7
Solvent	**Solubility Parameter (δ)**
Acetone	20.4
Isopropanol	23.4
Methanol	29.6
Water	47.7
Acetonitrile	25.1
Cyclohexane	16.7

low temperature bonding technique shows promise in reducing residual stresses caused by excessive heat. However, the use of HF is not always preferable.

Solvent-assisted bonding Solvent bonding is a commonly used method for bonding microfluidic chips due its attractive benefits, including strong bonds, minimization of surface damage and it's ability to be upscaled for production relatively simply [81]. This bonding technique employs the use of a solvent between the bonding interfaces. The solvation of the surface renders polymer chains at the interface mobile and facilitates diffusion between the materials. Entangled polymer chains are now present at the interface, resulting in strong bonds. Hildebrandt and Scott (1949) [82] adequately described a measure of the cohesive forces for both solvent and solute. The Hildebrandt parameter (δ) has units of $J/cm^{3\frac{1}{2}}$. When two materials exhibit similar solubility parameters, dissolution of the solute can occur [82]. Table 2.2.1.4 displays the solubility parameters of commonly used microfluidic materials and their relevant solvents. Researchers can select solvents that provide specific levels of polymer dissolution most applicable to their implementation. In general, solvent and polymers with dissimilar solubility parameters are selected to inhibit excessive solvent uptake into the polymer, a factor that leads to channel deformation [12]. Channel deformation can be further minimized by short solvent exposure periods.

Localized microwave fusion bonding Microwave radiation have been successfully used to bond PMMA sheets together. A metal thin-film is deposited on the desired bond area and exposed to microwave radiation. Localized heating around the metal film occurs, resulting in substrate bonding [83]. Lei et al.

[83] achieved localized bonding by depositing a 100nm metal chromium/gold film onto a PMMA substrate and placing the substrate in a microwave chamber operating at 2.4 GHz. Although this technique does provide accurate bonds with relatively high bond strengths, it has not been widely adopted, largely due to the extra fabrication techniques required to achieve bonding.

2.3 PCR microfluidics

2.3.1 Introduction

In recent years, a monumental amount of research is being done on microfluidics and its role in providing devices capable of replacing commonplace laboratory procedures, a large portion of which usually require expensive equipment or the aid of laboratory technicians [84].These LOC devices provide benefits over traditional methodology due to their reduced consumption of analytes and reagants, cost reduction, portability and their potential to be automated. This reduction in size translates to a higher surface to volume ration, a feature that can be of benefit to a multitude of fields. Biosensors, for example, require binding of target analytes to recognition elements and a higher surface area allows for more recognition elements to be bound resulting in increased sensitivity. The benefits that LOC devices can provide to the biological and analytical chemistry fields have led to the adoption of microfluidics as a platform for future laboratory procedures.

One application which shows particular promise in the microfluidics area is the Polymerase Chain Reaction (PCR), a precursory step to many diagnosis and analytical procedures. The PCR reaction amplifies sequences of genes through a thermo-circulatory process, whereby a liquid is exposed to 3 unique temperatures in the presence of some polymerase and nucleotides. Once the sample has cycled through the temperature zones the genetic sequence will be amplified. Microfluidics has been applied to PCR in a variety of forms, which can now be classified into distinct categories of PCR devices, i.e. stationary wells compared to continuous flow. The reduction in sample volume is especially beneficial to PCR due to it being a temperature dependent process. This reduction in liquid volumes directly translates to a reduction in thermal mass, which in turn results in better temperature ramping rates. Conventional PCR machines are large pieces of instrumentation and it is highly unlikely one would find such a device in rural areas. On the other hand, PCR on-chip devices can be fully portable, which would allow for more complex analytical procedures to be performed in an in-field environment. This review details an investigation into μTAS devices, with specific focus on a microfluidics approach to PCR.

2.3.2 The Polymerase Chain Reaction

Kary Mullis first developed the PCR in 1984, as a means of amplifying DNA [85]. The PCR is an important precursory step for a number of fields, including clinical diagnosis, medical, biological and forensic analysis [86]. It's LOC realization was not proposed until the 1990's, once the benefits of μTAS devices were realized. This section will introduce the concepts of DNA, enzymes and the PCR process, with specific attention to microfluidic realizations of PCR devices.

2.3.2.1 DNA

Deoxyribonucleic acid (DNA) consists of two long polynucleotide chains composed of four types of nucleotide subunits. These bases are adenine (A), guanine (G), cytosine (C), and thymine (T). DNA bases tend to form pairs, A with T and C with G. These bases are held together through hydrogen bonds [87]. Base pairs connected to a sugar and a phosphate molecule are called nucleotides. Nucleotides are arranged in a spiral structure referred to as a double helix. The structure can be seen in Figure 2.7 . An important property of DNA is it's ability to replicate itself, each strand within a double helix can serve as a pattern for replicating it's sequence. DNA encodes information through the sequencing of nucleotides in each strand. This information holds the instructions for all proteins an organism will ever synthesize [88]. This mechanism is responsible for passing down hereditary information between organisms and their offspring.

2.3.2.2 Enzymes

An enzyme is a biological catalyst that initiates specific biochemical reactions. These enzymes control the rates of a number of biochemical reactions within living cells, such as the biosynthesis of macromolecules, the controlled release of energy and digestion of food [88].

The mechanism by which enzymes catalyze chemical reactions is as a result of a substrate binding to the active site on an enzyme. This binding of the substrate and enzyme produces a change in the substrates electron distribution that ultimately leads to the formation of products [89]. The active site on the enzyme posses unique geometry, which only allows the binding of specific substrates. Two models exist for describing the way in which the active site and substrate interact with each other, namely the Lock and Key model and the Induced Fit model, see Figure 2.8. The theory proposes that the substrate plays an active role in the active site geometry and that the active site is partially flexible [89].

The discovery of the Taq polymerase, an enzyme from *Thermus aquaticus*,

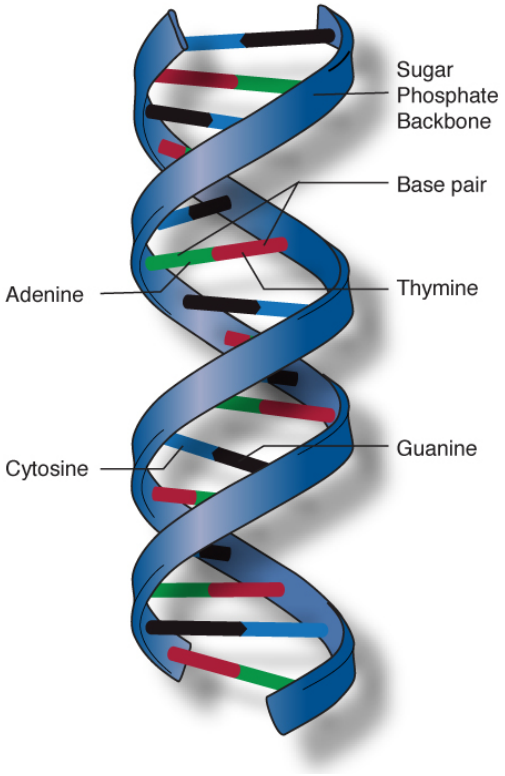

Figure 2.7: Structure of DNA [4].

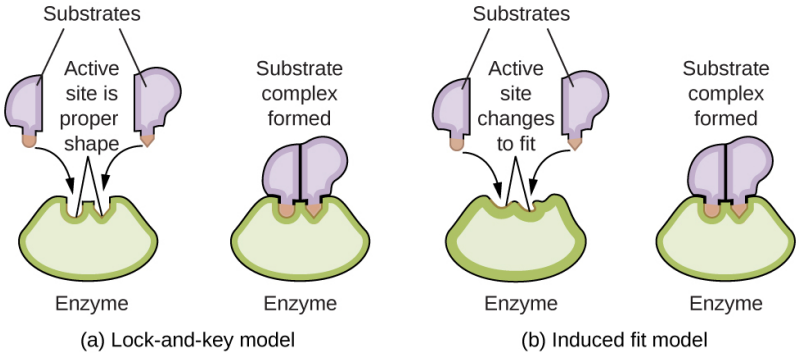

Figure 2.8: Enzyme models [5]

discovered in the Yellowstone National Park, is responsible for the development and functioning of the PCR technique [90].

2.3.2.3 The PCR process

The PCR process is an enzyme controlled technique that amplifies DNA, capable of creating millions of copies of specific segments of DNA from very small starting concentrations [88]. The process involves forming a solution containing Taq DNA polymerase, dNTPs, $MgCl_2$, reaction buffers, primers and template. The DNA polymerase is the enzyme responsible for the linking of the nucleotides that together form the DNA product. The primers are specified DNA fragments, complementary to the target DNA sequence, which specify the DNA product to be amplified [88].

Thermal cycling is necessary to perform the PCR and usually consists of 20-40 cycles of 3 temperature points. Denaturation, the first of the heating steps, raises the reaction above the melting point of the two complementary DNA strands, allowing for their separation into 2 single strands. Reaction temperatures are then lowered to allow specific primers to bond to DNA segments, a process known as hybridization or annealing. The last step, known as the extension step, involves increasing reaction temperatures to allow the DNA polymerase to extend the primers by addition of nucleotides. The process is depicted in Figure 2.9. Each cycle of the PCR results in a doubling of DNA fragments and thus, after thirty cycles, millions of copies can be present in the PCR product.

2.3.3 PCR microfluidic designs

The benefits that microfluidic devices bring to the PCR process are considerable. The lower thermal masses, more efficient heat transfer and reduced cost of reagents has stimulated much research on microfluidic PCR implementations. Initially a large number of designs were fabricated on silicon/glass substrates. However, silicon is not an ideal PCR substrate due to the bare silicon substrate acting as a PCR inhibitor [91]. Polymers/thermoplastics are very promising substrates for PCR microfluidics due to their cost, ease of fabrication and biocompatability. Conventional tabletop PCR devices are expensive, lack portability and reaction times are in the range of 90-150 minutes. Conversely, microfluidic PCR devices are portable and have demonstrated amplification times as fast as 1.7 min(5.2s/cycle) [17]. Researchers have reported PCR devices fabricated on a number of polymer/thermoplastic substrates [92, 93]. Varying designs have been developed for rapid DNA amplification and can be categorized under either stationary chamber PCR, continuous flow or droplet based PCR.

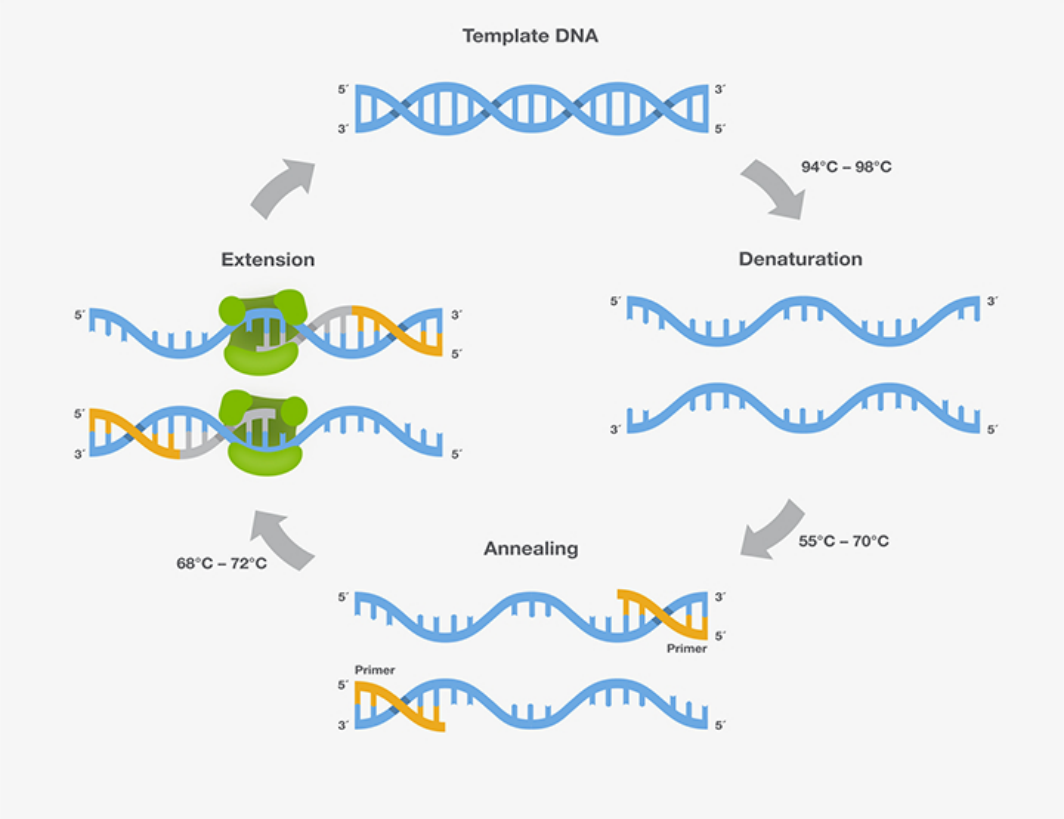

Figure 2.9: The PCR process cycles [6].

2.3.3.1 Stationary chamber PCR

Conventional PCR devices operate with a stationary chamber, whereby the chamber containing the PCR solution is cycled between the 3 temperature zones. The PCR product is then recovered from the chamber and detection is performed. Two groups of stationary chamber PCR implementations exist, namely single chamber and multi chamber.

Single chamber PCR In this design, PCR reaction constituents are placed in a single chamber and exposed to heating cycles of 3 temperatures. The first of these designs was created by Northrup et al. in 1993 [94]. Single chamber microfluidic PCR devices have been fabricated on glass/silicon hybrid chips reporting process times of around 50 minutes for 25 cycles [95] A microwave-assisted high-speed PCR device was reported by Fermer et al. [96] and was composed of a commercially available MicroWell 10 from Personal Chemistry (Uppsala, Sweden). The 100 μL sample was placed in a microwave chamber and heated for a total reaction time of 60 minutes, with amplification efficiencies comparable to those of conventional PCR devices.

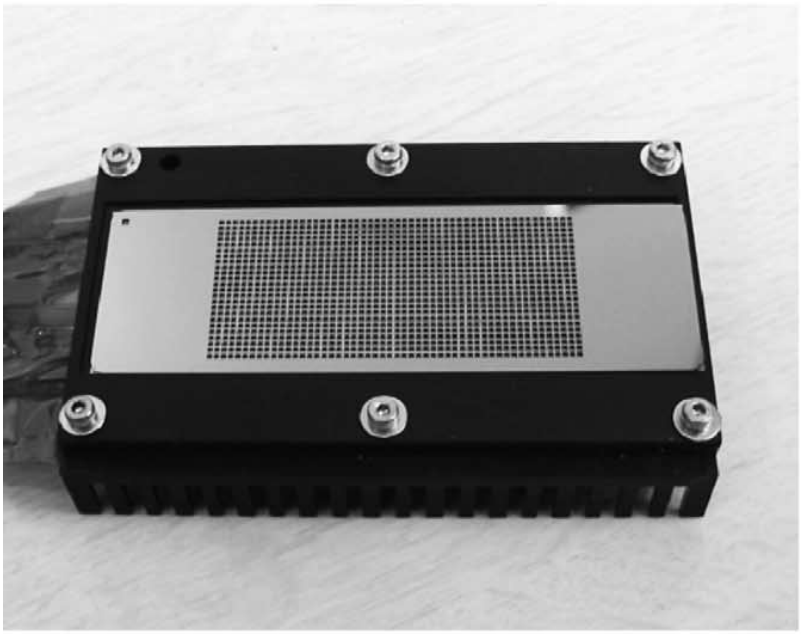

Figure 2.10: The multi-chamber PCR chip produced by Matsubra et al, 2006 [7].

Lui et al. [18] reported the fabrication of a fully integrated self-contained biochip capable of sample preparation (including magnetic bead-based cell capture, cell concentration, purification, and cell lysis), DNA amplification, DNA hybridization, and electrochemical detection. The process had a completion time of 3.5h of which sample preparation was 50 min, PCR amplification 90 min, pumping and valving 10 min, and hybridization 60 min. Integrated devices have been reported by a number of research groups [101, 102, 103], driven by the need for a fully-integrated self contained LOC realization.

Multi chamber PCR Sample throughput is addressed by a multi-chamber implementation of a PCR device, an example of which can be seen in Figure 2.10. Samples are loaded into an array of chambers and heating cycles are applied uniformly across all chambers. Significant investigation has been undertaken on these devices, however they suffer potential challenges. The miniaturization of chambers lead to an increased SVR, which promotes the adsorption of PCR reagents on chamber walls[41].

Matsubara et al. [7] reported the fabrication of a 60 chamber stationary PCR device. The chip was exposed to a 95°C hold for 10 min followed by 40 cycles of 95 °C for 10 s and 60 °C for 15 s. The device was capable of detecting DNA sequences related to E. coli and RhD genes within 1 hour, including amplification and detection. Parallel chambers have been reported [107, 108] to detect microorganisms in samples on the nL scale.

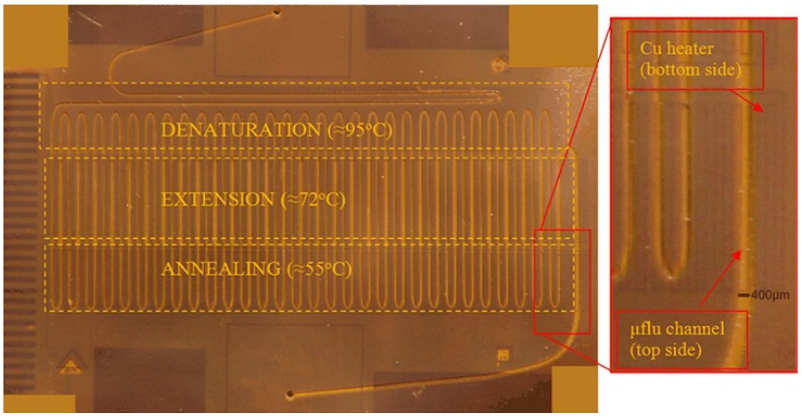

Figure 2.11: Example of a serpentine channel PCR chip by Moschou et al.[8]

2.3.3.2 Continuous Flow

An alternative to the conventional stationary PCR chambers is the continuous flow implementation, operating on a "time-space" principle, whereby the solution is continuously cycled through 3 stationary temperature zones. This method offer flexibility with regard to reaction time. Sample exposure to temperature zones can be regulated by altering flow rates. In general, processesing times are quicker than stationary chamber PCR due to the reduced thermal intertia/mass. The sample mass is the only mass required to change temperature [109].

Central to continuous flow PCR research is the serpentine channel design shown in Figure 2.11, reported by a number of researchers [110, 111, 112, 113, 114, 115]. Integration of post/pre sample treatment is an important characteristic of a truly self-contained LOC. Wang et al [59] reported a miniaturized PCR system that allowed for DNA amplification, which was integrated with an optical detection unit capable of quantitative detection, using fluorescent monitoring. More recently, integrated electrochemical sensors show promise for genetic detection, as there is no need for optical measurement devices, as well as being readily integrateable into microfluidic technologies. Hsieh et al. have reported an integrated PCR device, which for DNA detection, employ label-free, single-step, and sequence-specific electrochemical DNA (E-DNA) sensors [116]. A modified redox-reporter DNA probe is bound to the electrode, which generates current changes after hybridization. The samples are exposed to 2 genetic amplification techniques LAMP and PCR before being brought to the electrode for detection [116].

2.3.3.3 Droplet PCR

The use of droplets in PCR is new in terms of microfluidic research. Water-in-oil droplets are used in microchannels to function as independent reactors,

with sample volumes in the nL and pL range. These droplets are capable of individual reactions within themselves [117]. This technique offers significant advantages over conventional continuous flow PCR due to requiring less reagents and reduced SVR, thus leading to less unwanted adsorption onto channel walls, and droplets are unlikely to cross-contaminate one another, since samples are immersed in an oil carrier phase. An example of a droplet based PCR device can be seen in Figure 2.12.

Wang et al. reported the fabrication of a PCR device that utilizes biphasic droplets with volumes of 5-250 nL capable of DNA amplification comparable to benchtop techniques [59]. The device was able to achieve temperature ramp rates of 9.5°C and 3.5°C for heating and cooling. The author did not publish total reaction times for his device and amplification was performed on a very short fragment of only 56 base-pair.

Zhu et al [118] described the use of an agarose droplet based PCR device for highly sensitive, specific and quantitative detection of pathogens. It employs agarose droplets dispersed in an oil carrier phase. The droplets are produced at 300Hz, allowing for the formation of 10^6 droplets to form within an hour. Large numbers of multiplexed samples are possible with this technique, allowing for high-throughput multi-parameter comparisons to be made of large populations of cells at the single cell level [118]. Although dPCR shows considerable promise for future PCR devices, it is still an emerging area of research.

2.3.4 Temperature regulation

PCR amplification success depends on a number of factors and without the correct heating cycles, amplification of DNA fragments could not occur. It is thus vital that temperature be controlled accurately to alleviate fluctuations that would otherwise inhibit or prevent the PCR. Temperature regulation has been achieved through a number of heating techniques, namely thin-film heaters [119, 120], Peltier elements [121, 122], IR radiation [123], microwave radiation [96], and others. These devices can be categorized according to whether they are in contact with the PCR chip or are a non-contact heating configuration.

2.3.4.1 Contact heating

Two main forms of contact heaters are reported by most research groups, namely thin-film heaters and Peltier/heating blocks. Off-chip heating techniques provide easier control and reduced implementation complexity [124].

Thin film heaters Thin film heaters are deposited films of metals that possess advantageous resistance/temperature relationships, and when exposed

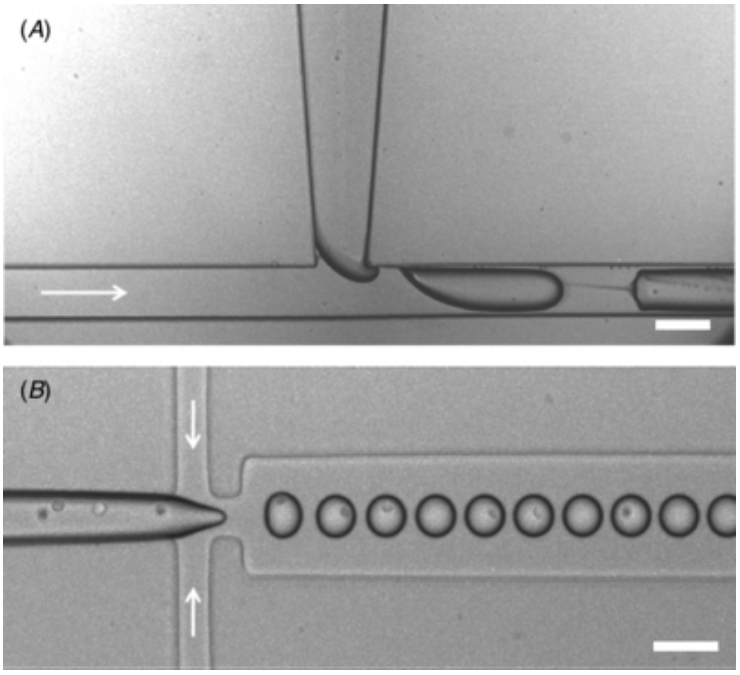

Figure 2.12: Two droplet based systems, namely (A) T-junction and (B) flow focusing [9].

to a voltage, produce heat. Platinum and polysilicon thin film heaters are most common [125]. However, other implementations do exist [33, 106]. A drawback to this technique is the increased fabrication complexity of the device. In general, we are not concerned with re-usability of PCR chips, due to cross-contamination of samples, and thus the cost efficiency of fabricating thin film heaters on single-use chips outweighs their potential benefits.

Peltier Elements Thermoelectric cooling operates based on the Peltier effect, namely when a current is passed between two electrically dissimilar materials, most commonly p- and n- type semiconductor materials, heat is absorbed or released at the junction [126]. The absorbtion/release of heat is dependent on the direction of current flow, and in Peltier elements this current flow produces a "hot" and "cold" on the device.

The use of PE in microfluidic applications has been extensive, largely due to their ease of operation, cost efficiency and their ability to function as a heater and cooler [127, 128, 16, 129]. Kim et al. reported the fabrication of a PDMS based CF-PCR device, where thermal regulation was achieved using 3 TE elements in conjunction with an external PID controller [127]. Detectable amounts of PCR product were observed after reactions of only 8-30 minutes.

The use of 2 platinum heating blocks, one for denaturation and the other

for annealing, extension, was reported by Tachibana et al. [130]. The device consisted of channels with a 150μm height and width, driven by capillary forces and no external flow control was required. The device was capable of successful amplification of DNA fragments within 14 minutes.

2.3.4.2 Non-contact heating

IR heating The use of infrared radiation (IR) sources to perform heating in microfluidic systems have been proposed by research groups. The small thermal mass associated with microfluidic samples can be leveraged and rapid heating/cooling rates have been demonstrated using IR sources. The use of a tungsten lamp as an IR radiation source for use in heating within a PCR system was demonstrated [131]. A hot mirror was used to reduce background thermal radiation and fluorescence detection was used to confirm the successful amplification of a 304 base-pair amplicon.

Microwave heating The use of external and integrated microwave heating systems have been reported for use in PCR devices. Microwave heating provides benefits, such as directive heating and localized heating can be achieved through the addition of metallic surfaces within the microfluidic device. Shaw et al. has demonstrated use of this principle to apply selective heating for bonding of lids, Figure 2.13 depicts the device. Heating and cooling rates of 65 °C/s have been demonstrated using an integrated microwave source and air impingement cooling [10]. The device was capable of performing rapid PCR orders of magnitude faster than conventional devices.

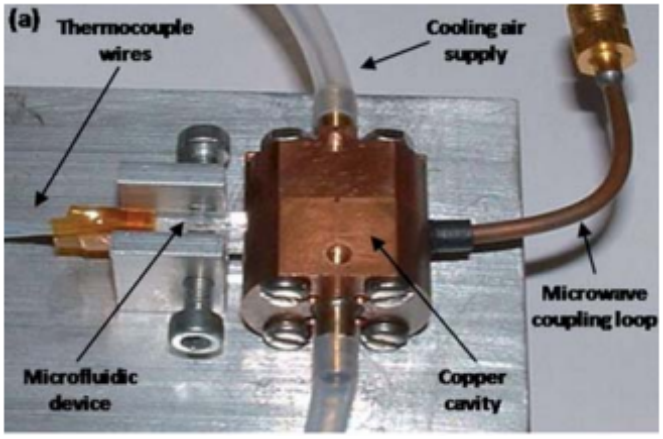

Figure 2.13: A custom built re-entrant microwave cavity operating at 8 GHz [10].

2.3.5 Flow control

The sheer variety of microfluidic pumps prevents the provision of an all encompassing description of available techniques and devices. Micropumps have long been a topic of research due to their wide spectrum of applications. The miniaturization of these systems has led to specific design parameters for micropumps. Relatively large back pressures are commonplace and in the order of 25 kPa, and as such pump designs should cater for this. Fluid parameters such as pH, viscosity, viscoelasticity, temperature, as well as bubble generation are important considerations.

Generally we can assume that pumps fall into two categories, namely displacement pumps and dynamic pumps [132]. The use of micropumps in μTAS systems is not commonplace and most likely due to lack of availability, cost and performance [132], with most researchers turning to external pumping methods. As such this section will briefly overview the most common implementations of pumps in use. Figure 2.14 depicts results from a study conducted by Elveflow [11]. The results depict the devices researchers claimed to use in their microfluidics research.

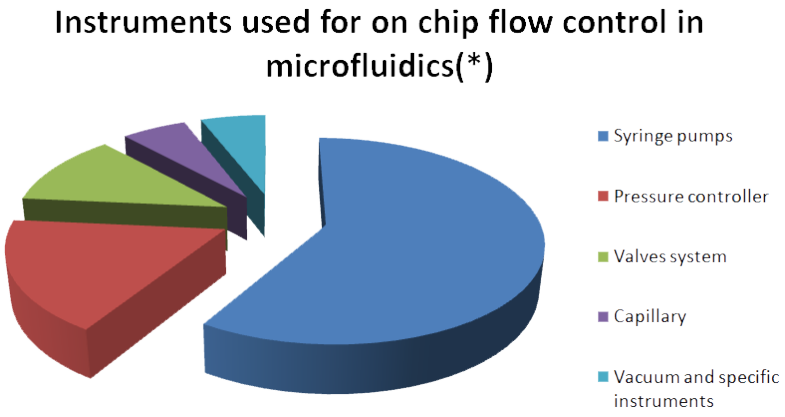

Figure 2.14: Fluid control systems employed in microfluidics research [11].

2.3.5.1 Common microfluidic flow control systems

Syringe pumps are the most commonly used flow control system used in microfluidic systems [11]. Syringe pumps can be divided into 2 categories, namely classic syringe pumps which are prone to generating flow oscillations, and pulseless microfluidic syringe pumps, which are more expensive, but generate more stable, pulse-free flows. Syringe pumps are widely adopted in microfluidics research due to their ease of use, quick configurability, allowing for rapid

switching of flow rates and their relative inexpensiveness. An example of a syringe pump can be seen in Figure 2.15.

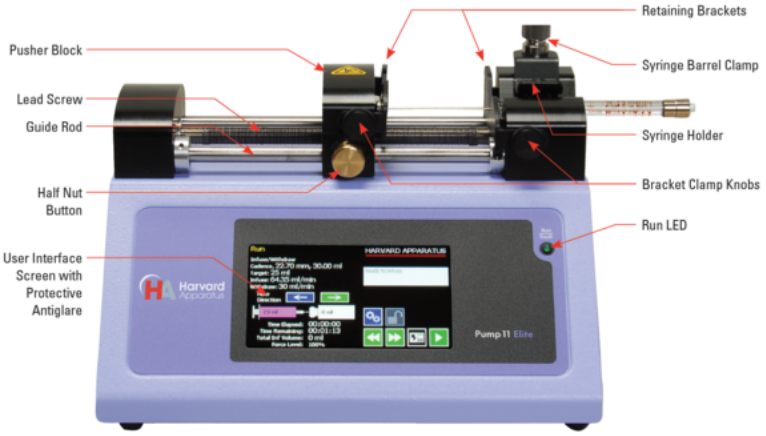

Figure 2.15: Microfluidic Dual Programmable Syringe Pump 11 Pico Plus Elite (Darwin Microfluidics).

Peristaltic pumps are another commonly used external flow control device in microfluidics. This class of pump drives fluid through positive displacement. This is achieved through compression and relaxation of the tube containing the liquid. Recently, micro-peristaltic pumps have shown great potential for integration into microfluidic circuits. These pumps offer simple control, while remaining relatively inexpensive [133].

Ideally, the flow control mechanism should be integrated into the device, improving portability, while reducing complexity of the system. A number of alternatives to external flow control have been demonstrated, although these devices are still not commonly used due to the increased complexity required for fabrication. Zhang et al. demonstrated the use of a micro-peristaltic pump integrated into a microfluidic system [134]. the device could generate pulse-free, stable flows with uniform velocity at rates ranging from 1 to 500 nL/s. Researchers have demonstrated the use of elastomeric valves integrated within the microfluidic system as a means for flow control. These valves can be controlled via electrical signals and can act as actuators by fluctuating a membrane constructed on a single substrate (e.g. PDMS) [135]. These devices offer a high-level of integration, but the complexity involved in their fabrication has stunted their widespread use.

2.4 Conclusion

The literature review provided a brief overview of the general microfluidics principles that researchers leverage to fabricate a variety of microfluidic devices. A detailed investigation on current fabrication technologies, substrates and devices was conducted and presented. Silicon/glass microfluidic devices have been largely abandoned, except in special cases, for the newer thermoplastic/polymer class of substrates, due to their favorable properties. Bonding techniques were described and flow mechanisms currently employed in literature were discussed. The PCR was detailed and microfluidic implementations were presented as a comparable basis for the

en design.

Chapter 3

Design and fabrication

3.1 Design overview

The importance of disposability and it's relation to cost is a key design consideration for PCR microfluidic chips. Cross-contamination of samples can be avoided by using cheap, readily disposable chips. Commercial grade PMMA was acquired for the substrate in an effort to conform to the disposability and cost criteria for POC PCR devices. A serpentine channel continuous-flow device was designed to transport the droplet through 3 static temperature regions on the device. Channels were etched using CO_2 laser ablation, a technique which allowed for the rapid fabrication of multiple prototype chips within minutes. The temperature regions were realized by Peltier heaters, coupled to OTS digital thermostats. Integration of heat measurements was avoided to provide disposability of chips, temperature probes were mounted on aluminum sheets and temperature was measured externally. Temperature gradients across PMMA chips were realized with 2 heater configurations. The avoidance of costly microfluidic connector components was avoided by designing inlet/outlet holes to allow for the tubing to fit within and applying an epoxy mixture to act as a sealant. A syringe pump was used to achieve flow control of 20 µL samples and a bench-top PSU was used as a supply for the electronics and heaters.

Although this device is not strictly "POC", through replacement of the PSU and flow control methods, a fully portable POC version could be realized. Conforming to low cost was a large factor in the realization of a fully POC device with acquisition of micro-pumps, micro-Peltiers being difficult and costly. As this was the prototype device, benchtop equivalents were used.

3.2 Heaters

A set of Peltier elements (GM250-127-14-16) were obtained from Adaptive Thermal Management (European Thermodynamics Limited). These devices

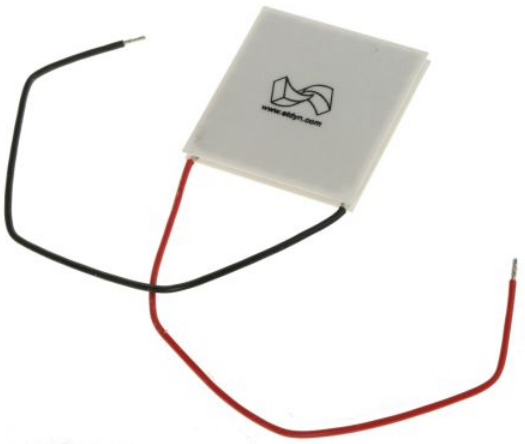

Figure 3.1: Peltier heaters obtained from RS-ZA (40x40 mm)

are light weight, portable, cost efficient and easy to operate. Devices were selected based on appropriate operation temperatures to ensure that the respective PCR zones could be heated to the required thresholds while considering thermal losses. Device characteristics can be found in Appendix B.

3.2.1 Physical configuration

A wooden base for the device was chosen and cut to specification. An aluminium sheet was fastened to the base to act as a heatsink for the "cold side" of the Peltier elements, as seen in Figure 3.2 . If insufficient heat is removed from these TEC devices they will overheat and stop functioning. To ensure proper thermal conduction, commercial grade silver paste was used to enhance heat transfer between base-sheet/Peltier interface. The Peltier elements were placed equally on the center of the sheet. This configuration allowed for the generation of the 3 temperature zones, as shown in Figure 3.3 . The heaters were placed with their cold side to the heatsink and silver paste was applied to ensure conductivity.

Peltier elements have known tendencies to create radial heat patterns. In an effort to improve uniformity of heat distribution, aluminum plates were cut to size and used as a heat dispersant layer. This layer served a secondary purpose of increasing the size of the temperature zones. The effective heating area required for temperature zones was 60 mm. A temperature zone of this

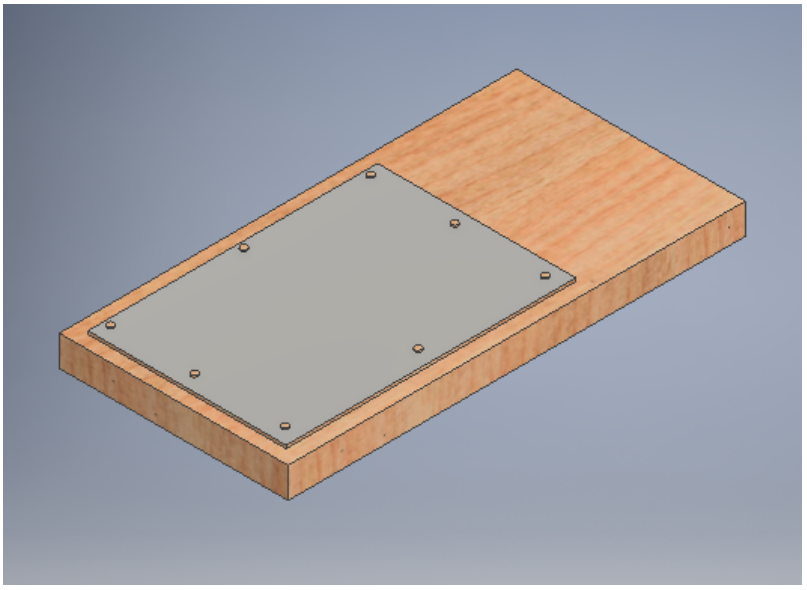

Figure 3.2: CAD representation of base with aluminum sheet.

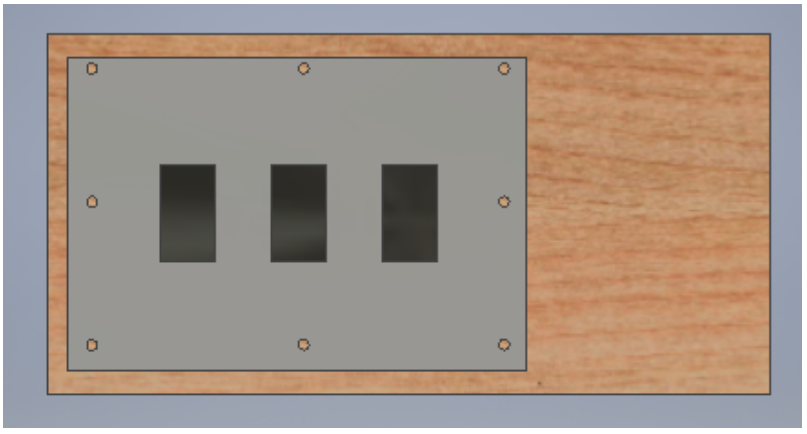

Figure 3.3: CAD representation of aluminum sheets with Peltier elements (black) placed on top.

width provided a heated surface sufficiently large enough to heat the 30 channel PCR chip. Aluminum sheets were cut and fastened to the "hot" side of the elements to provide a larger heating surface (Figure 3.4). Thermal paste was applied at the intersection of the heating side and the aluminum sheets (80x60 mm).

Device longevity was taken into account during the design and as such the heaters and aluminum sheets are replaceable and not permanently fixed. Steel bolts (60mm) were placed in points around the heating surfaces to maintain the position of the heaters by temporarily fastening them in place (Figure

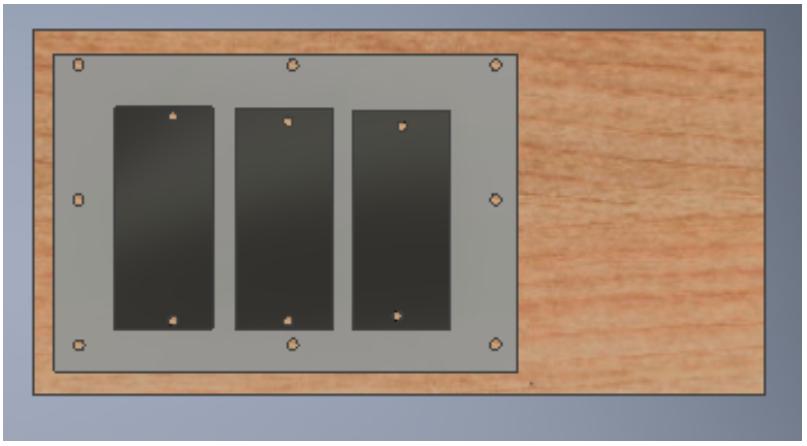

Figure 3.4: CAD representation of aluminum sheets increasing heating area in comparison with Figure 3.3

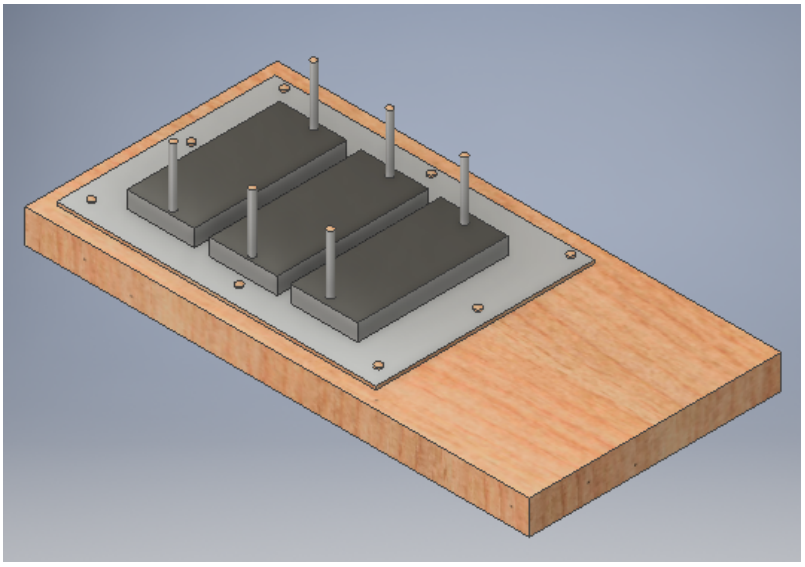

Figure 3.5: CAD representation of aluminum sheets and bolts extruding from base.

3.5). This ensured repeatability when testing, but still allowed for component replacement.

The microfluidics chip is placed in the center of the 3 heating zones, as shown in Figure 3.6. Steel plates were manufactured to act as fasteners, one plate for each zone. The thermistors were placed in the centre of each plate and fastened in place with a high-temperature sealant. A specialized sealant is required as the areas are exposed to temperatures around 100°C and as such needs to be heat resistant. The portability of the thermistors and fasteners allow for easy sample processing and simplified repair due to molecularity. Figure 3.7 shows the entire heating configuration.

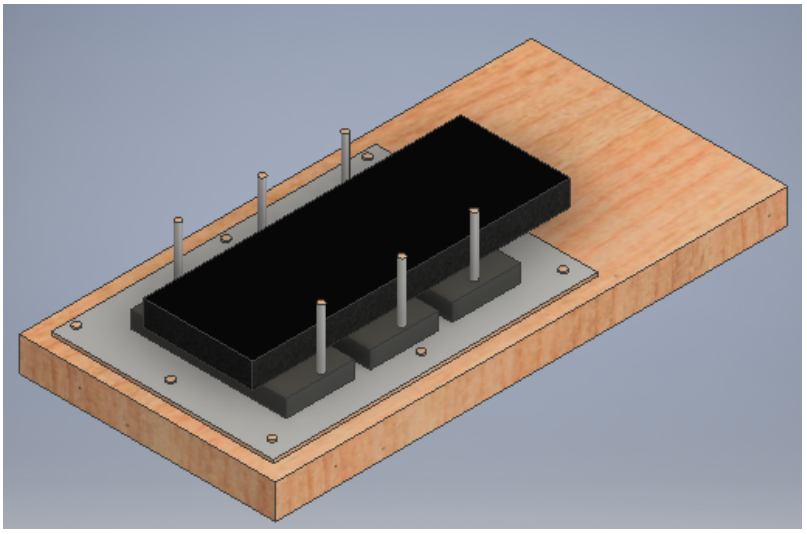

Figure 3.6: CAD representation of device configuration with microfluidics chip (black) in place.

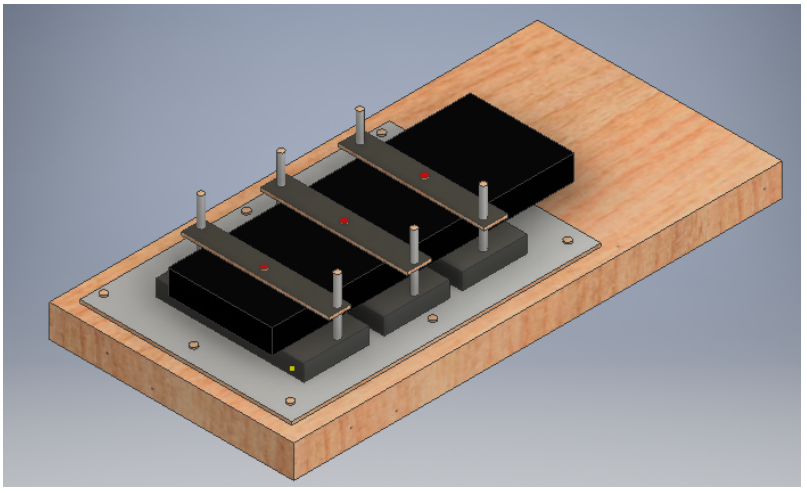

Figure 3.7: CAD representation of the entire device configuration.

3.3 Temperature Regulation

There are a number of ways to achieve temperature regulation when using heating elements. These fall into two main categories, namely custom built controllers that try to optimize efficiency and cater directly to the designs requirements or store bought controllers, an inexpensive alternative that with modification, can be altered to the designs needs. Due to the ease at which Peltier devices can be controlled, simple and inexpensive digital thermo-controller modules (W1209) were investigated and purchased from DIYElectronic, Figure 3.8. Thermo-controller modules were connected to the Peltier devices

and powered by a bench top power supply. To improve accuracy of thermal measurements, the default thermo-probes on the controllers were replaced by G1540 glass-encapsulated thermistors from EPCOS. The data sheet can be found in Appendix B. Calibration tests were performed to ascertain accuracy of the thermistors. Power usage measurements were performed to ensure that the Peltier devices were operating at ideal supply values.

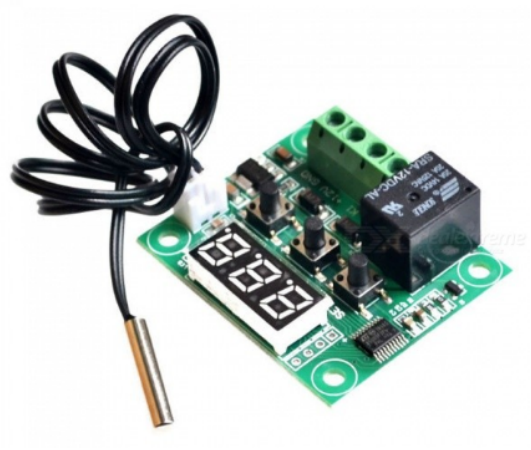

Figure 3.8: Image of W1209 digital thermostat used for temperature control of Peltier elements.

3.3.1 Circuit Schematic

Figure 3.9 shows the complete thermal regulatory circuitry, each module controls a single PE, all modules are powered by a common 12V rail, the 92°C PE has it's own 12V dedicated supply, while the 72°C and 55°C PE's share a common supply.

3.3.2 Power supply calibration

Conventionally, PID controllers are used to realize accurate temperature control, but they require custom built controllers or the use of a micro-controller coupled to some external circuitry. The W1209 thermo-controllers operate through the switching of a relay by an onboard micro-controller. The relay toggles between on/off to stabilize around a set temperature. This mechanism can lead to under/overshoot of temperatures realized by the PE's. This effect can be minimized by optimizing the power supplied to each heater/thermo-controller pairing, so as to prevent significant over/undershoot. Power calibration tests were performed for each heater/thermo-controller pair according to the following protocol:

- A sweep of input voltages was performed for each pair.

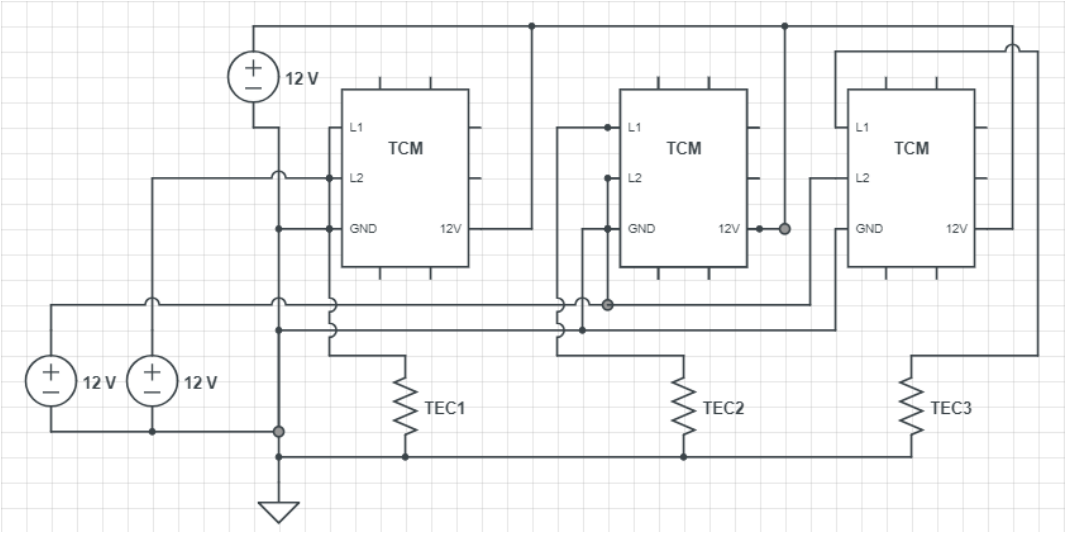

Figure 3.9: Circuit schematic for thermo-controller/Peltier coupling. Power supply values are representative of the maximum source values required.

- Temperature measurements were performed to record under/overshoot for each supply voltage.
- Supply voltage was determined for respective modules based on minimum under/overshoot values.

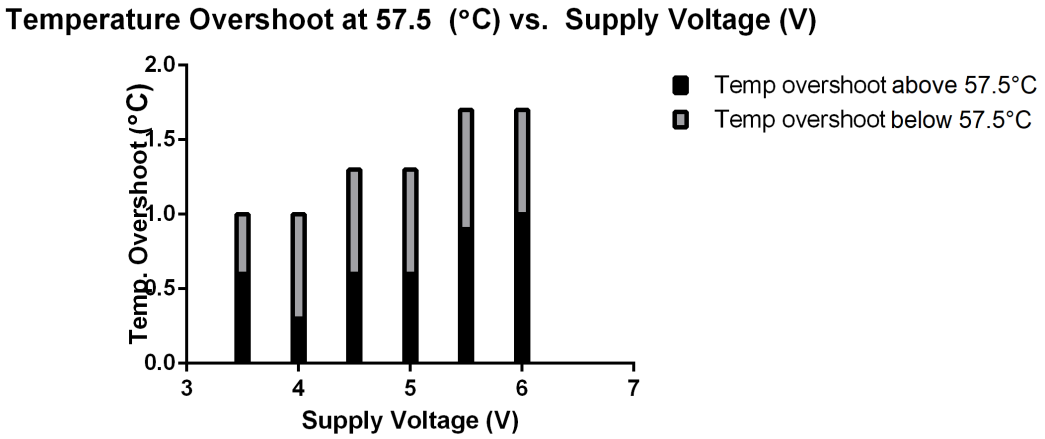

Figure 3.10: Peltier device heat pattern, with temperature set at 57.5°C.

Figures 3.10, 3.11, 3.12 show the respective total overshoot values for each temperature point. It was found that optimal temperatures for the PE were as follows:

- 57.5°C PE optimal supply was approximately 3.5-4 V.

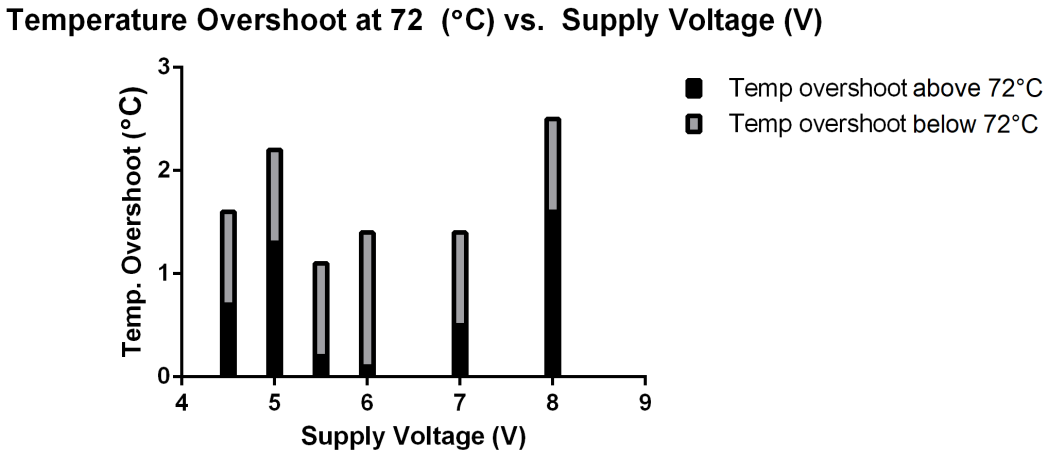

Figure 3.11: Peltier device heat pattern, with temperature set at 72°C.

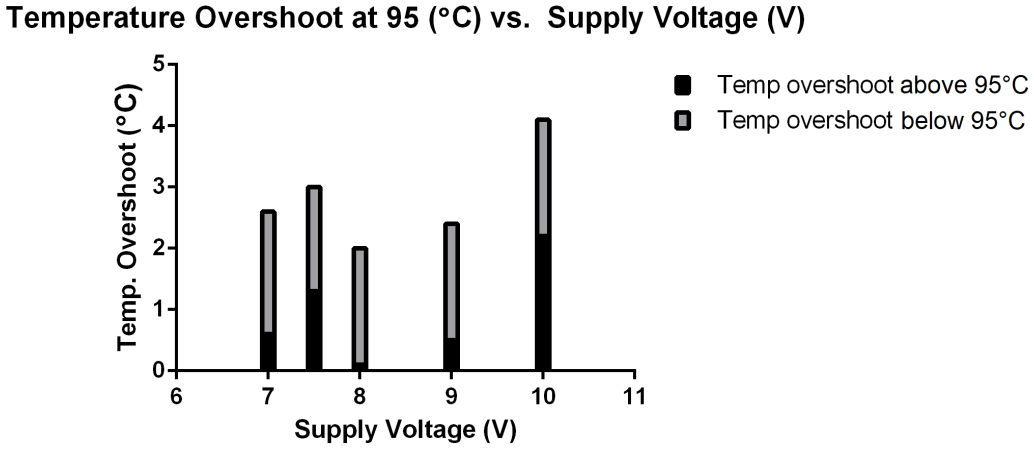

Figure 3.12: Peltier device heat pattern, with temperature set at 95°C.

- 72°C PE optimal supply was approximately 5.5 V.
- 95°C PE optimal supply was approximately 8 V.

Heating measurements were taken directly on Peltier surfaces with an IR temperature gun.

3.4 Channel Fabrication

3.4.1 PMMA substrate

Poly(methyl methacrylate) was obtained from Maizey Plastics in 1m^2 sheets. Sheets were cut into 30cm^2 workable pieces that could fit into the laser bed.

PMMA allows for the use of laser ablation as a fabrication technique, which is suitable for rapid prototyping of multiple channel designs. Due to it's low thermal conductivity (0.167-0.25 W/m.K.) it is an ideal substrate for creating temperature gradients. PMMA also displays reduced non-specific adsorption of DNA molecules, making it a good choice for the biocompatability requirements of PCR devices [41]. The PMMA itself is relatively inexpensive compared to conventional microfluidic substrates and thus fulfilled the criteria of cost and disposability.

3.4.2 Laser ablation

Channels were realized on PMMA substrate through use of a CO_2 laser (TS4040, Jinan Transcon CNC Equipment Co. LTD). The use of laser ablation allowed for rapid prototyping of multiple device geometries until a final design was settled upon. The laser ablation process produces channels of varying dimensions as a result of laser parameters. In order to obtain the ideal channel geometry, testing was performed to ascertain the relationship between laser parameters and channel dimensions.

3.4.3 Channel morphology testing

The relationship between channel morphology and CO_2 laser parameters was investigated. The CO_2 laser software allows for the adjustment of 3 parameters:

- Speed (mm/s)
- Power Minimum (%)
- Power Maximum (%)

The channel's top and side profiles were imaged using a Motic 1.3Mp microscope camera and measured in Motic's imaging software (Motic ImagePlus 2.0). Ideally we would like the parameters that reflect the smallest channel size and smoothest profiles.

3.4.3.1 Speed tests

The effect of the laser speed parameter was investigated by varying speed and keeping the power variables constant. Speed values less than 50mm/s resulted in cuts too large for the imaging area and thus speeds were investigated upwards to a speed of 100 mm/s. Table 3.1 depicts the values of parameters for the testing.

The initial testing indicated that an increase in speed resulted in a decrease of channel width, as shown in Figure 3.13. This was as expected as longer

Figure 3.13: Images displaying channel morphology (depth, width) for varying laser speeds.

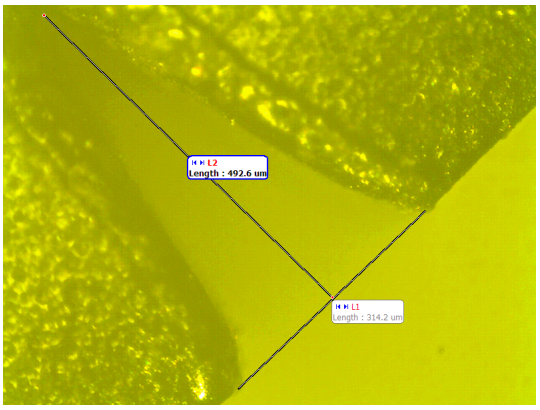

Speed: 50 mm/s

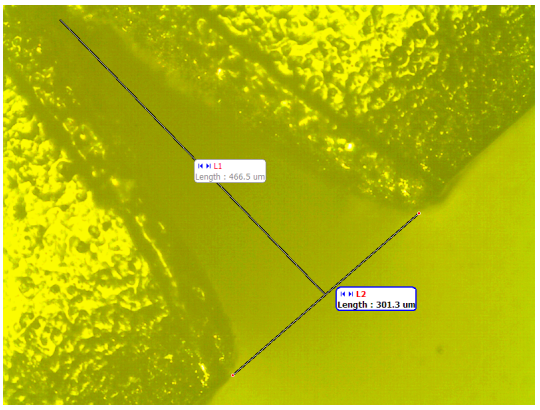

Speed: 60 mm/s

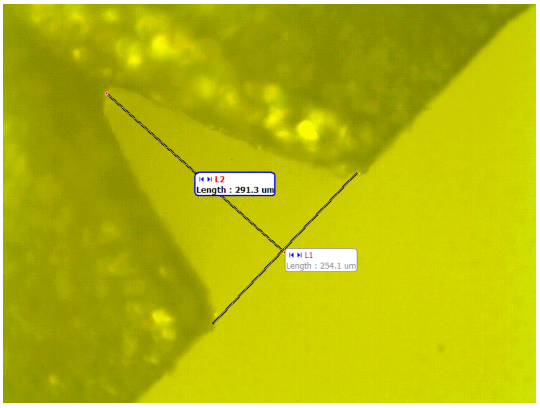

Speed: 70 mm/s

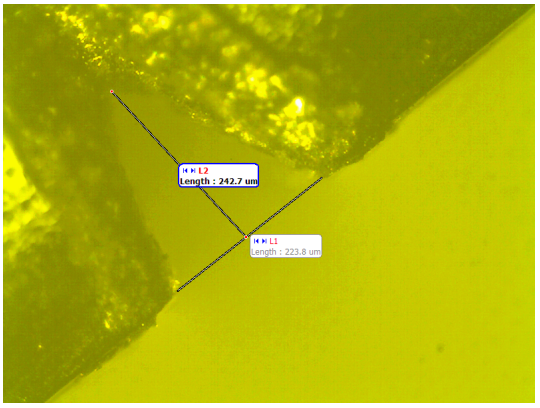

Speed: 80 mm/s

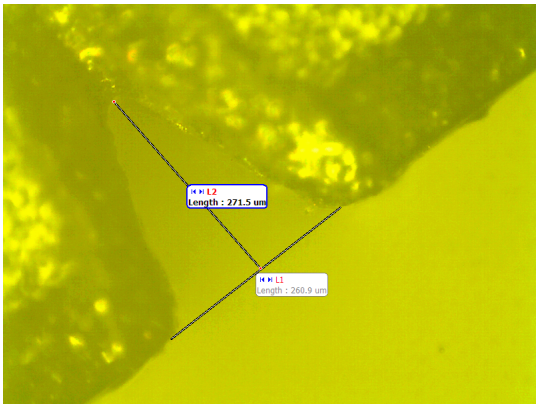

Speed: 90 mm/s

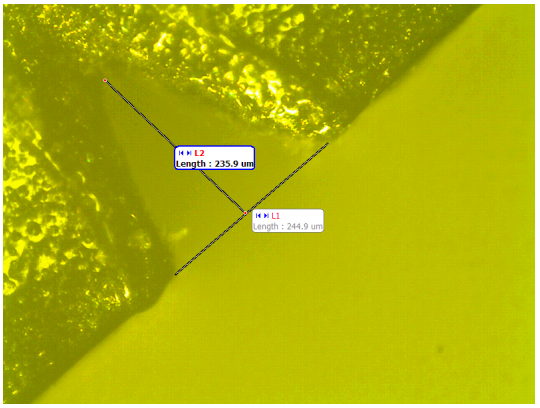

Speed: 100 mm/s

Table 3.1: Laser parameters used to investigate the relationship between speed and channel geometry.

Speed (mm/s)	Power Min. (%)	Power Max. (%)
50	15	40
60	15	40
70	15	40
80	15	40
90	15	40
100	15	40

residence times of the focal point result in increased energy absorbtion at the surface, resulting in larger deformation and increased cut depth.

3.4.3.2 Power tests

The combined effect of maximum and minimum power parameters was investigated by varying power settings while keeping speed constant. A series of 10 tests were performed according the parameter values in Table 3.4.3.2.

Table 3.2: Laser parameters used to investigate the relationship between channel morphology and power parameters.

Speed (mm/s)	Power Min. (%)	Power Max. (%)
100	10	30
100	12.5	30
100	15	30
100	10	40
100	12.5	40
100	15	40
100	20	40
100	25	50

Power tests confirmed the initial hypothesis that increased power settings result in an increase of channel width and depth. It was noted that lower power settings resulted in a more smooth channel surface and small channel dimensions, as shown in Figure 3.14. After considering all parameters settings, the laser settings for the final channel fabrication process chosen as:

- Speed: 100 mm/s
- Minimum power: 10 %
- Maximum power: 30 %

Figure 3.14: Images displaying channel morphology (depth, width) for varying laser power settings.

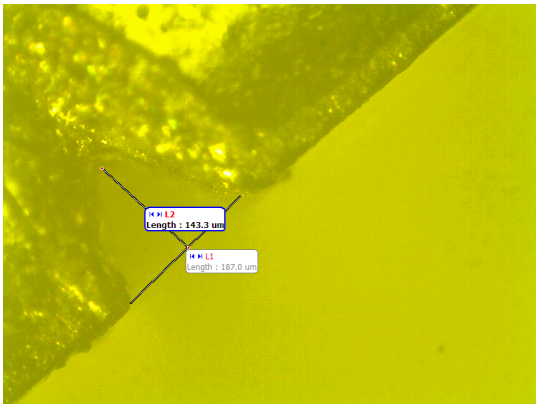

Min power(%): 10, Max power(%): 30

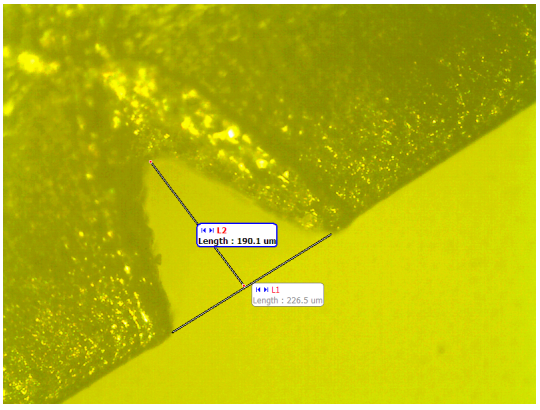

Min power(%): 12.5, Max power(%): 30

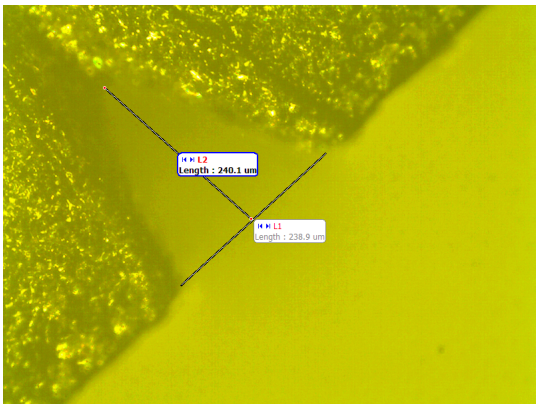

Min power(%): 15, Max power(%): 30

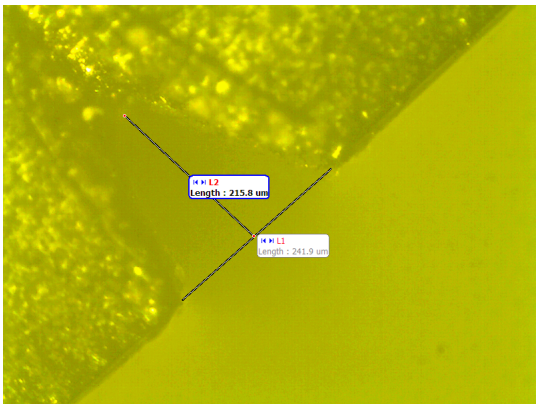

Min power(%): 10, Max power(%): 40

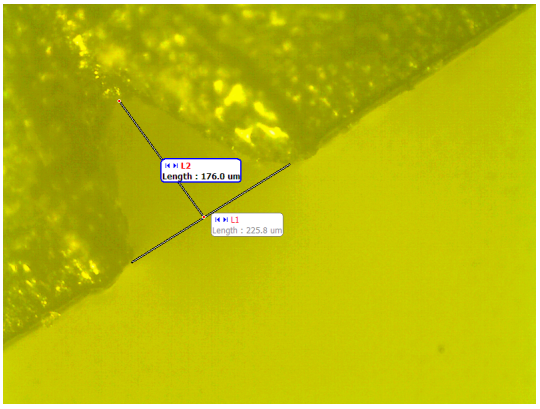

Min power(%): 12.5, Max power(%): 40

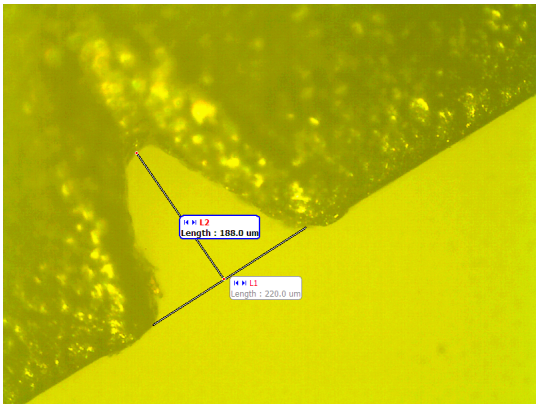

Min power(%): 15, Max power(%): 40

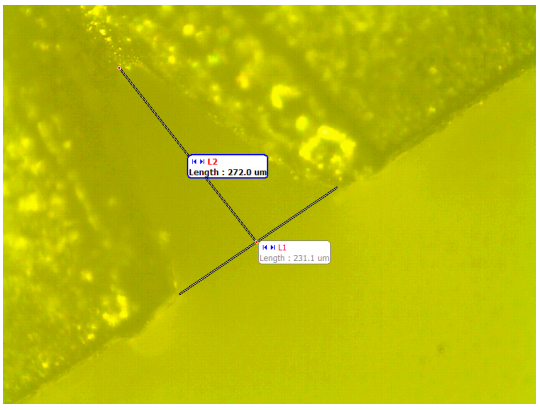

Min power(%): 20, Max power(%): 40

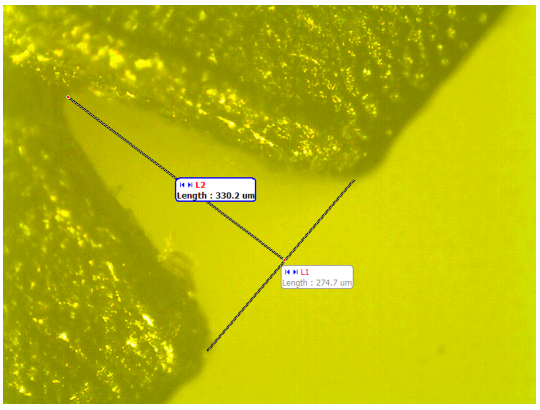

Min power(%): 25, Max power(%): 50

Figure 3.16 depicts an image of the channel geometry using the optimized parameters, this configuration was used to fabricate the channels in the final design. Figure 3.15 shows the dimension variance in channel geometries using the optimized parameters.

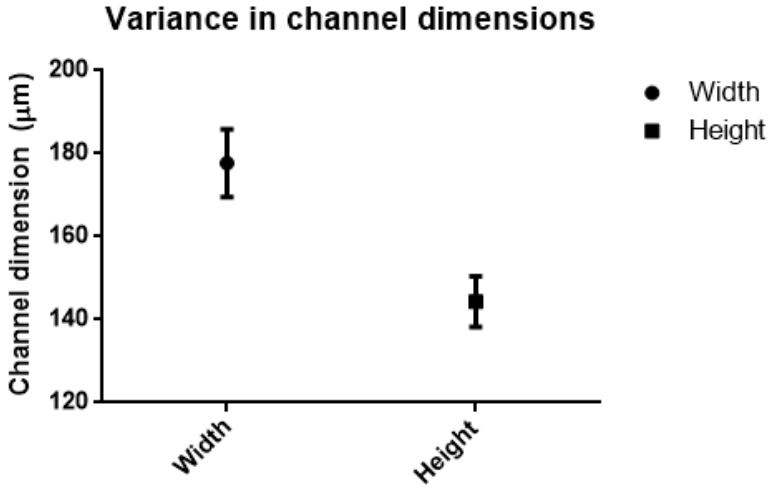

Figure 3.15: Channel dimensions variances (μm^2).

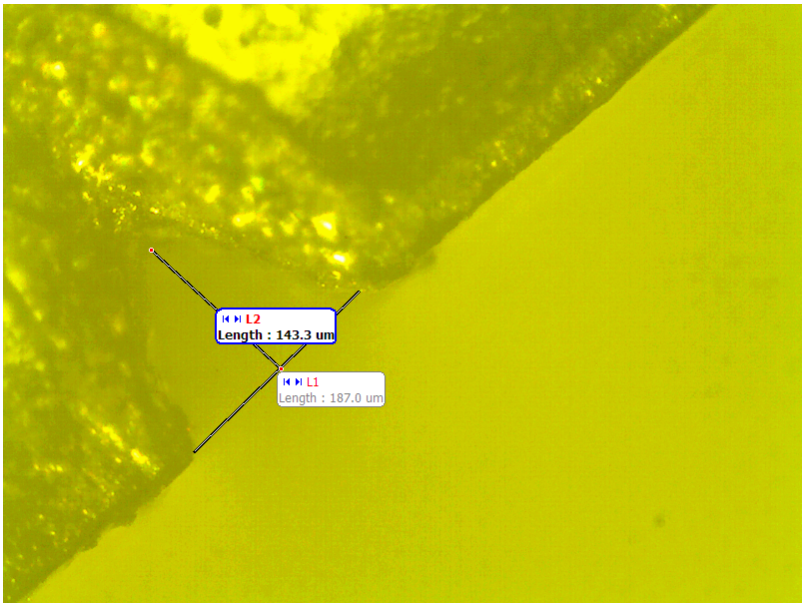

Figure 3.16: Final channel geometry based on optimized laser parameters.

3.4.4 Serpentine channel design

The serpentine channel was designed through an iterative process consisting of:

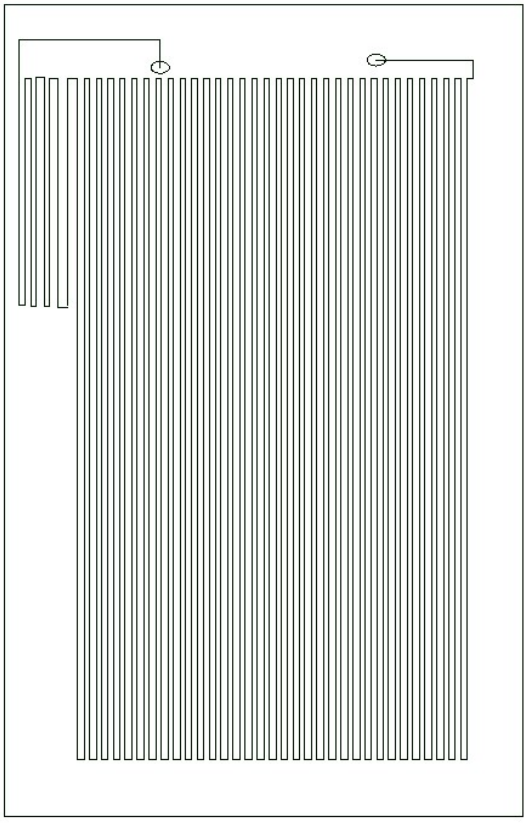

Figure 3.17: Schematic of the channel geometry, designed within RDWorkz.

- Drawing channel geometry through RDWorks (laser software).
- Bonding channel lid.
- Testing to see whether any channel blockages.
- Perform gradient heat measurements
- Repeat until required gradients were achieved.

The final microfluidics chip design consisted of a cut PMMA sheet with dimensions 100x60x3 mm. The geometrical design can be seen in Figure 3.18. The design was produced in RDWorkz. The 3 temperature zones are indicated in Figure 3.18 , red for denaturation, yellow for annealing and green for extension. The top right of the schematic depicts a pre-denaturation zone used in the "hot" start step of the reaction.

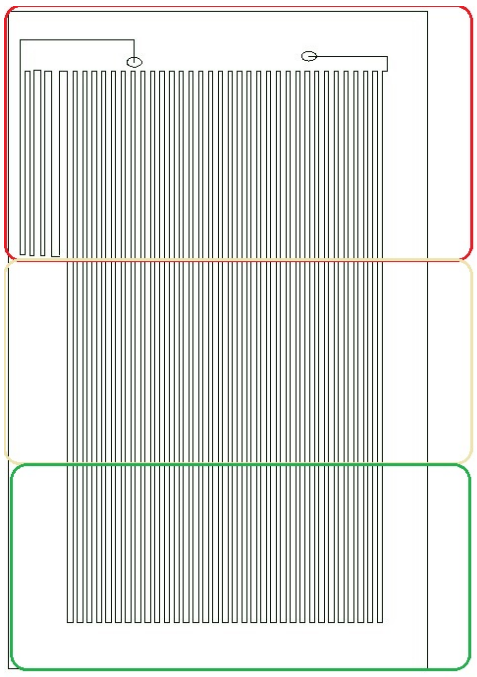

Figure 3.18: Schematic of the channel geometry, temperature zones indicated by colored areas.

The channel network etched into the PMMA had a total length of 6.2 m.

3.4.5 Lid bonding

The process of lid bonding is one that requires much optimization, in order to prevent channel deformation or clogging. Solvent-assisted thermal bonding was chosen as the technique to bond a PMMA lid to the PMMA channel substrate. Solvent bonding requires the choice of a solvent that has a Hildebrandt solubility parameter close enough to the PMMA's solubility parameter to allow dissolution of the polymer, but differs enough to prevent excessive solvent uptake into the substrate.

Acetone and isopropanol were investigated for use in the lid bonding. They were chosen to investigate bonding efficiencies of different solvents, one with a similar solubility parameter and one that differs slightly. The solubility parameters of the solvents and PMMA are:

- PMMA (δ): 20.1
- Acetone (δ): 20.4
- Isopropanol (δ): 23.4

Multiple tests were performed to ascertain bond efficiency. Bonds were evaluated by applying a flow rate of 50 μ L/min through channels and observing for external or cross channel leakages. Chips were also submerged in a water bath with external tubes leading to a syringe, while air was forced through the channels and air leakage was monitored.

The following protocol was used to perform the solvent-assisted bonding:

- PMMA lids were cut to size (100x60x3 mm)
- A 3 step wash was performed.
- Lids washed with deionized water(DI), left to air dry.
- An acetone wash was performed, left to air dry.
- A final DI water wash step, followed by air dry.
- PMMA lid was briefly exposed to solvent bath (1 min).
- Lid clamped to channel substrate through paper clips.
- The clamped device was placed in a laboratory oven at 72°C and left for 10 minutes.
- Bonding was evaluated as previously mentioned.

The use of acetone proved to be inefficient for bonding the PMMA substrates as poor bond quality and channel deformation was observed using this solvent. Air leakages and blockages were found in 80% of the trials.

Isopropanol was evaluated as a bonding solvent and initial testing resulted in far improved bond qualities compared to those of the acetone trials. Iterative trials were performed using varying solvent exposure time and heating periods. It was found that extremely brief exposure to solvent (<30 seconds) and oven residency times of 10 minutes provided optimal bond strength, while providing minimal channel deformation. Examining isopropanol's solubility parameter, we can see that it differs slightly from that of PMMA, allowing for the dissolution of polymer chains at the interface while minimizing excessive solvent uptake.

Channel morphology testing was performed by examining channel geometries prior and post bonding. However, due to the laser causing deformation of channels at the cut position, it was not possible to examine the effects of solvent bonding on the channel. Imaging equipment available proved insufficient and no conclusive images could be observed.

3.4.6 External connections

The use of commercial microfluidic connections was avoided due to cost and availability. Tygon flexible tubing (Saint-Gobain Performance Plastics France), with inner and outer diamaters (ϕ_i and ϕ_D) of 0.8 mm and 2.4 mm respectively, was used. External connections for the syringe pump (inlet) and outlet were laser ablated on the PMMA substrate and circular through-holes with dimensions of 2.35 mm were used. Due to the compressible nature of the tubing, end points of the tube could be inserted into external connection ports on the microfluidics chip with minimal air leakage, as shown in Figure 3.19. Epoxy (Quickset Clear, Pratley) was used to ensure that connections were secure and no air or fluid loss occurred during operation.

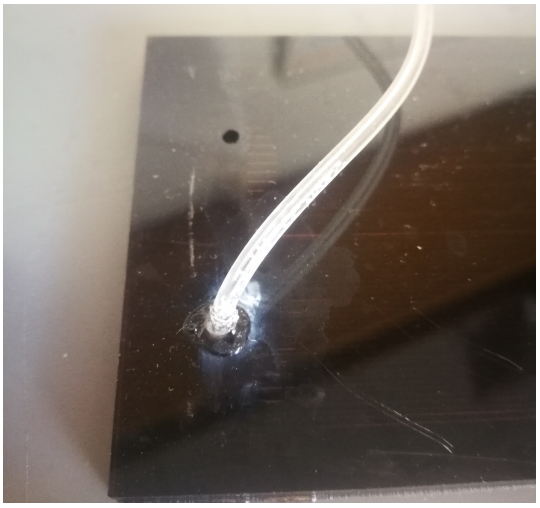

Figure 3.19: Tubing inserted into connections points. Epoxy (Quickset) can be seen surrounding the connection point.

3.4.7 Flow control

Flow control of the sample was achieved by using a NE-300 Syringe pump (New Era Pump Systems, Inc), as shown in Figure 3.20. The pump was connected to the microfluidics chip through placing the connector tube in the syringe's outlet and placing the syringe on the stage. Variable flow rates are possible and a number of these were tested. The results can be seen in Chapter 4.

3.5 Conclusion

A PCR microfluidic device was fabricated according to the methodologies and materials mentioned in Chapter 3. An image of the fabricated device can be

Figure 3.20: The NE-300 syringe pump used (New Era Pump Systems, Inc).

seen in Figure 3.21. This implementation of the device serves as a prototype and as such no effort was made to produce a polished user-end device. Chapter 4 will present the testing methodologies employed to characterize the fabricated device.

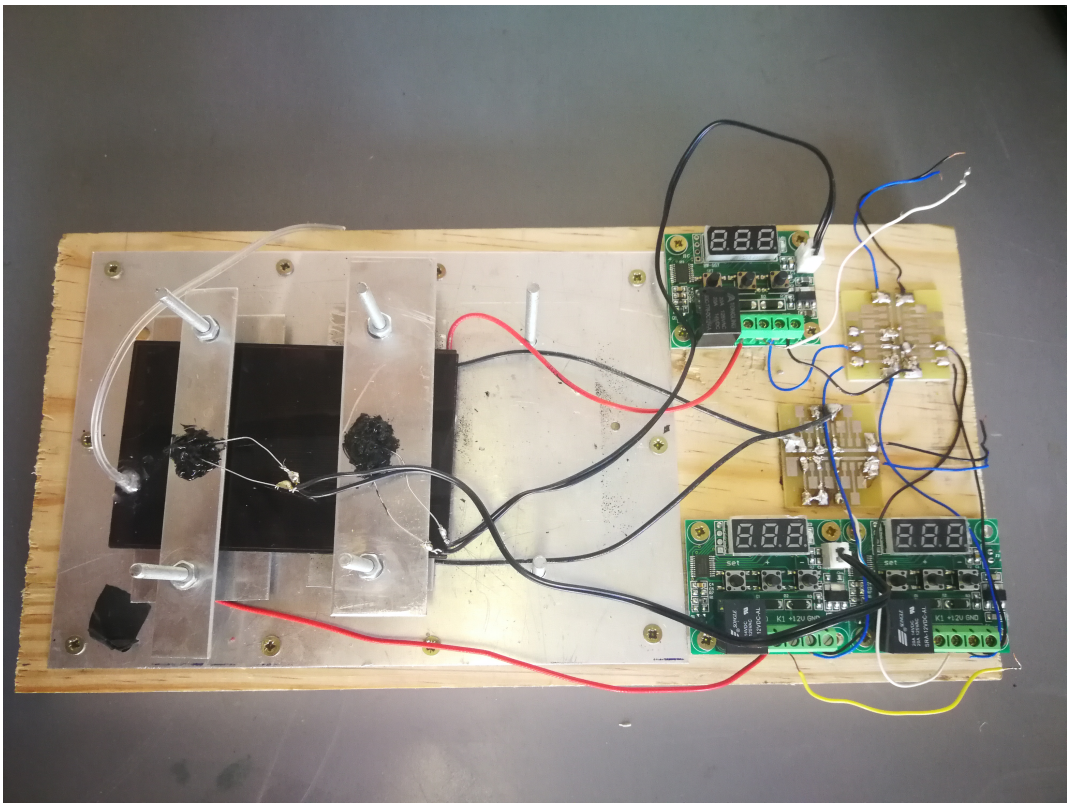

Figure 3.21: An image of the fabricated device with the microfluidics chip in place.

Chapter 4

Testing methodology and results.

4.1 Introduction

This chapter will present the testing methodology adapted to characterize the device fabricated according to the specifications in Chapter 3. Heating tests were performed to ensure that the correct temperature gradients were created across the PMMA microfluidics chip. Thermistor measurements were calibrated with an IR temperature gun. Flow rate was characterized by comparing predicted flow rates with actual flow through times. Fluid samples were imaged to verify that fluids remained within their channels, no cross channel flow occurred and bubble formation was minimal. These tests were necessary to validate that device conditions matched those required for correct PCR amplification, namely that temperature zones were accurate and distinct, and sample residency times within thermal zones were sufficient.

Amplification of a 200 bp DNA fragment was performed at varying flow rates. Amplification efficiencies at different sample residency times were compared and a conclusion on optimal flow rates was reached, based on amplification results.

4.2 Heating calibration tests

4.2.1 Test Protocols

Sets of temperature measurements were taken to confirm the thermistor accuracy against actual temperature. An Infrared(IR) thermometer, MT695 (MajorTECH), was used to calibrate thermistor measurements. The test protocol used was as follows:

- Heating zones were split into a grid of 12 elements.
- Controllers were with supplied power.

- Temperature points set on each controller. Denaturation, 95°C. Annealing, 55°C. Extension, 72°C.
- Heaters supplied with power.
- Wait until heating zones displayed the set temperature based on thermistor measurements.
- Record temperature measurements of every zone with IR thermometer and thermistor on all 3 PE's.

Figure 4.1 below depicts the portion of the heating surface that will actively have liquid flowing over it. The green rectangle references the chip positioning when superimposed on a heating surfaces heat pattern. Fluid flows along the direction shown by the arrow. Averages of the repeated temperature measurements were taken and placed in a table. The data points were extrapolated by placing three data points in between each successive measurement. The heat gradients were assumed to be linear for simplicity.

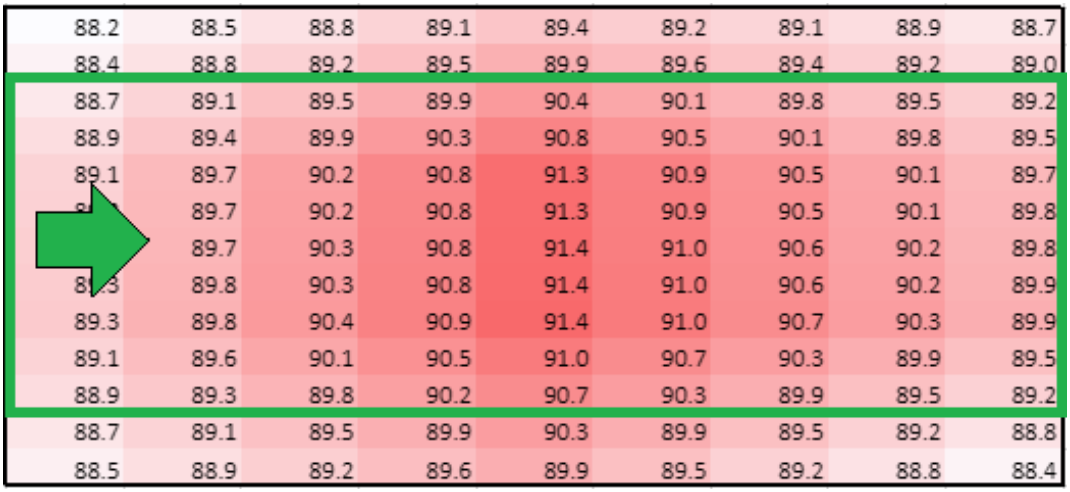

Figure 4.1: Peltier device heat pattern, with temperature set at 91°C.

4.2.2 Temperature calibration on Peltier surfaces.

Temperature measurements were taken directly on the "hot" surface of the Peltier device. These sets of tests were used to ascertain thermistor calibration without the thermal losses of the additional device layers. Measurements were taken according to the test protocol defined and 3 repeats were performed.

Figure 4.2: Heat patterns for temperature measured on "hot" Peltier surface.

89.7	89.8	89.9	89.9	90.0	89.9	89.8	89.7	89.6
89.9	90.0	90.1	90.2	90.4	90.2	90.0	89.9	89.7
90.2	90.3	90.4	90.6	90.7	90.5	90.3	90.1	89.9
90.4	90.5	90.7	90.9	91.1	90.8	90.5	90.2	90.0
90.6	90.8	91.0	91.2	91.4	91.1	90.8	90.4	90.1
90.5	90.8	91.0	91.2	91.4	91.1	90.8	90.5	90.2
90.5	90.7	91.0	91.2	91.5	91.1	90.8	90.5	90.2
90.4	90.7	90.9	91.2	91.5	91.2	90.9	90.6	90.3
90.3	90.6	90.9	91.2	91.5	91.2	90.9	90.6	90.3
90.3	90.5	90.8	91.0	91.3	91.0	90.7	90.4	90.2
90.2	90.4	90.6	90.8	91.0	90.8	90.5	90.3	90.1
90.2	90.3	90.5	90.6	90.8	90.5	90.3	90.1	89.9
90.1	90.2	90.3	90.4	90.5	90.3	90.2	90.0	89.8

Heat pattern of Peltier element surface (91°C).

67.3	67.4	67.5	67.6	67.7	67.7	67.7	67.7	67.7
67.7	67.8	67.9	68.0	68.1	68.0	67.9	67.9	67.8
68.1	68.2	68.3	68.4	68.5	68.3	68.2	68.0	67.9
68.4	68.5	68.6	68.7	68.8	68.6	68.4	68.2	67.9
68.8	68.9	69.0	69.1	69.2	68.9	68.6	68.3	68.0
68.7	68.8	68.9	69.0	69.1	68.8	68.5	68.2	67.9
68.6	68.7	68.8	68.8	68.9	68.6	68.3	68.0	67.7
68.5	68.6	68.6	68.7	68.8	68.5	68.2	67.9	67.6
68.4	68.5	68.5	68.6	68.6	68.3	68.0	67.7	67.4
68.2	68.3	68.3	68.4	68.5	68.2	67.9	67.6	67.4
68.1	68.1	68.2	68.2	68.3	68.1	67.8	67.6	67.3
67.9	67.9	68.0	68.1	68.2	67.9	67.7	67.5	67.3
67.7	67.8	67.9	67.9	68.0	67.8	67.6	67.4	67.2

Heat pattern of Peltier element surface (68°C).

54.0	54.1	54.1	54.2	54.2	54.0	53.9	53.7	53.5
54.4	54.5	54.6	54.6	54.7	54.4	54.2	53.9	53.7
54.9	54.9	55.0	55.1	55.2	54.8	54.5	54.1	53.8
55.3	55.4	55.5	55.5	55.6	55.2	54.8	54.4	54.0
55.7	55.8	55.9	56.0	56.1	55.6	55.1	54.6	54.1
55.8	55.8	55.9	55.9	56.0	55.6	55.2	54.8	54.4
55.9	55.9	55.9	55.9	55.9	55.6	55.3	55.0	54.7
55.9	55.9	55.8	55.8	55.7	55.5	55.3	55.1	54.9
56.0	55.9	55.8	55.7	55.6	55.5	55.4	55.3	55.2
55.8	55.7	55.6	55.6	55.5	55.4	55.4	55.3	55.3
55.6	55.5	55.5	55.4	55.4	55.4	55.4	55.3	55.3
55.3	55.3	55.3	55.3	55.3	55.3	55.3	55.3	55.4
55.1	55.1	55.2	55.2	55.2	55.3	55.3	55.4	55.4

Heat pattern of Peltier element surface (55°C).

4.2.3 Temperature calibration on steel heat dispersers.

Temperature measurements were taken directly on the steel plates placed on top of each PE. Silver paste was applied between the heaters and steel plates. These tests aimed to examine the heat pattern occurring on the new steel heating surfaces. Measurements were taken according to the test protocol defined and 3 repeats were performed.

The steel plates serve as a heat dissipation mechanism, not only to increase the heated surface area, but also to reduce the radial heat pattern generated by the Peltier elements. Figure 4.1 clearly depicts the radial heat pattern of the Peltier devices. In contrast,the heat pattern measured on the steel dispersers plates is more uniform, as shown in Figure 4.2.

Figure 4.3: Heat patterns for temperature measured on steel heat dispersers.

87.5	87.9	88.3	88.7	89.1	88.9	88.6	88.4	88.1
88.4	88.8	89.1	89.5	89.8	89.6	89.4	89.1	88.9
89.3	89.6	89.9	90.2	90.5	90.3	90.1	89.9	89.7
90.2	90.5	90.7	91.0	91.2	91.0	90.9	90.7	90.5
91.1	91.3	91.5	91.7	91.9	91.8	91.6	91.5	91.3
91.0	91.2	91.4	91.6	91.8	91.7	91.5	91.3	91.2
90.9	91.1	91.3	91.5	91.8	91.6	91.4	91.2	91.1
90.8	91.0	91.2	91.5	91.7	91.5	91.3	91.1	90.9
90.7	90.9	91.2	91.4	91.6	91.4	91.2	91.0	90.8
90.1	90.3	90.6	90.8	91.1	90.9	90.6	90.4	90.1
89.4	89.7	90.0	90.3	90.6	90.3	90.0	89.7	89.4
88.8	89.1	89.4	89.8	90.1	89.8	89.4	89.1	88.7
88.1	88.5	88.9	89.2	89.6	89.2	88.8	88.4	88.0

Heat pattern of steel heat dissipater (91°C).

66.5	66.7	66.8	67.0	67.1	66.9	66.7	66.4	66.2
66.9	67.1	67.2	67.4	67.5	67.3	67.1	66.9	66.7
67.4	67.5	67.6	67.8	67.9	67.7	67.5	67.3	67.1
67.8	67.9	68.0	68.2	68.3	68.1	67.9	67.7	67.6
68.2	68.3	68.5	68.6	68.7	68.5	68.4	68.2	68.0
68.2	68.3	68.3	68.4	68.5	68.4	68.3	68.1	68.0
68.2	68.2	68.2	68.3	68.3	68.2	68.2	68.1	68.0
68.1	68.1	68.1	68.1	68.1	68.1	68.1	68.0	68.0
68.1	68.1	68.0	68.0	67.9	67.9	68.0	68.0	68.0
67.8	67.8	67.8	67.8	67.8	67.8	67.8	67.8	67.8
67.6	67.6	67.7	67.7	67.8	67.7	67.7	67.6	67.6
67.3	67.4	67.5	67.6	67.7	67.6	67.5	67.4	67.3
67.0	67.2	67.3	67.5	67.6	67.5	67.4	67.2	67.1

Heat pattern of steel heat dissipater (68°C).

53.0	53.1	53.2	53.2	53.3	53.3	53.2	53.2	53.1
53.6	53.6	53.7	53.8	53.9	53.8	53.8	53.7	53.6
54.1	54.2	54.3	54.4	54.6	54.4	54.3	54.2	54.1
54.7	54.8	54.9	55.0	55.2	55.0	54.9	54.7	54.5
55.2	55.4	55.5	55.7	55.8	55.6	55.4	55.2	55.0
55.4	55.5	55.6	55.7	55.9	55.7	55.5	55.4	55.2
55.6	55.6	55.7	55.8	55.9	55.8	55.7	55.5	55.4
55.7	55.8	55.8	55.9	56.0	55.9	55.8	55.7	55.6
55.9	55.9	56.0	56.0	56.0	56.0	55.9	55.9	55.8
55.6	55.6	55.6	55.6	55.7	55.6	55.6	55.5	55.5
55.4	55.3	55.3	55.3	55.3	55.3	55.3	55.2	55.2
55.1	55.0	55.0	55.0	55.0	54.9	54.9	54.9	54.9
54.8	54.8	54.7	54.7	54.6	54.6	54.6	54.6	54.6

Heat pattern of steel heat dissipater (55°C).

4.2.4 Temperature calibration with PCR chip

Temperature measurements were taken with the PCR device (3.7) in full operation. This situation represented the device as would be in-field. This was used, in conjunction with the fluid transport tests, as a final confirmation indicator that PCR amplification testing could begin. Measurements were taken according to the following protocol:

- The PMMA microfluidic chip was subdivided into 16 quadrants
- Temperature measurements were performed with IR thermal gun
- Data points were extrapolated by placing 2 additional values between IR temperature measurements.

The temperature gradient pattern of the PMMA microfluidics chip can be seen in Figure 4.4, while Figure 4.5 depicts the same graphic with temperature values. It can be seen that a temperature gradient was achieved across the microfluidics chip, with 3 distinct temperature regions. However, the values in Figure 4.5 depict values lower than those required of PCR devices. These values represent thermal IR measurements on the chip's surface, but due to the low thermal conductivity and relative thickness of the chip (3 mm), a temperature gradient is created across the depth of the substrate. In order to account for this phenomenon, temperature measurements were taken on both sides of the substrate and a comparison drawn. These metrics were used to calculate the temperature at the channel depth, using the substrate thermal conductivity. A figure displaying the temperature pattern at this depth is presented in 4.6.

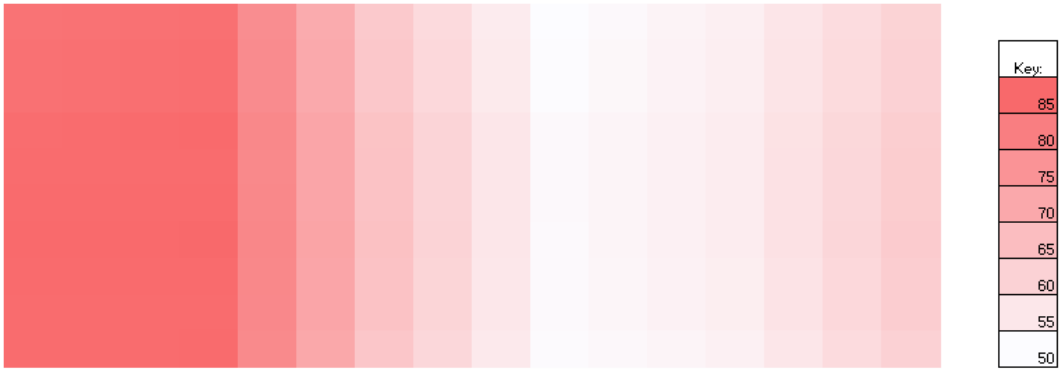

Figure 4.4: PMMA microfluidic chip measured temperature pattern. Temperatures set for 95°C, 57°C and 72°C, respectively.

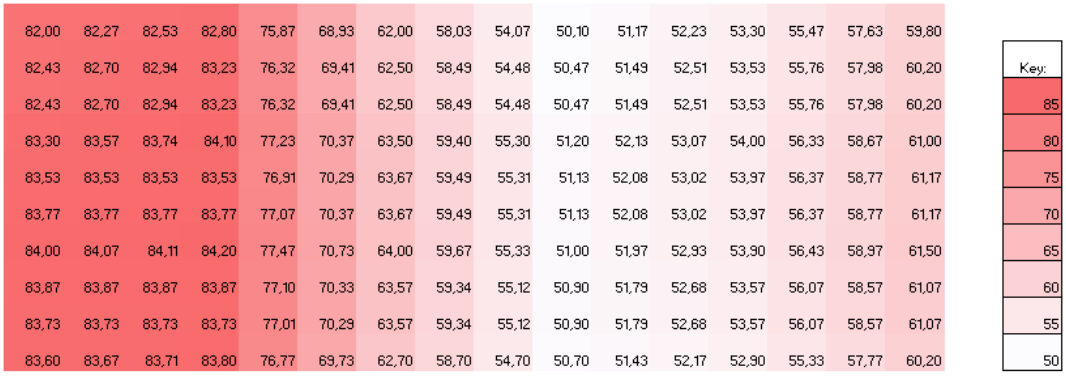

Figure 4.5: PMMA microfluidic chip measured temperature pattern with values. Temperatures set for 95°C, 57°C and 72°C, respectively.

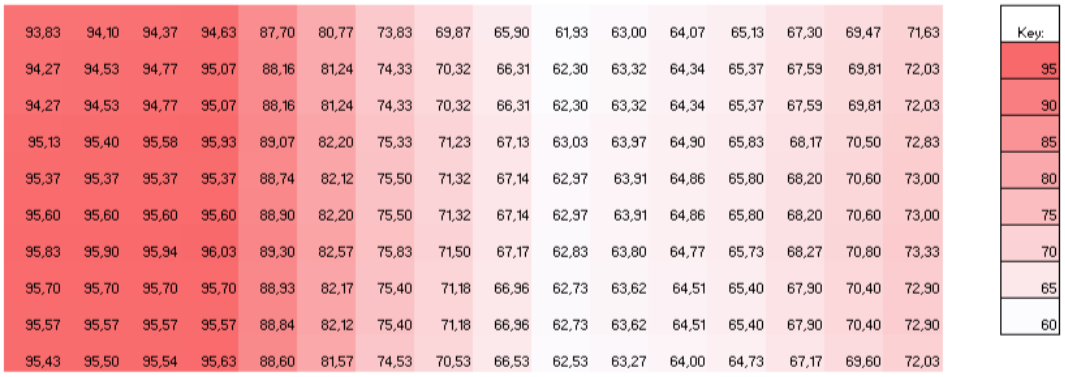

Figure 4.6: Temperature pattern at channel depth with calculated values. Temperatures set for 95°C, 57°C and 72°C, respectively.

As can be seen in Figure 4.6, when correcting the values using the aforementioned process, temperature values at the channel depth are well within the range for PCR device requirements. A stable temperature gradient is thus created across the microfluidics chip, with temperature zones well within the requirements for correct PCR operating conditions.

4.3 Microfluidics channel and transport.

The PMMA microfluidics chip fabricated in Chapter 3 is characterized in the following section. Sample encapsulation refers to the ability of a microfluidics chip to ensure fluids are contained within channels and with no cross-channel flow. This is of paramount importance, as sample leakage results in unpredictable flow rates, bubble formation and non-functioning of the device, and as such, ensuring samples are retained in channels is a necessary requirement.

Flow rates were also considered. Theoretical flow rates for the device are calculated based on channel dimensions and syringe pump rates and these are compared to actual measured flow rates. The importance of flow rates in PCR cannot be understated. Constant and predictable flow rates are necessary to ensure that samples have sufficient residency times within the respective temperature regions to ensure correct PCR amplification. A number of flow rates were tested and corresponding residency times were calculated.

4.3.1 Sample encapsulation.

Sample encapsulation was validated in a number of ways. The device was tested for air leakages by connecting inlet/outlet tubing and submerging the device in a water bath. A syringe pump was connected to the inlet and air was forced through the channel network, while the presence of air bubbles

being ejected from the device was monitored. A device was considered air tight if no air bubbles were formed. Once a microfluidics chip had passed this initial validation step, microscopic images were taken of samples within their channels to confirm encapsulation.

4.3.1.1 Samples in microfluidic channels.

Microscopy imaging was performed to ascertain whether sample encapsulation was achieved. Liquid samples were passed into the microfluidic channels via inlet tubing and sample encapsulation was validated by checking for the presence of cross-channel flow and excessive bubble formation. Figure 4.7 depicts the start of the sample emerging into the image field-of-view as seen in the top left. Liquid samples can be distinguished from empty channels, as channels filled with liquid are transparent. This figure validates that no unwanted flow has occurred.

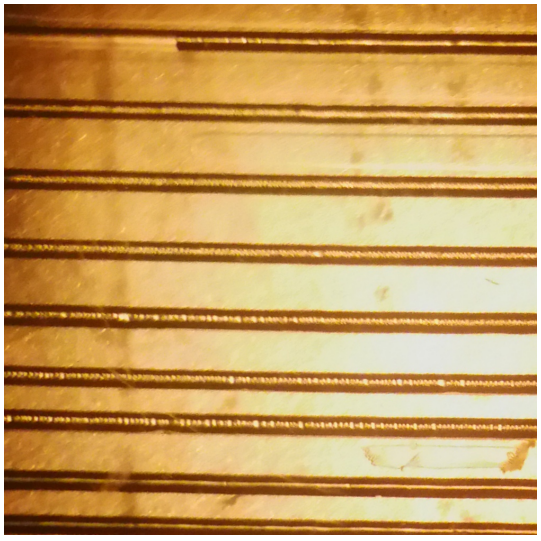

Figure 4.7: Image of a liquid sample (top left) encapsulated in the microfluidic channel.

In Figure 4.8, the top two channels are filled with liquid, while a small volume sample (20 µL) can be seen surrounded by air and is depicted in black. This figure depicts the capability of the microfluidics channels to hold samples within the PCR reaction volume range. These figures and discussion serve as validation for sample encapsulation within the microfluidic channel network.

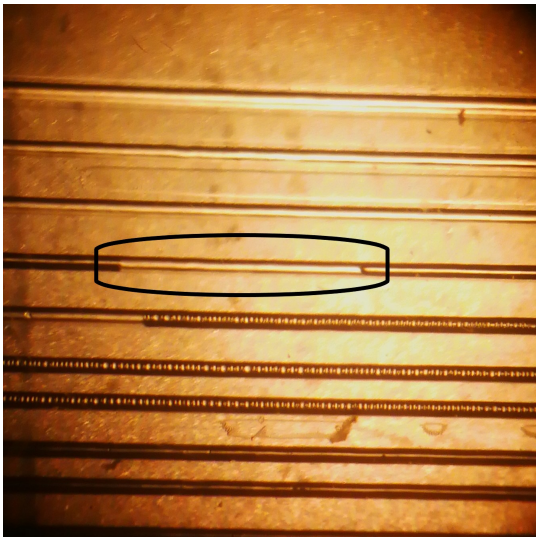

Figure 4.8: Image of small volume liquid sample in channel (indicated). The top 3 channels also contain liquid.

4.3.2 Flow rates.

The flow of samples throughout the channel network was validated in order to ascertain whether the microfluidics chip provided predictable flow rates, an important feature necessary for correct PCR amplification. Theoretical flow rates were calculated based on channel geometry and compared to measured flow-through times. Due to the nature of microfluidics, theoretical and actual flow rates should coincide closely.

Ensuring that samples reside in the appropriate temperature zones is key to performing successful PCR amplification. Sample residency time were calculated using theoretical and actual flow rates. These validation tests were used in the final DNA amplification testing presented in Chapter 4.

4.3.2.1 Theoretical calculations.

The channel geometry used in the final microfluidics network is depicted in Figure 3.15 and has dimensions of (150μm x 150μm). Theoretical values were calculated for average linear velocity, Reynold's number and flow-through time, using the following assumptions:

- Total channel length: 6200 mm.
- Cross-sectional area: 0.01125 mm^3.
- Flow rates: 100, 50, 30, 20, 10 μL/min.
- The dynamic viscosity of water : 8×10^{-4} Pa.s^{-1}.

Table 4.1: Theoretically calculated values of average velocity and total flow through time.

Flow rate (μ L/min)	v_{ave} (mm/s)	Flow through time (min)
100	148.13	0:42
50	74.06	1:23
30	44.45	2:19
20	29.63	3:29
10	14.81	6:58

Table 4.2: Theoretical Reynold's numbers for varying flow rates.

Flow rate (μ L/min)	Theoretical Reynold's numbers (Re)
100	14.81
50	7.40
30	4.44
20	2.96
10	1.48

Table 4.3: Calculated average linear velocity using measured values.

Flow rate (μL/min)	v_{ave} (mm/min)	Flow through time (min)
100	29.52	3:30
50	16.02	6:27
30	8.38	12:20
20	6.42	16:05
10	3.75	27:33

- The density of water: 1000 kg/m^3.

Chapter 4.3.2.4 compares the differences between theoretical and measured values.

4.3.2.2 Calculations using measured values.

This section details the calculations done using the actual flow rates coupled with the measured total flow through times of a sample through the microfluidic network. Average linear velocity was calculated using the measured values and this was used to calculate Reynold's numbers for the device in operation. A comparison between measured device parameters and theoretical device characteristics can be found in Chapter 4.3.2.4.

4.3.2.3 Measured residency times.

The PCR requires that the sample be exposed to the correct temperature zones for a minimum amount of time, usually determined by the type of Taq

Table 4.4: Actual Reynold's numbers for varying flow rates.

Flow rate (μL/min)	Theoretical Reynold's numbers (Re)
100	2.95
50	1.59
30	0.84
20	0.64
10	0.37

polymerase used. Table 4.5 depicts the calculated residency times in each temperature zone, based on the average velocity calculated from the total flow times (Table tab:Vavereal). The values in Chapter 4.3.1 were used alongside the measured total flow through time to calculate the actual Reynolds numbers. These values give an indication whether a given flow rate will result in successful amplification. Residency times that are too short do not give the polymerase sufficient time to perform it's function, resulting in failed or poor amplification. Literature states that residency times less than 1 second for a temperature zone result in very little to no amplification. The channel geometry was defines a ratio of 1:0.47:1 for denaturation, extension and annealing respectively. This ratio is as a result of the initial channel design which inferred this ratio from it's geometry. Figure 4.9 depicts the lengths of each zone for a cycle. Comparing Figure 4.9 to 4.10 we can see that lengths described in Figure 4.9 refer to channel length within each temperature zone per cycle.

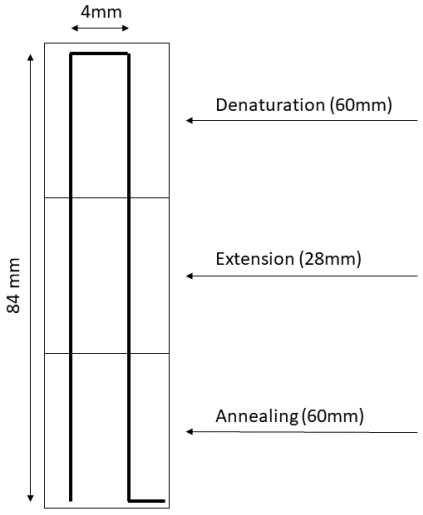

Figure 4.9: Length of temperature zones.

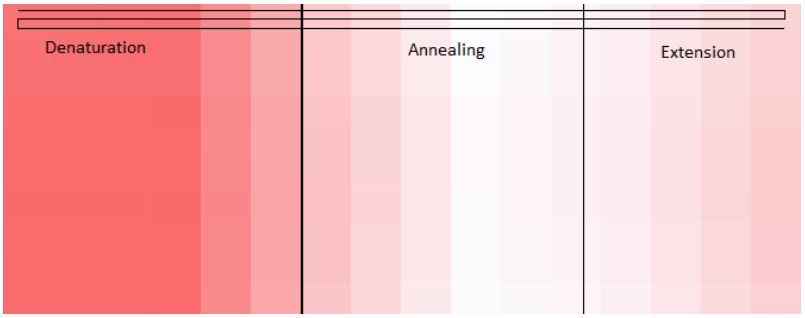

Figure 4.10: Depiction of temperature zones with a channel indicated in black.

Table 4.5: Residency times (seconds) per cycle for flow rates (mm/s)

Flow rate ($mm/second$)	Denaturation	Annealing	Extension
29.52	2.03	0.95	2.03
16.02	3.75	1.74	3.75
8.38	7.16	3.34	7.16
6.42	9.34	4.36	9.34
3.75	16	7.47	16

4.3.2.4 Comparison between theoretical and actual flow rates/residency times.

Comparing the results of the actual and theoretical values for the device reveal a disparity between the two. If we examine Figure 4.11 we can see that the actual Reynold's numbers are substantially lower than the theoretical Reynold's values. Similarly, the theoretical flow through times are much higher than the actual flow through times measured, as shown in Figure 4.12. These two metrics are linked and can be explained by back pressure in the channels, as well as channel morphology. Notable back pressure is produced in microfluidic channels, especially when using positive pressure driven flow. This can lead to substantially slower flow rates than expected and this could explain the considerably slower flow rates noted in the measured results.

The Reynold's number is linked to the average linear velocity, which is derived from the total flow through time over the length of the entire microfluidics network. Slower flow through times result in lower average linear velocities which result in lower Reynold's numbers. This is evident if we compare Table 4.2 and Table 4.4, where the actual Reynold's numbers are far lower than their theoretical counterparts. This is as a direct result of far slower flow through times compared to the theoretically predicted values as seen in Table 4.2. This is a deviation that bodes well for the device, as lower Reynold's numbers result in more predictable flows. If we compare the average velocities in Table 4.2 and Table 4.4 it is clear that the actual device was unable to achieve flow rates

similar to the theoretically predicted values. This follows on from the slower than expected flow through times when comparing Table 4.1 and Table 4.3. This disparity is a result of approximating values for the theoretical calculations as well as viscous drag induced in the channels. Channel morphology is assumed to be uniform along the entire channel length, but in practice variations of channel geometries exist, and it is these variations that contribute to the difference between the actual and theoretical values for the microfluidics device.

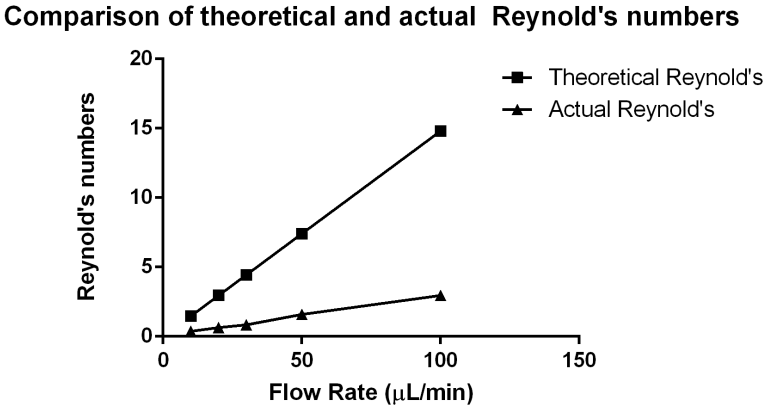

Figure 4.11: Theoretical vs. actual Reynold's numbers.

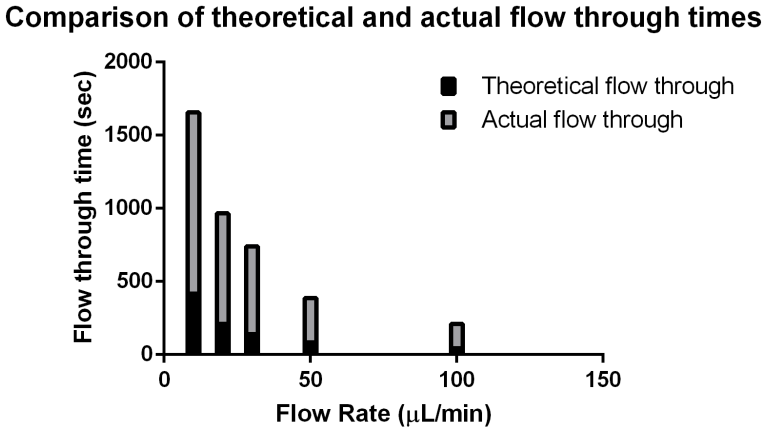

Figure 4.12: Theoretical vs. actual flow through times.

4.4 DNA amplification

DNA amplification was performed using the microfluidics device constructed according to the methodologies detailed in Chapter 3. Amplification of *NisinA*, a 250 base-pair fragment, was tested at varying flow rates in order to ascertain optimal device parameters. A BioDrop (Fischer Scientific) was used to confirm amplification results of tests. Positive tests were compared to control tests to provide additional proof that no non-specific amplification of primers had occurred. The DNA sample solution was composed of the following reagents:

- MilliQ water 28.75 μL
- 5X Flexi Buffer 10 (New England Biolabs) μL
- dNTPs (New England Biolabs) M(ea) 1 μL
- Fwd Primer (Inqaba Biotechnical Industries (Pty) Ltd.) M 1 μL
- Rev Primer (Inqaba Biotechnical Industries (Pty) Ltd.) M 1 μL
- Q5 High-Fidelity DNA Polymerase (New England Biolabs) U/uL 0.25 μL
- Template DNA 50 (in-house) ng/uL 3 μL

The use of the Q5 High-Fidelity DNA Polymerase requires special operating procedures in comparison to more conventional Taq polymerases. The Q5 requires a denaturation temperature of 98°C, which is higher than traditional denaturation temperatures, usually around 95°C. The benefit of the digital thermostats implemented in the design is the ability to change the temperature zone's desired temperature at will. NEB also provides an optimal temperature zone residency time for the polymerase, as seen in Figure 4.13. Comparing Figure 4.13 with Table 4.3 displaying the measured residency times for the DNA tests, we can see that the residency times of the tests were shorter than those specified by the polymerase for optimal amplification. This was done on purpose to ascertain the minimum residency times that would result in amplification, and as a byproduct, the fastest possible reaction time for the device. Residency times far below the recommended optimal times resulted in no amplification. As residency times approached the recommended values, increased amplification was noted.

4.4.1 DNA test protocol:

The testing protocol to determine whether successful amplification of a DNA fragment had occurred was as follows:

- Power was supplied to the device, desired temperatures were set on thermocontrollers.

STEP	TEMP	TIME
Initial Denaturation	98°C	30 seconds
25–35 Cycles	98°C *50–72°C 72°C	5–10 seconds 10–30 seconds 20–30 seconds/kb
Final Extension	72°C	2 minutes
Hold	4–10°C	

Figure 4.13: Optimal temperature zone residency times for the Q5 polymerase.

- Device was left to reach the required temperatures which typically took around 10 minutes.
- DNA template was added to PCR mixture.
- 20 μL of the sample containing DNA fragment and PCR mixture was loaded into syringe.
- Syringe was connected through tubing to the device.
- Sample was manually injected into the extended denaturation zone and left for typically around 2 minutes to ensure a correct "hot-start"
- Syringe pump was set to desired flow rate. Syringe pump was turned on and sample was now driven through the channels.
- Samples were collected at the output tube into standard laboratory reaction vessels (1 mL). Sample volumes at the output varied with an average sample volume of 11 μL being recovered. This reduced volume at the output can be attributed to sample evaporation during the heating cycles.
- Samples were analyzed by the BioDrop device to ascertain final DNA concentration. Concentrations were recorded.

The BioDrop device allows the exclusion of the background fluid for the sample in question. As the sample solution contained not only the amplified DNA fragments, but also the PCR mixture, a solution containing the primers, polymerase and buffer solution devoid of any DNA fragment was used as a background calibration. This allows for more accurate detection of DNA fragments and avoids the non-specific detection of these other molecules.

A further control test was performed containing the aforementioned constituents, namely the same solution used in the test protocol, but without any DNA fragments. This solution was run through the same protocol detailed above and analyzed by the BioDrop. This solution is identical to the solution used as the

background calibrator and as such no presence of DNA was detected. These two techniques serve as validation that no non-specific detection of DNA was noted by the BioDrop.

4.4.2 Amplification results.

Amplification results were tabulated in 4.6 according to their respective flow rates. Research has shown that flow rates leading to insufficient residency times within temperature zones resulted in poor to no amplification occurring and this was confirmed through testing. It was found that flow rates exceeding 50 μL led to insufficient residency times and resulted in final DNA concentrations of less than 50 ng/μL. These high flow rate tests proved the hypothesis that the Taq polymerase should be exposed to the appropriate temperature zones for periods around and exceeding 2 seconds, any less than that led to little to no amplification.

Flow rate tests were performed on the lower end of the spectrum, (10-50 μL/min). As predicted, the longer the total reaction time, the greater the final concentration of DNA present in the final solution. Table 4.6 and 4.7 reference the results measured, 30 μL and below resulted in notable amplification with 10 μL/min producing a final concentration of around 1.5 μg/μL, a notable increase from the original 100 ng/μL starting concentration. It should be noted that without the BioDrop's feature for excluding the background solution, control tests would not have produced an absolutely negative results, as detailed. Instead, control tests would most likely express a small variance in concentration, although still not significant. If one examines Table 4.7, it can be seen that the concentration values for the respective flow rates do not deviate from their mean significantly. This bodes well for the possible accuracy of the constructed device, allowing for future iterations to provide an accurate quantitative assessment of concentration ranges that the samples fall within.

Figure 4.14 depicts the concentrations detected post amplification for various flow rates. As can be seen, the concentration exponentially increases for decreasing flow rate speeds. This is as expected and is corroborated by Figure 4.13, displaying the optimal residency times for each temperature zone. Lower flow rates result in longer residency times and as residency times approach optimal values depicted in Figure 4.13, amplification efficiency increases. When comparing Figure 4.13 to Table 4.2 we can see that the 3.75 mm/second flow rate residency times are still below the optimal residency periods. This indicates that amplification efficiency could be further improved by increasing temperature zone residency times. This is the exact result we expect to see. If we examine Table 4.8 and compare with Figure 4.14 a relationship between residency times, flow rates and amplification efficiencies can be drawn. Figure

Table 4.6: Comparison of flow rates, total reaction time and amplification concentrations.

Flow rate (μL/min)	Flow through time (min)	Concentration (ng/μL)
100	3:30	0
50	6:27	60.5
30	12:20	227.5
20	16:05	687.5
10	27:33	1469
20 (Control)	15:42	0

4.14 confirms that the device operates as expected and produces amplification efficiencies according to the expected pattern.

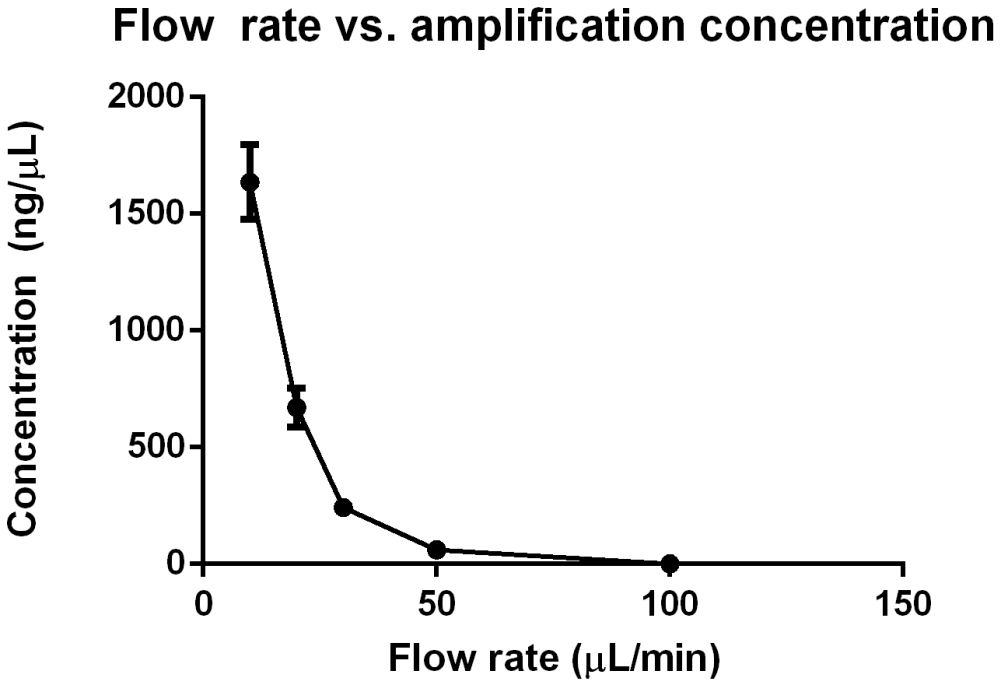

Figure 4.14: Concentration post amplification for respective flow rates.

4.5 Conclusion

A microfluidic PCR device was constructed capable of notable DNA amplification, and more rapidly than conventional laboratory equipment. Successful amplification of a 250 base-pair sequence was demonstrated. Amplification efficiencies were compared to flow rates to ascertain optimal sample throughput

Table 4.7: Comparison of flow rates, amplification concentrations and standard error of the mean(SEM).

Flow rate (μL/min)	Concentration (ng/μL)	Mean error (SEM)
100	0	0
50	60.5	7.48
30	227.5	8.03
20	687.5	48.20
10	1469	92.42
20 (Control)	0	0

Table 4.8: Residency times (seconds) per cycle for flow rates (μL/*second*)

Flow rate (μL/*second*)	Denaturation	Annealing	Extension
100	2.03	0.95	2.03
50	3.75	1.74	3.75
30	7.16	3.34	7.16
20	9.34	4.36	9.34
10	16	7.47	16

times. It was found that longer sample residency periods within the appropriate temperature zones resulted in higher final concentration of DNA detected. This was corroborated with current literature which presents similar findings. A minimum flow rate that achieved notable amplification was found. Non-specific amplification was discounted through a 2-fold process. Negative controls containing all reagents, but devoid of the DNA fragment were run through the device and produced no detectable amplification. The BioDrop device also allows for the calibration of a background fluid and this ensures that no other genetic material besides the amplified fragment is detected in the sample.

Chapter 5

Conclusion

An investigation was performed on portable microfluidic PCR devices to improve POC approaches to patient diagnosis, as well as investigate an alternative to conventional bench top PCR equipment. A relevant literature, pertaining to the construction of microfluidic devices was performed, with a focus on PCR implementations. A serpentine-channel PCR device was constructed on a PMMA substrate using laser ablation, solvent-assisted thermal bonding for lid fabrication and a syringe pump for flow control. The thermal control system comprised of OTS thermo-controllers coupled to a set of 3 Peltier heaters. The constructed device was evaluated by performing amplification of a 250 base-pair fragment, *NisinA*. A relationship between temperature zone residency times and amplification efficiency was determined. The device was capable of notable amplification within 30 minutes, representing a considerable improvement over conventional labratory techniques (150-180 minutes).

The following list constitutes the main contributions made by this project:

- A review was supplied that provided a brief overview of fundamental microfluidic principles and microfluidic fabrication techniques for both glass/silicon and thermoplastic devices. PCR devices were discussed in detail and various implementations were presented.
- Conventional methodology for performing PCR was investigated and it was found that conventional equipment does not meet portability, cost or simplicity criteria.
- A microfluidics PCR device was fabricated. The techniques used to fabricate the device can be seen as low cost, with some processes being scalable. The fabrication of the device can be performed in a "low-tech" labratory, as none of the procedures required the use of specialized equipment. This serves as proof that such LOC devices can be produced in a "low-cost" labratory environment. Commercial microfluidics connectors were avoided and a low-cost in-house connection scheme was devised.

- The fabricated device was capable of noteable DNA amplification of a *NisinA* fragment within 30 minutes. This represents a far improved rate of amplification in comparison to conventional amplification procedures.
- A specification is provided to be used in future work and can be seen in 6.1. The specification details a similar approach, however substitutes the components that are not truly portable in the current implementation.

The project suceeded in achieving it's main objectives. However, due to environmental constraints, there were some limitations on the work done. The device fabricated is not portable in it's current form.

The Peltier elements used are not micro-Peltier versions and as such draw considerable power. This requires the use of a benchtop power supply unit to provide sufficient power. Micro-Peltier elements were not obtainable within the time or cost frame, but the use of these devices in the future will allow the powering of the device by a battery configuration. Secondly, the syringe pump used is also a benchtop device, further hindering the portability of the device. The solution to this would be the use of micro-peristaltic or micro-syringe pump types of devices, which can be powered via batteries. This would allow the fluid control mechanism to conform to portability criteria. The cost of these devices was outside the scope of the budget for the project and acquisition of these devices within a South African context is difficult.

The device was tested over a range of flow rates and a relationship was determined between temperature zone residency times and the final amplification concentration. However, future research should look at optimizing this process to obtain a more distinct relationship between the parameters in question in order increase amplification efficiency. Although sufficient amplification was observed it can be noted that this procedure should be repeated at lower flow rates. The Q5 High Fedility Polymerase specifies optimal residency times and future research can investigate the redesign of channel geometry to match the optimal residency times specified. Slower flow rates should be investigated to determine a point at which further increase of residency periods no longer results in increasing amplification efficiencies. Secondarily, future research should focus on the portability criteria for future design iterations.

The following presents a list of work for future research:

- Optimization of laser ablation process to produce configurable channel dimensions from determined laser parameters.
- Investigation of lid bonding strengths for a number of solvent combination/mixtures, using solvent-assisted thermal bonding.
- Design and implementation of a portable fluid control mechanism/device.

- Use of a portable heating system, either in the form of micro-Peltier elements or the design of a Joule heating system.
- Determination of ideal residency periods for a number of polymerases to achieve maximum amplification.

The use of microfluidic PCR devices can be incorporated into a number of areas. They could function as a possible replacement of conventional benchtop devices in a laboratory context, providing improvements in terms of cost and time. Their use in the LOC context is well-documented and can be considered the main driving force behind the research done on this category of devices. Their possibility to provide in-field diagnostics to improve diagnostic response times is hugely attractive and once incorporated into devices capable of pre-sample treatment and end-point detection, these devices could revolutionize the way that genetic diseases are diagnosed.

A prototype portable PCR device was constructed based on a microfluidic framework. The device was constructed in a cost efficient manner in a "low-tech" laboratory environment, avoiding the use of excessively complex equipment or fabrication techniques. The device produced notable amplification of a *NisinA* DNA fragment within 30 minutes. This device could serve as a prototype for future implementations that would adhere more strictly to the portability, cost and simplicity criteria.

Chapter 6

Future work and recommendations.

6.1 Evaluation of current implementation.

A device capable of rapid PCR was fabricated and although successful in its primary goal, it did not adhere to its secondary purpose of conforming to portability criteria. This chapter will address this and other limitations of the device's current implementation and propose requirements and a potential design for future work. The end goal of such a device is to form part of a LOC device for possible use in rural settings, where populations lack access to sufficient diagnostic technologies. The proposed specification will focus on the use of more energy efficient heaters, a self-contained, low power pumping solution and the use of a low power, integrateable power supply.

The heating system used in the current implementation involves Peltier elements requiring around 4 A in operation and thus powered by a bench-top power supply. The peltier elements obtained are relatively large devices (40 x 40 mm) and as such draw a substantial amount of power. Initially, the heaters that were to be used in the design were micro-counterparts of these Peltier elements, but due to availability they were not implemented. The use of more energy efficient heaters will allow for the downsizing of the PSU and heating system, which will greatly increase the device's portability. Temperature probes can be positioned better in future iterations, as multiple calibration tests were required in the current implementation.

The syringe pump used to create pressure driven flow in the current implementations has advantages in a prototyping environment. Flow rates can be adjusted on the fly allowing for rapid flow rate testing to be performed, but due to it's size can not be considered completely portable. A fully integrated PCR device requires the use of a micro-pump, or alternatively centrifugal driven

flow.

The device was fabricated in what can be considered a "low-tech" laboratory, when compared to the environments in which other research groups fabricate their microfluidic devices. This was initially a challenge, but due to the techniques and methodology required to fabricate in such an environment, some of these procedures show potential for automated scalable production. The device channels and lid bonding can be automated to allow large-scale production. The device, including heating, temperature control and flow control form a separate system from the microfluidics chip. This allows for the use of multiple microfluidic chips, possibly with a variety of channel geometries, to be used in the device.

The CO_2 laser ablation methodology for creating channels is easily up-scalable and commercial lasers should be able to theoretically fabricate thousands of chips a day. The bonding technique used requires a solvent, a mechanism for applying pressure to the device and an oven. Lids could be submerged into large solvent baths, and then placed in an oven with constant pressure applied to them. The connection of the external connectors needs to be revised in order for it to be performed with some autonomy.

Fabrication of a microfluidics device was demonstrated using "low-tech" machinery and techniques. Although successful in amplifying DNA rapidly, the devices can be improved in future iterations, allowing for the production of a fully-integrated μTAS.

6.2 Proposed specifications for future design.

The device proposed focuses on an implementation for use in-field and as such the specifications detailed outline criteria for such a device. The device should be fully portable, requiring no external equipment, adhere to low costs and simple operation. The following list details requirements that future devices should try to adhere to:

- portable-involving no external equipment
- low-cost
- robust-for use in-field
- easily up-scalable
- provide rapid diagnosis at a POC level
- low-power, can be battery or 220V operatable.

- reliable
- specific
- quantifiable
- simple to use
- easily integrateable (universal external connectors)
- preferably hand-held
- data output system

A future design is proposed in Table 6.1 which attempts to adhere to as many of the aforementioned criteria as possible, while still attempting to remain low-cost. The future design should be principally concerned with addressing the

Requirement Specifications				
Component	**Requirement**	**Implementation**	**Ease of fabrication/implementation**	**Cost**
Substrate	Biocompatibility	PMMA	Easy	+
	Ease of fabrication	PC	Easy	+
	Cheap	PDMS	Medium	+++
Heating element	Low energy	Micro-peltier elements	Easy	++
	Digitally controllable	Joule heating used metallic thin films	Hard	+++
	Appropriate dimensions	IR laser	Medium	++
	Accurate heating patterns			
Temperature control	Accurate	Custom built PID controller	Hard	+
	Reliable	Store bough digital thermocontroller	Easy	+
	Digital			
	Easily integrateable			
Fluid control	Portable	Micro-peristaltic pumps	Easy	++++
	Configurable flow rates	Micro-syringe pump	Easy	++++
	Low power	Motor-based centrifugal system	Medium	++
	Ideally programmable			
Lid	Air-tight	Solvent-assisted thermal bonding	Easy	+
	Simple procedure	Microwave assisted thermal bonding	Hard	++
	Reliable			
	Upscalable			
External connections	Cost efficient	In-house connection schema	Medium	+
	Easily implementable			
	As universal as possible			
Power supply	Small, portable	Battery powered regulator circuitry	Medium	++
	Battery or conventional plug powered	Regulation of 220 V wall input	Medium	+++

Table 6.1: Future design specification for a portable PCR device.

portability of the heating, fluid control and power supply systems. A reduction in these systems will greatly improve the portability of the future device.

6.3 Future development.

The following details concluding remarks for future development of this device:

- The heating system used should ideally be low power ($<$12 V), integrateable and easily controllable. Micro-Peltier elements provide an applicable solution.

- Improving the energy efficiency of the heating system will allow for a smaller power supply to be used. Ideally a custom built supply powered by batteries will be designed.
- The fluid control mechanism should be integrable and easily controllable, preferably programmable for interfacing with a microcontroller. Micro-persistaltic/syringe pumps are attractive for this purpose.
- The use of a micro-controller for control of the power supply, heating system and fluid flow would allow for a fully-programmable device capable of configurable parameters.
- The design should conform to low cost materials and fabrication techniques, while keeping mass production in mind.
- The device could contain an integrated sensing mechanism, be it on-board fluorescence detection or a means of resistive testing to confirm amplification post-PCR.

A fully-integrated, portable PCR device is possible with current technologies and materials. The proposed design aims to help guide future researchers towards a more LOC approach. The use of a micro-controller will allow for the configurability of the subsystems and allowing device parameters to be fine-tuned for specific applications. These devices show potential to solving a number of critical health issues pertaining to early diagnosis and accessibility and the fabrication of a portable PCR device will aid in this pursuit.

Appendices

Appendix A

Technical drawings

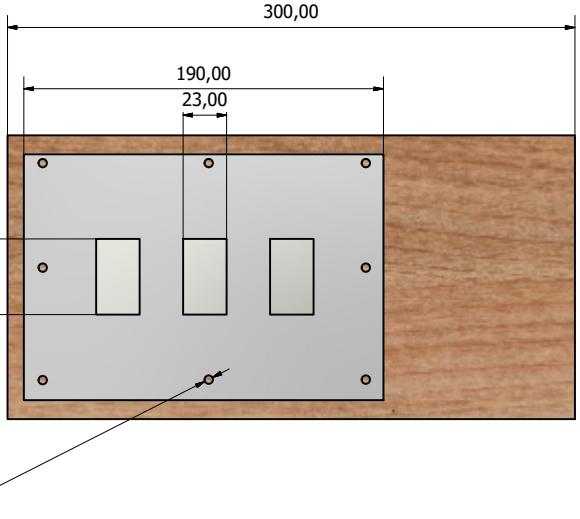

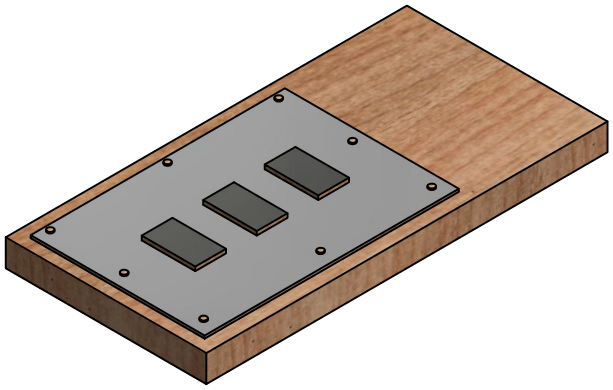

Designed by	Checked by	Approved by	Date		Date	
Giles					2018/11/26	

Device base with heaters and steel plate

Edition	Sheet
	1 / 1

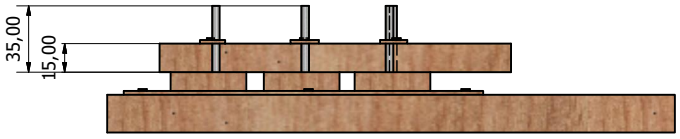

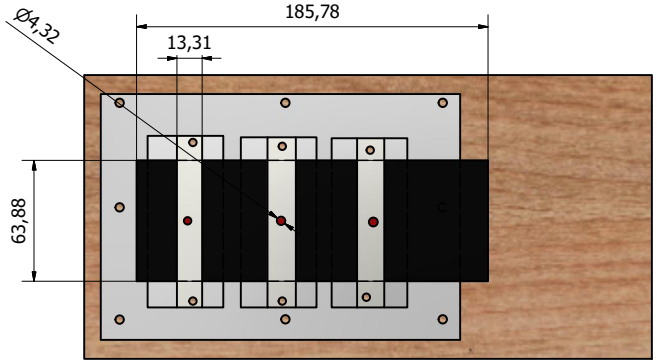

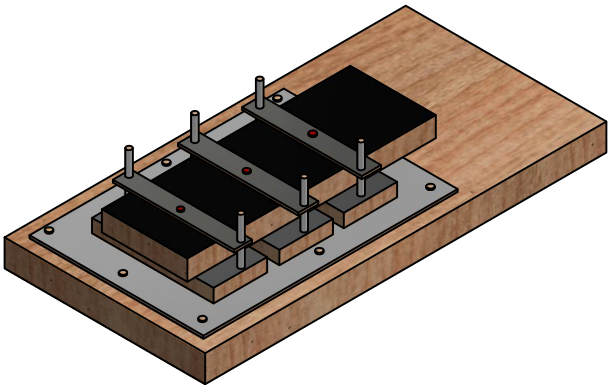

Designed by	Checked by	Approved by	Date		Date	
Giles					2018/11/26	

Device with chip, thermoprobes and fasteners in place

Edition	Sheet
	1 / 1

Appendix B

Datasheets

GM250-127-14-16

Thermoelectric generator module

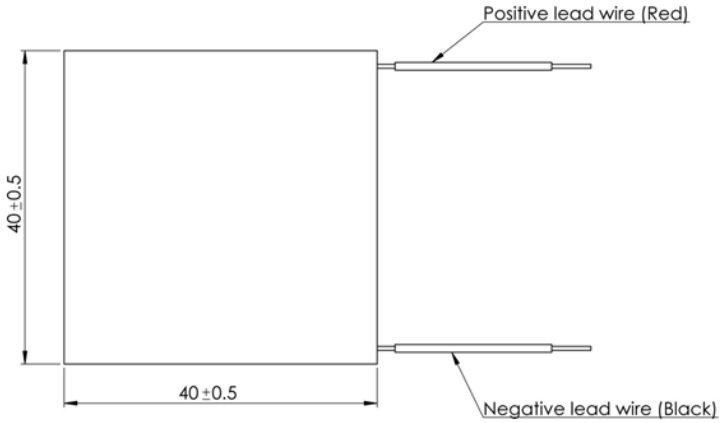

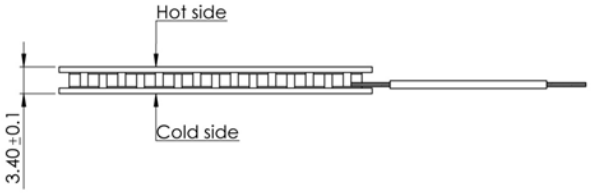

Parameters for hot side temp 250°C and cold side temp 30°C

Matched load output power	6.99W
Matched load resistance	3.65Ω ± 15%
Open circuit voltage	10.11V
Matched load output	1.38A
Matched load output voltage	5.05V
Heat flow through module	~ 139.8W
Maximum compress (non-destructive)	1.2MPa
Maximum operation temperature	Hot side - 250°C. Cold side - 175°C

Features

- Compact structure (no moving parts)
- Reliable performance
- Maintenance-free
- Noise-free operation
- Low-carbon, green technology

Adaptive® Power Management

Web: www.etdyn.com Tel: +44(0)116 279 6899 E-mail: info@etdyn.com

GM250-127-14-16

Thermoelectric generator module

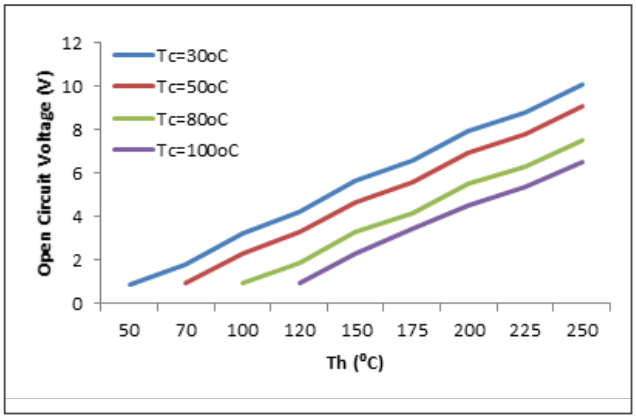

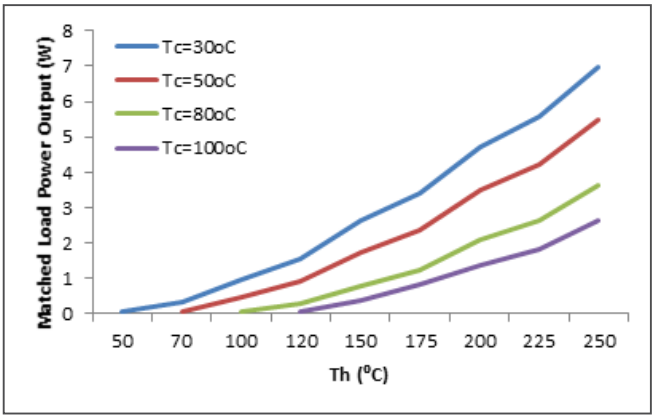

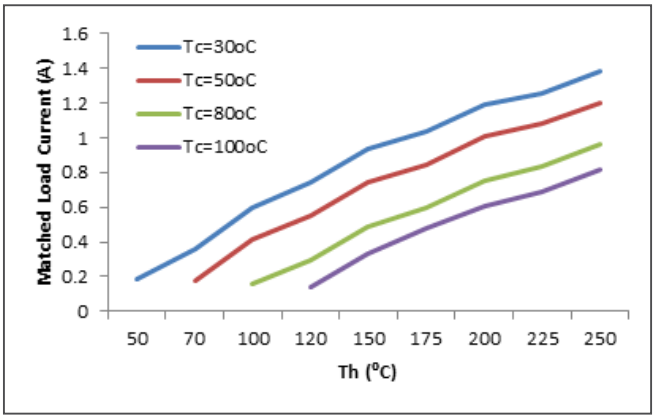

Note: Th = hot side temperature

Adaptive® Power Management

GM250-127-14-16

Thermoelectric generator module

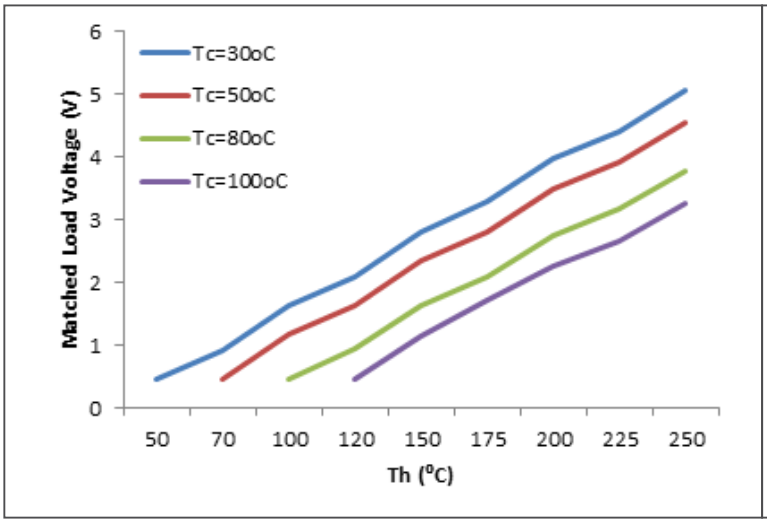

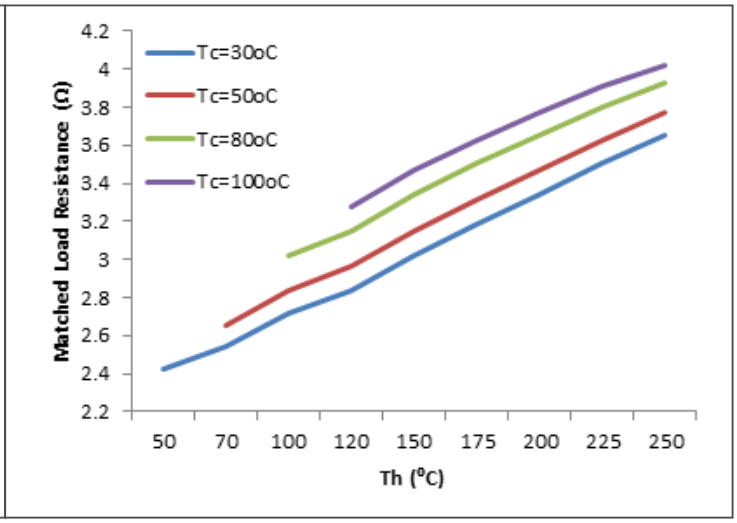

Note: Th = hot side temperature

GM250-127-14-16

Thermoelectric generator module

Formulae for calculating thermoelectric properties (best fit derived from measured material characteristics)

Thermal conductivity

- $k_n = (0.0000334545 \times T^2 - 0.023350303 \times T + 5.606333)$ W/mK
- $k_p = (0.0000361558 \times T^2 - 0.026351342 \times T + 6.22162)$ W/mK

Seebeck coefficient

- $a_n = (0.001530736 \times T^2 - 1.08058874 \times T - 28.338095) \times 10^{-6}$ V/K
- $a_p = (-0.003638095 \times T^2 + 2.74380952 \times T - 296.214286) \times 10^{-6}$ V/K

Electrical conductivity

- $o_p = (0.015601732 \times T^2 - 15.708052 \times T + 4466.38095) \times 10^2$ S/m
- $o_n = (0.01057143 \times T^2 - 10.16048 \times T + 3113.71429) \times 10^2$ S/m

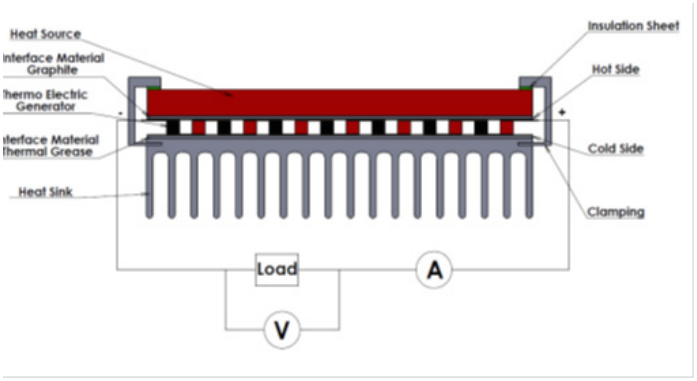

Where the subscript *n* refers to the n-type thermoelement and the subscript *p* refers to the p-type thermoelement.It should be noted here that the electrical conductivity relates to the electrical resistivity as follows: p = 1/o Thus, where electrical resistivity is needed, one can calculate the electrical conductivity through the aforementioned formulae and then reverse to calculate the electrical resistivity.

W1209 Temperature Control Switch

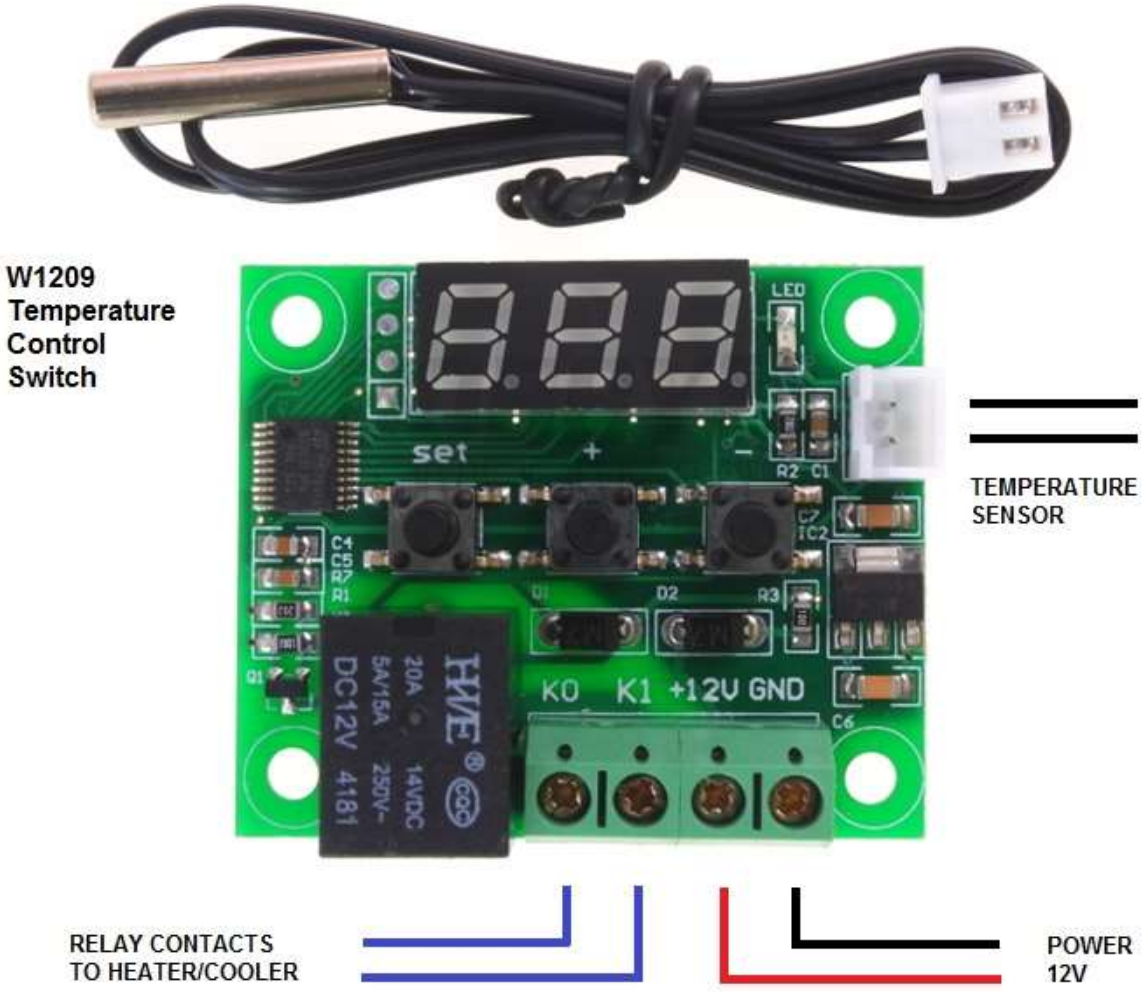

DESCRIPTION:

The W1209 is an incredibly low cost yet highly functional thermostat controller. With this module you can intelligently control power to most types of electrical device based on the temperature sensed by the included high accuracy NTC temperature sensor. Although this module has an embedded microcontroller no programming knowledge is required. 3 tactile switches allow for configuring various parameters including on & off trigger temperatures. The on board relay can switch up to a maximum of 240V AC at 5A or 14V DC at 10A. The current temperature is displayed in degrees Centigrade via its 3 digit seven segment display and the current relay state by an on board LED.

SPECIFICATION:

Temperature Control Range: -50 ~ 110 C
Resolution at -9.9 to 99.9: 0.1 C
Resolution at all other temperatures: 1 C
Measurement Accuracy: 0.1 C
Control Accuracy: 0.1 C
Refresh Rate: 0.5 Seconds
Input Power (DC): 12V
Measuring Inputs: NTC (10K 0.5%)
Waterproof Sensor: 0.5M
Output: 1 Channel Relay Output, Capacity: 10A

Power Consumption
Static Current: <=35mA
Current: <=65mA

Environmental Requirements
Temperature: -10 ~ 60 C
Humidity: 20-85%

Dimensions
48mm x 40mm x 14mm

Settings Chart
Long press the “SET” button to activate the menu.

Code Description Range Default Value
P0 Heat C/H C
P1 Backlash Set 0.1-15 2
P2 Upper Limit 110 110
P3 Lower Limit -50 -50
P4 Correction -7.0 ~ 7.0 0
P5 Delay Start Time 0-10 mins 0
P6 High Temperature Alarm 0-110 OFF

Long pressing +- will reset all values to their default

Displaying the current temperature:
The thermostat will display the current temperature in oC by default. When in any other mode making no input for approximately 5 seconds will cause the thermostat to return to this default display.

Setting the trigger temperature:
To set the trigger temperature press the button marked 'SET'. The seven segment display will flash. You can now set a trigger temperature (in oC) using the '+' and '-' buttons in 0.1 degree increments. If no buttons are pressed for approximately 2 seconds the trigger temperature will be stored and the display will return back to the current temperature.

Setting the parameters:
To set any parameter first long press the 'SET' button for at least 5 seconds. The seven segment display should now display 'P0'. This represents parameter P0. Pressing the '+' or '-' buttons will cycle though the various parameters (P0 to P6). Pressing the 'SET' button whilst any of there parameters are displayed will allow you to change the value for that parameter using the '+' and '-' buttons (see below). When finished setting a parameter press the set button to exit that option. If no buttons are pressed for approximately 5 seconds the thermostat will exit the parameter options and will return back to the default temperature display.

Setting the cooling or heating parameter P0:
The parameter P0 has two settings, C and H. When set to C (default) the relay will energise when the temperature is reached. Use this setting if connecting to an air-conditioning system. When set to H the relay will de-energise when the temperature is reached. Use this setting if controlling a heating device.

Setting the hysteresis parameter P1:
This sets how much change in temperature must occur before the relay will change state. For example if set to the default 2oC and the the trigger temperature has been set to 25oC, it will not de-energise until the temperature falls back below below 23oC. Setting this hysteresis helps stop the thermostat from continually triggering when the temperature drifts around the trip temperature.

Setting the upper limit of the thermostat parameter P2:
This parameter limits the maximum trigger temperature that can be set. It can be used as a safety to stop an excessively high trigger temperature from accidentally being set by the user.

Setting the lower limit of the thermostat parameter P3:
This parameter limits the minimum trigger temperature that can be set. It can be used as a safety to stop an excessively low trigger temperature from accidentally being set by the user.

Setting temperature offset correction parameter P4:
Should you find there is a difference between the displayed temperature and the actual temperature (for instance if the temperature probe is on a long run of cable) you can make minor corrections to the temperature reading with this parameter.

Setting the trigger delay parameter P5:
This parameter allows for delaying switching of the relay when the trigger temperature has be reached. The parameter can be set in one minute increments up to a maximum of 10 minutes.

Setting the high temperature alarm parameter P6:
Setting a value for this parameter will cause the relay to switch off when the the temperature reaches this setting. The seven segment display will also show '---' to indicate an alarm condition. The relay will not re-energise until the temperature falls below this value. The default setting is OFF.

Mounting instructions

1 Soldering

1.1 Leaded NTC thermistors

Leaded thermistors comply with the solderability requirements specified by CECC.

When soldering, care must be taken that the NTC thermistors are not damaged by excessive heat. The following maximum temperatures, maximum time spans and minimum distances have to be observed:

	Dip soldering	*Iron soldering*
Bath temperature	max. 260 °C	max. 360 °C
Soldering time	max. 4 s	max. 2 s
Distance from thermistor	min. 6 mm	min. 6 mm

Under more severe soldering conditions the resistance may change.

1.2 Leadless NTC thermistors

In case of NTC thermistors without leads, soldering is restricted to devices which are provided with a solderable metallization. The temperature shock caused by the application of hot solder may produce fine cracks in the ceramic, resulting in changes in resistance.

To prevent leaching of the metallization, solder with silver additives or with a low tin content should be used. In addition, soldering methods should be employed which permit short soldering times.

1.3 SMD NTC thermistors

SMD NTC thermistors can be provided with a nickel barrier termination or on special request with silver-palladium termination. The usage of mild, non-activated fluxes for soldering is recommended as well as a proper cleaning of the PCB.

- Nickel barrier termination

The nickel barrier layer of the silver/nickel/tin termination (see figure 1) prevents leaching of the silver base metalization layer. This allows great flexibility in the selection of soldering parameters.

The tin prevents the nickel layer from oxidizing and thus ensures better wetting by the solder. The nickel barrier termination is suitable for all commonly-used soldering methods.

Note: SMD NTCs with AgPd termination are not approved for lead-free soldering.

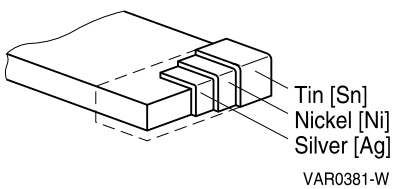

Figure 1

SMD NTC thermistors, structure of nickel barrier termination

1.3.1 Solderability (test to IEC 60068-2-58)

Preconditioning: Immersion into flux F-SW 32.
Evaluation criterion: Wetting of soldering areas ≥95%.

Solder	Bath temperature (°C)	Dwell time (s)
SnPb 60/40	215 ±3	3 ±0.3
SnAg (3.0 ... 4.0), Cu (0.5 ... 0.9)	245 ±3	3 ±0.3

1.3.2 Resistance to soldering heat (test to IEC 60068-2-58)

Preconditioning: Immersion into flux F-SW 32.
Evaluation criterion: Leaching of side edges ≤1/3.

Solder	Bath temperature (°C)	Dwell time (s)
SnPb 60/40	260 ±5	10 ±1
SnAg (3.0 ... 4.0), Cu (0.5 ... 0.9)	260 ±5	10 ±1

Wave soldering

Temperature characteristic at component terminal with dual wave soldering

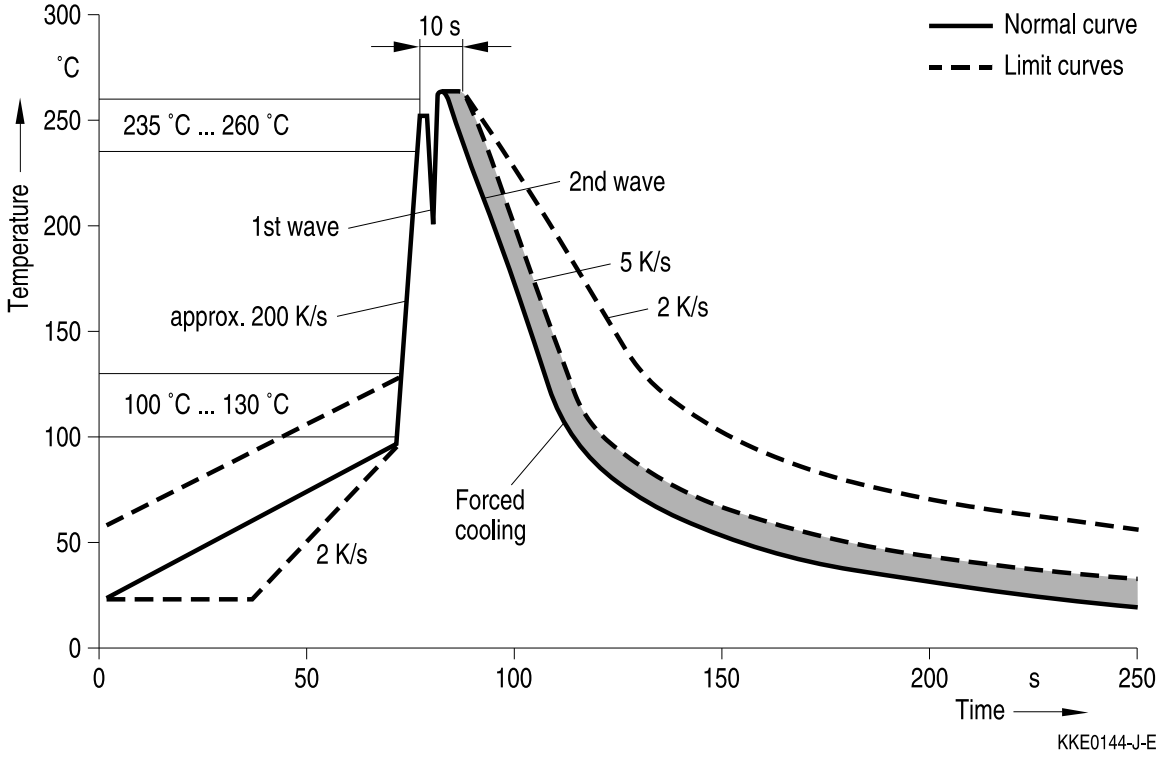

Solder joint profiles for silver/nickel/tin terminations

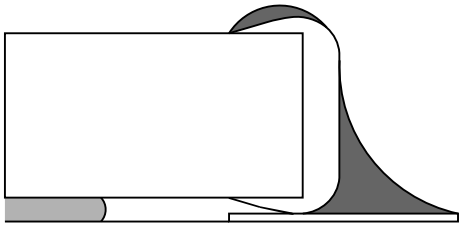

Good solder joint KKE0287-9-E

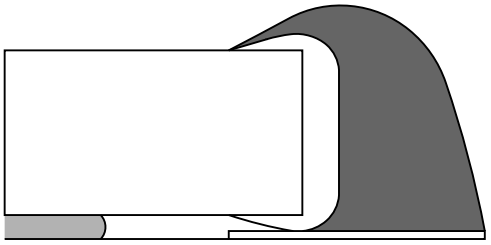

Too much solder
Pad geometry too large,
not soldered in preferred direction KKE0288-H-E

Reflow soldering

Recommended temperature characteristic for reflow soldering following JEDEC J-STD-020D

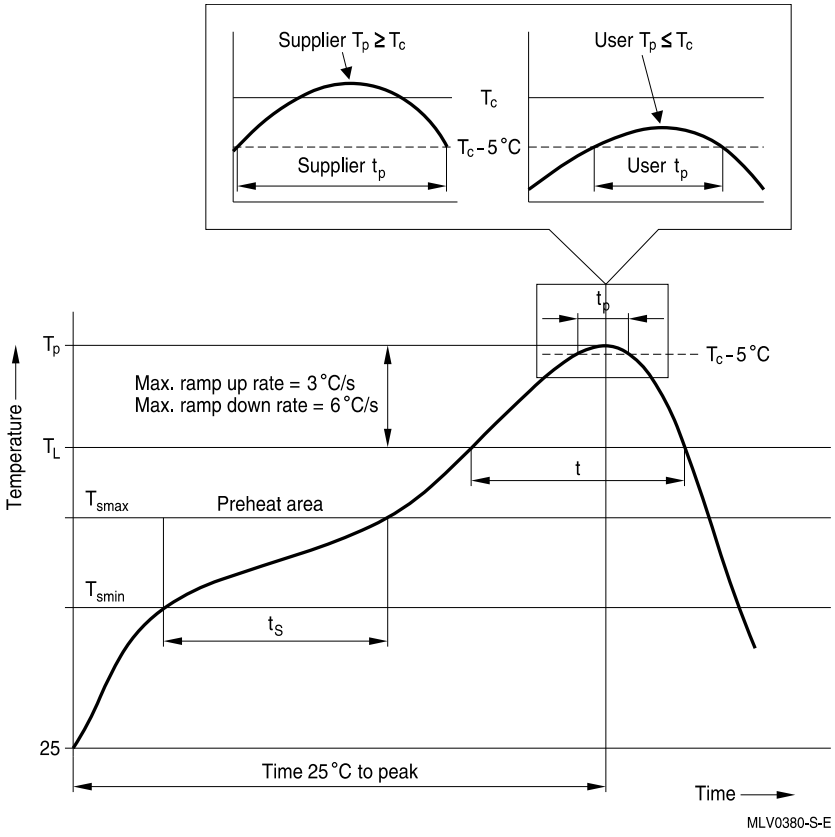

Profile feature		Sn-Pb eutectic assembly	Pb-free assembly
Preheat and soak - Temperature min - Temperature max - Time	 T_{smin} T_{smax} t_{smin} to t_{smax}	 100 °C 150 °C 60 ... 120 s	 150 °C 200 °C 60 ... 180 s
Average ramp-up rate	T_{smax} to T_p	3 °C/ s max.	3 °C/ s max.
Liquidous temperature Time at liquidous	T_L t_L	183 °C 60 ... 150 s	217 °C 60 ... 150 s
Peak package body temperature	T_p [1)]	220 °C ... 235 °C [2)]	245 °C ... 260 °C [2)]
Time (t_P) [3)] within 5 °C of specified classification temperature (T_c)		20 s [3)]	30 s [3)]
Average ramp-down rate	T_p to T_{smax}	6 °C/ s max.	6 °C/ s max.
Time 25 °C to peak temperature		maximum 6 min	maximum 8 min

1) Tolerance for peak profile temperature (T_P) is defined as a supplier minimum and a user maximum.
2) Depending on package thickness. For details please refer to JEDEC J-STD-020D.
3) Tolerance for time at peak profile temperature (t_P) is defined as a supplier minimum and a user maximum.

Note: All temperatures refer to topside of the package, measured on the package body surface. Number of reflow cycles: 3

Solder joint profiles for silver/nickel/tin terminations

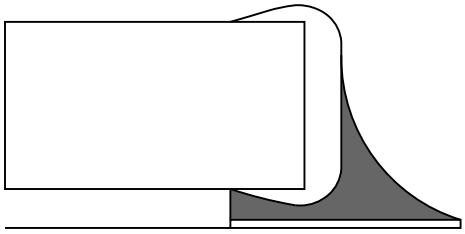

Good solder joint TNT0565-G-E

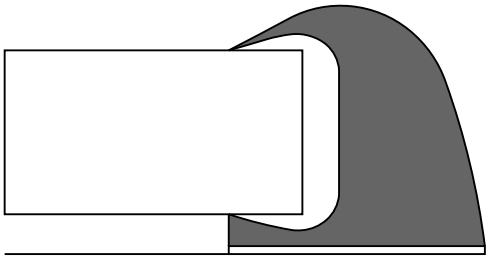

Too much solder
Pad geometry too large KKE0071-A-E

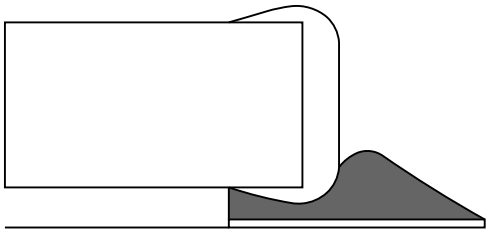

Poor wetting KKE0072-I-E

1.3.3 Recommended geometry of solder pads

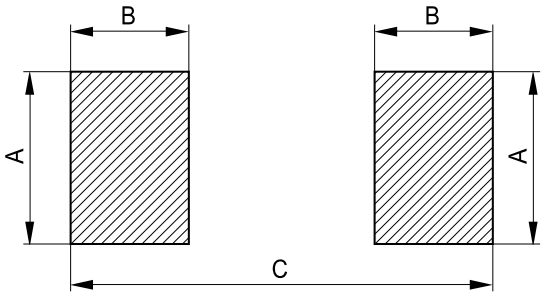

KKE0092-X

Recommended maximum dimensions (mm)

Case size inch/mm	A	B	C
0402/1005	0.6	0.6	1.7
0603/1608	1.0	1.0	3.0
0805/2012	1.3	1.2	3.4
1206/3216	1.8	1.2	4.5

1.3.4 Notes

Iron soldering should be avoided, hot air methods are recommended for repair purposes.

2 Conductive adhesion

An alternative to soldering is the gluing of thermistors with conductive adhesives. The benefit of this method is that it involves no thermal stress. The adhesives used must be chemically inert.

3 Clamp contacting

Pressure contacting by means of clamps is particularly suitable for applications involving frequent switching and high turn-on powers.

4 Robustness of terminations (leaded types)

The leads meet the requirements of IEC 60068-2-21. They may not be bent closer than 4 mm from the solder joint on the thermistor body or from the point at which they leave the feed-throughs. During bending, any mechanical stress at the outlet of the leads must be removed. The bending radius should be at least 0.75 mm.

Tensile strength: Test Ua1:

Leads		∅ ≤0.25 mm =	1.0 N
	0.25 <	∅ ≤0.35 mm =	2.5 N
	0.35 <	∅ ≤0.50 mm =	5.0 N
	0.50 <	∅ ≤0.80 mm =	10.0 N
	0.80 <	∅ ≤1.25 mm =	20.0 N

Bending strength: Test Ub:

Two 90°-bends in opposite directions at a weight of 0.25 kg.

Torsional strength: Test Uc: severity 2

The lead is bent by 90° at a distance of 6 to 6.5 mm from the thermistor body.

The bending radius of the leads should be approx. 0.75 mm. Two torsions of 180° each (severity 2).

When subjecting leads to mechanical stress, the following should be observed:

Tensile stress on leads

During mounting and operation tensile forces on the leads are to be avoided.

Bending of leads

Bending of the leads directly on the thermistor body is not permissible.

A lead may be bent at a minimum distance of twice the wire's diameter +2 mm from the solder joint on the thermistor body. During bending the wire must be mechanically relieved at its outlet. The bending radius should be at least 0.75 mm.

Bibliography

[1] "Electroosmosis." [Online]. Available: http://www.kirbyresearch.com/microfluidicsnanofluidicsch6.html

[2] A. Gerardino, "Top-Down approach to nanotechnology for cell-on-chip applications . TOP-DOWN APPROACH TO NANOTECHNOLOGY FOR CELL-ON-CHIP APPLICATIONS," no. May 2014, 2010.

[3] J. Giboz, T. Copponnex, and P. Mélé, "Microinjection molding of thermoplastic polymers: A review," *Journal of Micromechanics and Microengineering*, vol. 17, no. 6, 2007.

[4] "Structure of the double helix - geneed - genetics, education, discovery." [Online]. Available: https://geneed.nlm.nih.gov/topic$_s$*ubtopic.php?tid* = 15*sid* = 16

[5] N. Scholars, "Enzyme structure and function â catalysis | chemical kinetics," Oct 2018. [Online]. Available: https://nigerianscholars.com/tutorials/kinetics/enzyme-structure-and-function/

[6] "Pcr cycling parameters-six key considerations for success." [Online]. Available: https://www.thermofisher.com/za/en/home/life-science/cloning/cloning-learning-center/invitrogen-school-of-molecular-biology/pcr-education/pcr-reagents-enzymes/pcr-cycling-considerations.html

[7] Y. Matsubara, K. Kerman, M. Kobayashi, S. Yamamura, Y. Morita, and E. Tamiya, "Microchamber array based DNA quantification and specific sequence detection from a single copy via PCR in nanoliter volumes," *Biosensors and Bioelectronics*, vol. 20, no. 8 SPEC. ISS., pp. 1482–1490, 2005.

[8] D. Moschou, N. Vourdas, G. Kokkoris, G. Papadakis, J. Parthenios, S. Chatzandroulis, and A. Tserepi, "All-plastic, low-power, disposable, continuous-flow pcr chip with integrated microheaters for rapid dna amplification," *Sensors and Actuators B: Chemical*, vol. 199, pp. 470 – 478, 2014. [Online]. Available: http://www.sciencedirect.com/science/article/pii/S0925400514004079

[9] J. Hong, A. J. Demello, and S. N. Jayasinghe, "Bio-electrospraying and droplet-based microfluidics: Control of cell numbers within living residues," *Biomedical Materials*, vol. 5, no. 2, 2010.

[10] K. J. Shaw, P. T. Docker, J. V. Yelland, C. E. Dyer, J. Greenman, G. M. Greenway, and S. J. Haswell, "Rapid PCR amplification using a microfluidic device with integrated microwave heating and air impingement cooling," *Lab on a Chip*, vol. 10, no. 13, pp. 1725–1728, 2010.

[11] "How to choose the right microfluidic flow control system?" [Online]. Available: https://www.elveflow.com/microfluidic-tutorials/microfluidic-reviews-and-tutorials/how-to-choose-right-microfluidic-flow-control-system/

[12] C.-W. Tsao, "Polymer microfluidics: Simple, low-cost fabrication process bridging academic lab research to commercialized production," *Micromachines*, vol. 7, p. 225, 12 2016.

[13] L. J. Fitzpatrick and J. R. Dean, "Extraction solvent selection in environmental analysis," *Analytical Chemistry*, vol. 74, no. 1, pp. 74–79, 2002.

[14] G. M. Whitesides, "The origins and the future of microfluidics," *Nature*, vol. 442, no. 7101, pp. 368–373, 2006.

[15] K. Orrling, P. Nilsson, M. Gullberg, and M. Larhed, "An efficient method to perform milliliter-scale PCR utilizing highly controlled microwave thermocycling." *Chemical communications (Cambridge, England)*, no. 7, pp. 790–1, 2004. [Online]. Available: http://www.ncbi.nlm.nih.gov/pubmed/15045065

[16] J. Khandurina, T. E. McKnight, S. C. Jacobson, L. C. Waters, R. S. Foote, and J. M. Ramsey, "Integrated system for rapid PCR-based DNA analysis in microfluidic devices," *Analytical Chemistry*, vol. 72, no. 13, pp. 2995–3000, 2000.

[17] M. Hashimoto, P. C. Chen, M. W. Mitchell, D. E. Nikitopoulos, S. A. Soper, and M. C. Murphy, "Rapid PCR in a continuous flow device," *Lab on a Chip*, vol. 4, no. 6, pp. 638–645, 2004.

[18] P. Liu, T. S. Seo, N. Beyor, K. J. Shin, J. R. Scherer, and R. A. Mathies, "Integrated portable polymerase chain reaction-capillary electrophoresis microsystem for rapid forensic short tandem repeat typing," *Analytical Chemistry*, vol. 79, no. 5, pp. 1881–1889, 2007.

[19] M. Amasia, M. Cozzens, and M. J. Madou, "Centrifugal microfluidic platform for rapid PCR amplification using integrated thermoelectric heating and ice-valving," *Sensors and Actuators, B: Chemical*, vol. 161, no. 1, pp. 1191–1197, 2012.

[20] S. L. Anna, N. Bontoux, and H. A. Stone, "Formation of dispersions using "flow focusing" in microchannels," *Applied Physics Letters*, vol. 82, no. 3, pp. 364–366, 2003.

[21] G. M. Walker and D. J. Beebe, "A passive pumping method for microfluidic devices," *Lab on a Chip*, vol. 2, no. 3, pp. 131–134, 2002.

[22] "Hiv and AIDS in Southern Africa," ://www.avert.org/professionals/hiv-around-world/sub-saharan-africa/south-africa.

[23] "www.unaids.org/en/regionscountries/countries/southafrica," ://www.unaids.org/en/regionscountries/countries/southafrica.

[24] "Genetic Testing for HIV," ://stanfordhealthcare.org/medical-conditions/sexual-and-reproductive-health/hiv-aids/diagnosis/genetic-testing.html.

[25] S. C. Terry, J. H. Herman, and J. B. Angell, "A Gas Chromatographic Air Analyzer Fabricated on a Silicon Wafer," *IEEE Transactions on Electron Devices*, vol. 26, no. 12, pp. 1880–1886, 1979.

[26] B. Giri, "Introduction to Microfluidics," *Laboratory Methods in Microfluidics*, pp. 1–7, 2017. [Online]. Available: http://linkinghub.elsevier.com/retrieve/pii/B9780128132357000015

[27] J. C. T. Eijkel and A. V. den Berg, "The use of capillarity for passive flow handling in lab on a chip devices," vol. 6, 2006.

[28] UTP, "Informe De Caracterización De Vertimientos Propios De La Actividad De La Minería De Oro En Risaralda," vol. 8, no. 6, pp. 1–30, 2017.

[29] A. Olanrewaju, M. Beaugrand, M. Yafia, and D. Juncker, "Capillary microfluidics in microchannels: From microfluidic networks to capillaric circuits," *Lab on a Chip*, vol. 18, no. 16, pp. 2323–2347, 2018.

[30] H. A.Manz, N.Graber, "Miniaturized total chemical analysis systems: A novel concept for chemical sensing," vol. 1, no. 6, pp. 244–248, 1990.

[31] N. B. A. Manz, C. S. Effenhauser, "Electroosmotic pumping and electrophoretic separa- tion for miniaturised chemical analysis systems," vol. 4, p. 257â265, 1994.

[32] A. M. a. T. F. von Heeren, E. Verpoorte, "Electroosmotic pumping and electrophoretic separa- tion for miniaturisMicellar electrokinetic chromatography separations and analyses of biological samples on a cyclic planar microstructure," *Anal. Chem.*, vol. 68, p. 2044â2053, 1996.

[33] S. Zeng, C. H. Chen, J. C. Mikkelsen, and J. G. Santiago, "Fabrication and characterization of electroosmotic micropumps," *Sensors and Actuators, B: Chemical*, vol. 79, no. 2-3, pp. 107–114, 2001.

[34] S. Liu and P. K. Dasgupta, "Flow-injection analysis in the capillary format using electroosmotic pumping," *Analytica Chimica Acta*, vol. 268, no. 1, pp. 1–6, 1992.

[35] B. Çetin and D. Li, "Dielectrophoresis in microfluidics technology," *Electrophoresis*, vol. 32, no. 18, pp. 2410–2427, 2011.

[36] J. Wehking, "Electrohydrodynamic Manipulation of Liquid Droplet Emulsions in a," 2013.

[37] G. Masahide and W. Masao, "Self-propulsion of a water droplet in an electric field," *Journal of Physics D: Applied Physics*, vol. 38, pp. 2417–2423, 2005.

[38] F. e. a. Incropera, *Introduction to Heat Transfer 5th edition.*, 2006.

[39] P. Rai-Choudhury, *Handbook of microlithography, micromachining, and microfabrication: microlithography*, 1997.

[40] C. Iliescu, H. Taylor, M. Avram, J. Miao, and S. Franssila, "A practical guide for the fabrication of microfluidic devices using glass and silicon," *Biomicrofluidics*, vol. 6, no. 1, pp. 1–16, 2012.

[41] C. Zhang and D. Xing, "Miniaturized PCR chips for nucleic acid amplification and analysis: Latest advances and future trends," *Nucleic Acids Research*, vol. 35, no. 13, pp. 4223–4237, 2007.

[42] S. Ji, C. Academy, C. Ye, C. Academy, and S. Ji, "Thermal response of transparent silver nanowire / PEDOT : PSS film heaters Thermal Response of Transparent Silver Nanowire / PEDOT : PSS Film Heaters," no. December 2014, 2015.

[43] w. MicroChemicalsÂ®, "Lift off photolithography."

[44] K. L. Berkowski, K. N. Plunkett, Q. Yu, and J. S. Moore, "Introduction to Photolithography : Preparation of Microscale Polymer Silhouettes W," vol. 82, no. 9, 2005.

[45] "SU-8 Photoresists,Copyright Â© 2018 MicroChem Corp." ://www.microchem.com/Prod-SU8.htm.

[46] F. Laermer, S. Franssila, L. Sainiemi, and K. Kolari, "Chapter 21 - deep reactive ion etching," in *Handbook of Silicon Based MEMS Materials and Technologies (Second Edition)*, second edition ed., ser. Micro and Nano Technologies, M. Tilli, T. Motooka, V.-M. Airaksinen, S. Franssila, M. Paulasto-KrÃ¶ckel, and V. Lindroos, Eds. Boston: William Andrew Publishing, 2015, pp. 444 – 469. [Online]. Available: http://www.sciencedirect.com/science/article/pii/B978032329965700021X

[47] R. Dussart, T. Tillocher, P. Lefaucheux, and M. Boufnichel, "Plasma cryogenic etching of silicon: From the early days to today's advanced technologies," *Journal of Physics D: Applied Physics*, vol. 47, p. 123001, 03 2014.

[48] M. Morita, T. Ohmi, E. Hasegawa, M. Kawakami, and M. Ohwada, "Growth of native oxide on a silicon surface," *Journal of Applied Physics*, vol. 68, no. 3, pp. 1272–1281, 1990.

[49] J. Haneveld, H. Jansen, E. Berenschot, N. Tas, and M. Elwenspoek, "Wet anisotropic etching for fluidic 1D nanochannels," *Journal of Micromechanics and Microengineering*, vol. 13, no. 4, pp. 3–7, 2003.

[50] S. Tang and G. Whitesides, "Basic microfluidic and soft lithographic techniques," *Optofluidics: Fundamentals, Devices, and Applications*, pp. 7–32, 2010. [Online]. Available: http://www2.egr.uh.edu/ nvaradar/private/Refs/Litho.pdf

[51] H. Becker and L. E. Locascio, "Polymer microfluidic devices," *Talanta*, vol. 56, no. 2, pp. 267 – 287, 2002. [Online]. Available: http://www.sciencedirect.com/science/article/pii/S003991400100594X

[52] J. Friend and L. Yeo, "Fabrication of microfluidic devices using polydimethylsiloxane," *Biomicrofluidics*, vol. 4, no. 2, pp. 1–5, 2010.

[53] L. E. Locascio, C. E. Perso, and C. S. Lee, "Measurement of electroosmotic flow in plastic imprinted microfluid devices and the effect of protein adsorption on flow rate," *Journal of Chromatography A*, vol. 857, no. 1, pp. 275 – 284, 1999. [Online]. Available: http://www.sciencedirect.com/science/article/pii/S0021967399007748

[54] H.-J. Chiang, S.-L. Yeh, C.-C. Peng, W.-H. Liao, and Y.-C. Tung, "Polydimethylsiloxane-polycarbonate Microfluidic Devices for Cell Migration Studies Under Perpendicular Chemical and Oxygen Gradients," *Journal of Visualized Experiments*, no. 120, pp. 1–8, 2017. [Online]. Available: http://www.jove.com/video/55292/polydimethylsiloxane-polycarbonate-microfluidic-devices-for-cell

[55] J. Chen, Y. Lin, and G. Chen, "Fabrication of poly(methyl methacrylate) microfluidic chips by redox-initiated polymerization," *Electrophoresis*, vol. 28, no. 16, pp. 2897–2903, 2007.

[56] X. Zhang, Z. Zhu, Z. Ni, N. Xiang, and H. Yi, "Inexpensive, rapid fabrication of polymer-film microfluidic autoregulatory valve for disposable microfluidics," *Biomedical Microdevices*, vol. 19, no. 2, pp. 1–9, 2017.

[57] C. I. Rogers, J. B. Oxborrow, R. R. Anderson, L.-F. Tsai, G. P. Nordin, and A. T. Woolley, "Microfluidic valves made from polymerized polyethylene glycol diacrylate," *Sensors and Actuators B: Chemical*, vol. 191, pp. 438 – 444, 2014. [Online]. Available: http://www.sciencedirect.com/science/article/pii/S092540051301191X

[58] C. W. Tsao and D. L. DeVoe, "Bonding of thermoplastic polymer microfluidics," *Microfluidics and Nanofluidics*, vol. 6, no. 1, pp. 1–16, 2009.

[59] J. H. Wang, L. J. Chien, T. M. Hsieh, C. H. Luo, W. P. Chou, P. H. Chen, P. J. Chen, D. S. Lee, and G. B. Lee, "A miniaturized quantitative polymerase chain reaction system for DNA amplification and detection," *Sensors and Actuators, B: Chemical*, vol. 141, no. 1, pp. 329–337, 2009.

[60] D. C. Duffy, J. C. Mcdonald, O. J. A. Schu, and G. M. Whitesides, "Polydimethylsiloxane (PDMS) on SU-8 Mold," vol. 73246, no. 617, pp. 2–4, 1998.

[61] S. A. Soper, K. Brown, A. Ellington, B. Frazier, G. Garcia-Manero, V. Gau, S. I. Gutman, D. F. Hayes, B. Korte, J. L. Landers, D. Larson, F. Ligler, A. Majumdar, M. Mascini, D. Nolte, Z. Rosenzweig, J. Wang, and D. Wilson, "Point-of-care biosensor systems for cancer diagnostics/prognostics," *Biosensors and Bioelectronics*, vol. 21, no. 10, pp. 1932 – 1942, 2006. [Online]. Available: http://www.sciencedirect.com/science/article/pii/S0956566306000121

[62] B. . Jo, L. M. V. Lerberghe, K. M. Motsegood, and D. J. Beebe, "Three-dimensional micro-channel fabrication in polydimethylsiloxane (pdms) elastomer," *Journal of Microelectromechanical Systems*, vol. 9, no. 1, pp. 76–81, March 2000.

[63] Robert Langer and A. Jaklenec, "Fabrication of fillable microparticles and other complex 3D microstructures," *Materials Science*, vol. 1142, no. September, pp. 1138–1142, 2017.

[64] U. M. Attia, S. Marson, and J. R. Alcock, "Micro-injection moulding of polymer microfluidic devices," *Microfluidics and Nanofluidics*, vol. 7, no. 1, pp. 1–28, 2009.

[65] S. C. Chen, W. R. Jong, Y. J. Chang, J. A. Chang, and J. C. Cin, "Rapid mold temperature variation for assisting the micro injection of high aspect ratio microfeature parts using induction heating technology," *Journal of Micromechanics and Microengineering*, vol. 16, no. 9, pp. 1783–1791, 2006.

[66] D. Yao and B. Kim, "Development of rapid heating and cooling systems for injection molding applications," *Polymer Engineering and Science*, vol. 42, no. 12, pp. 2471–2481, 2002.

[67] "Micro & nano technologies published 2008 1." vol. 0, p. 8155, 2008.

[68] L. P. D. Melo, G. V. Salmoria, E. A. Fancello, and C. R. D. M. Roesler, "Influence of Processing Conditions on the Mechanical Behavior and Morphology of Injection Molded Poly(lactic-co-glycolic acid) 85:15," *International Journal of Biomaterials*, vol. 2017, no. 2005, 2017.

[69] L. Martynova, L. E. Locascio, M. Gaitan, G. W. Kramer, R. G. Christensen, and W. A. MacCrehan, "Fabrication of plastic microfluid channels by imprinting methods," *Analytical Chemistry*, vol. 69, no. 23, pp. 4783–4789, 1997, pMID: 9406529. [Online]. Available: https://doi.org/10.1021/ac970558y

[70] J. Han, J. Han, B. S. Lee, J. Lim, S. M. Kim, H. Kim, and S. Kang, "Elimination of nanovoids induced during electroforming of metallic nanostamps with high-aspect-ratio nanostructures by the pulse reverse current electroforming process," *Journal of Micromechanics and Microengineering*, vol. 22, no. 6, 2012.

[71] R. M. McCormick, R. J. Nelson, M. G. Alonso-Amigo, D. J. Benvegnu, and H. H. Hooper, "Microchannel Electrophoretic Separations of DNA in Injection-Molded Plastic Substrates," *Analytical Chemistry*, vol. 69, no. 14, pp. 2626–2630, 1997.

[72] H. Wilski, "The radiation induced degradation of polymers," *International Journal of Radiation Applications and Instrumentation. Part C. Radiation Physics and Chemistry*, vol. 29, no. 1, pp. 1 – 14, 1987. [Online]. Available: http://www.sciencedirect.com/science/article/pii/1359019787900543

[73] A. d. C. Eduard Arzt, "Fabrication Approaches for Generating Complex Micro- and Nanopatterns on Polymeric Surfaces," *Journal of Physics: Conference Series*, vol. 326, no. 1, 2011.

[74] Y. Wang, Y. Xie, P. Wei, R. B. King, H. F. Schaefer, P. von R. Schleyer, and G. H. Robinson, "A stable silicon(0) compound with a si=si double bond," *Science*, vol. 321, no. 5892, pp. 1069–1071, 2008. [Online]. Available: http://science.sciencemag.org/content/321/5892/1069

[75] C. Ageorges, L. Ye, and M. Hou, "Advances in fusion bonding techniques for joining thermoplastic matrix composites: a review," *Composites Part A: Applied Science and Manufacturing*, vol. 32, no. 6, pp. 839 – 857, 2001. [Online]. Available: http://www.sciencedirect.com/science/article/pii/S1359835X00001664

[76] L. Y. Shang, Z. L. Zhang, and B. Skallerud, "Fracture of anodic-bonded silicon-thin film glass-silicon triple stacks," *Engineering Fracture Mechanics*, vol. 75, no. 5, pp. 1064–1082, 2008.

[77] S. Queste, R. Salut, S. Clatot, J.-Y. Rauch, and C. G. Khan Malek, "Manufacture of microfluidic glass chips by deep plasma etching, femtosecond laser ablation, and anodic bonding," *Microsystem Technologies*, vol. 16, pp. 1485–1493, 01 2010.

[78] I.-M. H. Thomas M.H. Lee, Debbie H.Y. Lee, Connie Y.N. Liaw, Alex I.K. Lao, "Detailed characterization of anodic bonding process between glass and thin-film coated silicon substrates," *Sensors and Actuators*, vol. 86, no. 3, pp. 103–107, 2000.

[79] C. S. Goh, S. C. Tan, K. T. May, C. Z. Chan, and S. H. Ng, "Adhesive bonding of polymeric microfluidic devices," *Proceedings of the Electronic Packaging Technology Conference, EPTC*, pp. 737–740, 2009.

[80] K. Sun, A. Yamaguchi, Y. Ishida, S. Matsuo, and H. Misawa, "A heater-integrated transparent microchannel chip for continuous-flow pcr," *Sensors and Actuators B: Chemical*, vol. 84, no. 2, pp. 283 – 289, 2002. [Online]. Available: http://www.sciencedirect.com/science/article/pii/S0925400502000163

[81] S. P. Ng, F. E. Wiria, and N. B. Tay, "Low Distortion Solvent Bonding of Microfluidic Chips," *Procedia Engineering*, vol. 141, pp. 130–137, 2016. [Online]. Available: http://dx.doi.org/10.1016/j.proeng.2015.09.212

[82] J. H. HILDEBRAND, "A critique of the theory of solubility of non-electrolytes.'," pp. 37–45, 1949.

[83] K. F. Lei, S. Ahsan, N. Budraa, W. J. Li, and J. D. Mai, "Microwave bonding of polymer-based substrates for potential encapsulated micro/nanofluidic device fabrication," *Sensors and Actuators A: Physical*, vol. 114, no. 2, pp. 340 – 346, 2004, selected papers from Transducers 03. [Online]. Available: http://www.sciencedirect.com/science/article/pii/S0924424703007209

[84] S. Haeberle and R. Zengerle, "Microfluidic platforms for lab-on-a-chip applications," *Lab Chip*, vol. 7, pp. 1094–1110, 2007. [Online]. Available: http://dx.doi.org/10.1039/B706364B

[85] K. B. Mullis and F. A. Faloona, "[21] specific synthesis of dna in vitro via a polymerase-catalyzed chain reaction," in *Recombinant DNA Part F*, ser. Methods in Enzymology. Academic Press, 1987, vol. 155, pp. 335 – 350. [Online]. Available: http://www.sciencedirect.com/science/article/pii/0076687987550236

[86] M. Agne, A. Valones, R. L. Guimarães, L. André, and C. Brandão, "usefulness of PCR in mmb," pp. 1–11, 2009.

[87] "What is dna? - genetics home reference - nih." [Online]. Available: https://ghr.nlm.nih.gov/primer/basics/dna

[88] B. Alberts, "The structure and function of dna," Jan 1970. [Online]. Available: https://www.ncbi.nlm.nih.gov/books/NBK26821/

[89] "Mechanism of enzyme action." [Online]. Available: http://chemistry.elmhurst.edu/vchembook/571lockkey.html

[90] K. Mullis, "The polymerase chain reaction," 1994.

[91] W. Wang, H.-B. Wang, Z.-X. Li, and Z.-Y. Guo, "Silicon inhibition effects on the polymerase chain reaction: A real-time detection approach," *Journal of Biomedical Materials Research Part A*, vol. 77A, no. 1, pp. 28–34. [Online]. Available: https://onlinelibrary.wiley.com/doi/abs/10.1002/jbm.a.30627

[92] K. Liu and Z. H. Fan, "Thermoplastic microfluidic devices and their applications in protein and dna analysis," *Analyst*, vol. 136, pp. 1288–1297, 2011. [Online]. Available: http://dx.doi.org/10.1039/C0AN00969E

[93] A. Bhattacharyya and C. M. Klapperich, "Thermoplastic microfluidic device for on-chip purification of nucleic acids for disposable diagnostics," *Analytical Chemistry*, vol. 78, no. 3, pp. 788–792, 2006.

[94] M. Allen Northrup, C. Gonzalez, S. Lehew, and R. Hills, "Development of a pcr-microreactor," pp. 139–139, 01 1995.

[95] Y. Hong and Æ. F. Wang, "Flow rate effect on droplet control in a co-flowing microfluidic device," pp. 341–346, 2007.

[96] C. Fermér, P. Nilsson, and M. Larhed, "Microwave-assisted high-speed PCR," *European Journal of Pharmaceutical Sciences*, vol. 18, no. 2, pp. 129–132, 2003.

[97] Y. Hataoka, L. Zhang, T. Yukimasa, and Y. Baba, "Rapid microvolume PCR of DNA confirmed by microchip electrophoresis." *Analytical sciences : the international journal of the Japan Society for Analytical Chemistry*, vol. 21, no. 1, pp. 53–6, 2005. [Online]. Available: http://www.ncbi.nlm.nih.gov/pubmed/15675516

[98] C. Ke, A.-M. Kelleher, H. Berney, M. Sheehan, and A. Mathewson, "Single step cell lysis/pcr detection of escherichia coli in an independently controllable silicon microreactor," *Sensors and Actuators B: Chemical*, vol. 120, pp. 538–544, 01 2007.

[99] S. Kondo, N. Morimoto, K. Hori, E. Shinohara, and K. Kano, "Development of a microreactor for pcr," *IEEJ Transactions on Sensors and Micromachines*, vol. 119, pp. 448–453, 01 1999.

[100] B. Shi, G. He, and W. Wu, "A pcr microreactor machinery with passive micropump and battery-powered heater for thermo-cycled amplifications of clinical-level and multiplexed dna targets," *Microchimica Acta*, vol. 185, 10 2018.

[101] B. Batule, H. Mun, and W.-B. Shim, "Development of hrpzyme-integrated pcr platform for colorimetric detection of foodborne pathogens," 03 2018.

[102] S. Jha, Y.-C. Jang, R. Chand, K. Islam, and Y.-S. Kim, "A pdms based integrated pcr microchip for genetic analysis," pp. 273–275, 01 2011.

[103] K. Cheng, D. Pan, J. Teng, L. Yao, Y. Ye, F. Xue, F. Xia, and W. Chen, "Colorimetric integrated pcr protocol for rapid detection of vibrio parahaemolyticus," *Sensors (Basel, Switzerland)*, vol. 16, 09 2016.

[104] N. Ho Bae, S. Young Lim, Y. Song, S. Woo Jeong, S. Yi Shin, Y. Tae Kim, T. J. Lee, K. Lee, S. Lee, Y.-J. Oh, and Y. Min Park, "A disposable and multi-chamber film-based pcr chip for detection of foodborne pathogen," *Sensors*, vol. 18, p. 3158, 09 2018.

[105] D. Park, P.-C. Chen, B. H. You, N. Kim, T. Park, P. Datta, Y. Desta, S. A. Soper, D. Nikitopoulos, and M. Murphy, "Optimization of geometry for continuous flow pcr devices in a titer plate-based pcr multi-reactor platform," 01 2007.

[106] Z.-Q. Zou, X. Chen, Q.-H. Jin, M.-S. Yang, and Z. Jianlong, "A novel miniaturized pcr multi-reactor array fabricated using flip-chip bonding techniques," *Journal of Micromechanics and Microengineering*, vol. 15, p. 1476, 06 2005.

[107] J. S. Marcus, W. F. Anderson, and S. R. Quake, "Parallel picoliter rt-pcr assays using microfluidics," *Analytical Chemistry*, vol. 78, no. 3, pp. 956–958, 2006, pMID: 16448074. [Online]. Available: https://doi.org/10.1021/ac0513865

[108] E. A. Ottesen, J. W. Hong, S. R. Quake, and J. R. Leadbetter, "Microfluidic digital pcr enables multigene analysis of individual environmental bacteria," *Science*, vol. 314, no. 5804, pp. 1464–1467, 2006. [Online]. Available: http://science.sciencemag.org/content/314/5804/1464

[109] M. U. Kopp, "Chemical Amplification: Continuous-Flow PCR on a Chip," *Science*, vol. 280, no. 5366, pp. 1046–1048, 1998. [Online]. Available: http://www.sciencemag.org/cgi/doi/10.1126/science.280.5366.1046

[110] A. Shamloo and A. Mashhadian, "Inertial particle focusing in serpentine channels on a centrifugal platform," *Physics of Fluids*, vol. 30, p. 012002, 01 2018.

[111] C. M. Karale, S. Bhagwat, and V. Ranade, "Flow and heat transfer in serpentine channels," *AIChE Journal*, vol. 59, 05 2013.

[112] R. Poole, A. Lindner, and M. Alves, "Viscoelastic secondary flows in serpentine channels," *Journal of Non-Newtonian Fluid Mechanics*, vol. 201, pp. 10–16, 11 2013.

[113] X. Cui, J. Guo, X. Huai, K. Cheng, H. Zhang, and M. Xiang, "Numerical investigation on convective heat transfer of supercritical pressure co2 in serpentine channel," 08 2018.

[114] J. Zilz, C. SchÃ¤fer, C. Wagner, R. Poole, M. Alves, and A. Lindner, "Serpentine channels: Micro-rheometers for fluid relaxation times," *Lab on a chip*, vol. 14, 11 2013.

[115] A. Mohammed, A. Adeniyi, and A. Hassan, "Modelling of serpentine continuous flow polymerase chain reaction microfluidics," *International Journal of Engineering Science and Technology (IJEST)*, vol. 4, pp. 1183–1189, 03 2012.

[116] K. Hsieh, B. Scott Ferguson, M. Eisenstein, K. W. Plaxco, and H. Tom Soh, "Integrated electrochemical microsystems for genetic detection of pathogens at the point of care," *Accounts of Chemical Research*, vol. 48, no. 4, pp. 911–920, 2015.

[117] F. Schuler, M. Trotter, M. Geltman, and S. et al., "Digital droplet pcr on disk," *Lab Chip*, vol. 16, 11 2015.

[118] Z. Zhu, W. Zhang, X. Leng, M. Zhang, Z. Guan, J. Lu, and C. J. Yang, "Highly sensitive and quantitative detection of rare pathogens through agarose droplet microfluidic emulsion PCR at the single-cell level." *Lab on a chip*, vol. 12, no. 20, pp. 3907–3913, 2012.

[119] L. Yao, B. Liu, T. Chen, S. Liu, and T. Zuo, "Micro flow-through pcr in a pmma chip fabricated by krf excimer laser," *Biomedical microdevices*, vol. 7, pp. 253–7, 10 2005.

[120] Z. Zhan, C. Dafu, Y. Zhongyao, and W. Li, "Biochip for pcr amplification in silicon," pp. 25 – 28, 02 2000.

[121] X. Qiu and J. Yuan, "Temperature control for pcr thermocyclers based on peltier-effect thermoelectric," in *2005 IEEE Engineering in Medicine and Biology 27th Annual Conference*, Jan 2005, pp. 7509–7512.

[122] W. Benett and J. B. Richards, "Pcr thermocycler," 11 2018.

[123] K. A. Hagan, C. R. Reedy, M. L. Uchimoto, D. Basu, D. A. Engel, and J. P. Landers, "An integrated, valveless system for microfluidic purification and reverse transcription-PCR amplification of RNA for detection of infectious agents," *Lab on a Chip*, vol. 11, no. 5, pp. 957–961, 2011.

[124] Y. Zhang and H.-R. Jiang, "A review on continuous-flow microfluidic pcr in droplets: Advances, challenges and future," *Analytica Chimica Acta*, vol. 914, pp. 7 – 16, 2016. [Online]. Available: http://www.sciencedirect.com/science/article/pii/S000326701630191X

[125] J. El-Ali, I. Perch-Nielsen, C. Poulsen, D. Bang, P. Telleman, and A. Wolff, "Simulation and experimental validation of a su-8 based pcr thermocycler chip with integrated heaters and temperature sensor," *Sensors and Actuators A: Physical*, vol. 110, no. 1, pp. 3 – 10, 2004, selected Papers from Eurosensors XVI Prague, Czech Republic. [Online]. Available: http://www.sciencedirect.com/science/article/pii/S0924424703004710

[126] M. K. Rawat, H. Chattopadhyay, and S. Neogi, "A review on developments of thermoelectric refrigeration and air conditioning systems : a novel potential green refrigeration and air conditioning," *International Journal of Emerging Technology and Advanced Engineering*, vol. 3, no. 3, pp. 362–367, 2013.

[127] J. A. Kim, J. Y. Lee, S. Seong, S. H. Cha, S. H. Lee, J. J. Kim, and T. H. Park, "Fabrication and characterization of a PDMS-glass hybrid continuous-flow PCR chip," *Biochemical Engineering Journal*, vol. 29, no. 1-2, pp. 91–97, 2006.

[128] R. M. Niemi, I. Heiskanen, K. Wallenius, and K. LindstrÃ¶m, "Extraction and purification of dna in rhizosphere soil samples for pcr-dgge analysis of bacterial consortia," *Journal of Microbiological Methods*, vol. 45, no. 3, pp. 155 – 165, 2001. [Online]. Available: http://www.sciencedirect.com/science/article/pii/S0167701201002536

[129] B. Giordano, J. Ferrance, S. Swedberg, A. HÃ¼hmer, and J. Landers, "Polymerase chain reaction in polymeric microchips: Dna amplification in less than 240 seconds," *Analytical Biochemistry*, vol. 291, no. 1, pp. 124 – 132, 2001. [Online]. Available: http://www.sciencedirect.com/science/article/pii/S0003269700949741

[130] H. Tachibana, M. Saito, S. Shibuya, K. Tsuji, N. Miyagawa, K. Yamanaka, and E. Tamiya, "On-chip quantitative detection of pathogen genes by autonomous microfluidic pcr platform," *Biosensors and Bioelectronics*, vol. 74, pp. 725 – 730, 2015. [Online]. Available: http://www.sciencedirect.com/science/article/pii/S0956566315302554

[131] K. D. Foust and B. K. Kaspar, "NIH Public Access," vol. 8, no. 24, pp. 4017–4018, 2010.

[132] D. J. Laser and J. G. Santiago, "A review of micropumps," *Journal of Micromechanics and Microengineering*, vol. 14, no. 6, p. R35, 2004. [Online]. Available: http://stacks.iop.org/0960-1317/14/i=6/a=R01

[133] Dolomite, "Peristaltic pump." [Online]. Available: https://www.dolomite-microfluidics.com/product/peristaltic-pump/

[134] X. Zhang, Z. Chen, and Y. Huang, "A valve-less microfluidic peristaltic pumping method," *Biomicrofluidics*, vol. 9, no. 1, pp. 1–8, 2015. [Online]. Available: http://dx.doi.org/10.1063/1.4907982

[135] B. Mosadegh, T. Bersano, J. Park, M. A Burns, and S. Takayama, "Next-generation integrated microfluidic circuits," *Lab on a chip*, vol. 11, pp. 2813–8, 09 2011.